Photo- and Electrochemical Methods for Biomass Valorization

by

Gabriel Magallanes

A dissertation submitted in partial fulfillment
of the requirements for the degree of
Doctor of Philosophy
(Chemistry)
in the University of Michigan
2019

Doctoral Committee:

        Professor Corey R. J. Stephenson, Chair
        Assistant Professor Andrew P. Ault
        Professor John Montgomery
        Assistant Professor Corinna S. Schindler

Gabriel Magallanes

gmagalla@umich.edu

ORCID iD: 0000-0003-2097-1325

Dedication

To my parents, family, and Bailey – for your constant support

Acknowledgements

This dissertation represents the apex of my educational career in the physical sciences. I could not fathom reaching this point without the support of so many people. As I have progressed through my college and graduate career, I have increasingly recognized the importance of the people of my life and how they have helped me through the highs and the lows. It is with a great sense of gratitude that I have the opportunity to thank them all, although this writing does not do justice to the impact these people have had in my life. First and foremost, I have to thank my Ph.D. advisor, Professor Corey Stephenson. Corey's ability to guide but not take hold of the wheel has given me the space to grow as an independent scientist. His mentorship has allowed me to experience the ebbs and flows of research in the physical sciences while having opportunities to network, mentor, teach, and engage with my colleagues. Corey has also set a high standard of professionalism and knowledge in the field of chemistry. He has shown me how to think critically in a manner that can continuously improve the state of chemistry, and to question everything with a sense of curiosity and pragmatism. The lessons I have learned while working for Corey, both in science and in professionalism will be carried with me for years to come.

I would be remiss if I did not give proper acknowledgment to the genuinely talented and hard-working faculty and staff at the University of Michigan that have aided in my learning throughout my graduate career. Firstly, I want to thank my dissertation committee members, Andy Ault, John Montgomery, and Corinna Schindler for being an engaging and guiding group of intellects throughout my graduate studies. Alison Narayan served as my Original Research

the lab. I truly owe them so much for everything they taught me and their comradery throughout our projects. Mathilde Rigoulet was also a pivotal student in one of the projects I worked on and helped set the stage for successful paper submission. I want to make a special shout out to Tim Monos. Tim taught all of us in the lab how to keep composure when it seemed the worst was coming. He is a walking, living beacon of civility and wisdom. Finally, the mentees with whom I have worked with are just as important as the mentors I have had. Cheng Yang was a visiting student from China when I first started mentoring him, and now he is a slick, skilled experimentalist with a sense of urgency in all of the work he does. I am so excited to see his future work and how he will make an impact in the field of chemistry. Lastly, Kim Chan was an undergraduate I mentored for three years. Kim's hard work and perseverance earned her a position at Takeda Pharmaceutical Company, and now she has been admitted to the University of Pittsburgh for medical school. I am so proud of her hard work, her commitment to our lab, and the direction she is moving toward in her life.

I cannot go without mentioning all of my fantastic housemates. The day I moved into 903 S. Main St was the first day I had ever met Nick Ragazzone, Martin Sevrin, Jake Ludwig, and Alec Valenta. Although Martin left us to marry his beautiful wife Maggie, we have really stuck together this entire five-year journey and have grown close to each other like family. The newer housemates, Naish Lalloo and Cara D'amico, have also provided a great and meaningful friendship that has made my life so enjoyable. I have been so lucky to call these people my friends, and I hope that my future brings me the good fortune of making friends as great as they have been.

Finally, I want to thank my family and my best friend, Bailey. My parents immigrated to this country before I was born in hopes that I could have an unlimited scope of opportunity for my future. All they have ever wanted for me to that I follow my dreams and passions and that I do

what makes me happy. Their support has been steadfast, and I am thankful for that. My brothers, John, Javier, and Luis, have been a great source of support and wisdom, and knowing that they will always be there makes me happy. All of my family–nieces, nephews, aunts, uncles, and grandparents–bring great joy to my life. Finally, Bailey has been the best friend a man could ask for. Her companionship means a lot to me, and I am excited for what the future will bring to our lives as we move forward together.

These are my acknowledgments. These few pages only begin to represent the importance and impact these people have had on my life, both personally and professionally. I hope that I can continue to encounter great mentors and friends as I make my next move in the up-and-coming chapter of my life.

Table of Contents

Lists of Tables

Lists of Figures

List of Abbreviations

A (mA)	amps (milliamps)
Ac	acetyl
Acr	acridinium
AIBN	azobisisobutyronitrile
aq	aqueous
Ar (italicized)	aryl group
BDE	bond dissociation enthalpy
Bn	benzyl
bp	boiling point
bpy	2,2'-bipyridine
BRSM	based on returned starting material
BTX	benzene, toluene, and xylene
cat	catalysis/catalytic
CE	counter electrode
cm	centimeter
CV	cyclic voltammetry
DABCO	1,4-diazabicyclo[2.2.2]octane
DCA	9,10-dicyanoanthracene
dF(CF$_3$ppy)$_2$	2-(2,4-difluorophenyl)-5-trifluoromethyl pyridine
DMA	*N,N*-dimethylformamide
dtbbpy	4,4'-di-tert-butyl-2,2'-bipyridyl
E	potential (expressed in volts)
EA	electron affinity
E$_{ox}$	oxidation potential
E$_{pc}$	potential at peak current
E$_{red}$	reduction potential
GPC	gel permeation chromatography
HAT	hydrogen-atom transfer
HSQC	heteronuclear single quantum coherence
Hz	hertz
IEA	International Energy Agency
IP	ionization potential
ISC	intersystem crossing
IUPAC	international union of pure and applied chemistry
j	charge density
kcal	kilocalorie
KIE	kinetic isotope effect
lb	pound
LED	light emitting diode
lut	2,6-lutidine

Me	methyl
MeCN	acetonitrile
med	mediator
Mes	mesityl
MLCT	metal to ligand charge transfer
mol	mole
MV	methyl viologen
nm	nanometer
[O]	oxidation
Ox	oxidant
PC	photocatalyst
PET	photoinduced electron transfer
Ph	phenyl
PINO	phthalimide *N*-oxyl radical
pmp	para-methoxyphenyl
ppy	2-phenylpyridine
RE	reference electrode
Red	reductant
R_f	retention factor
RSM	returned starting material
rt	room temperature
RVC	reticulated vitreous carbon
SCE	standard calomel electrode
SET	single-electron-transfer
τ	lifetime of fluorescence
^{t}Bu	tert-butyl
TEMPO	2,2,6,6-tetramethyl-1-piperidinyloxy
TFA	trifluoracetic acid
TFAA	trifluoroacetic anhydride
TLC	thin-layer chromatography
TPP	tetraphenylporphyrin
Ts	*p*-toluenesulfonyl
UV	ultraviolet
V (mV)	volts (millivolts)
WE	working electrode

Abstract

Over the last eight years, the United States has experienced a rapid reduction of greenhouse gases with concomitant economic growth. This phenomenon can be attributed to substantial investments in clean energy production; reluctantly, similar attention has eluded the industry for commodity chemicals manufacturing. Lignin is an abundant biopolymer and the only renewable source of aromatic carbons on the planet. Depolymerization of lignin to monomeric material could provide a source of commodity chemicals more sustainably compared to crude oil processing. There are currently no technologies that efficiently convert lignin to fine chemicals. Our lab considers the conversion of lignin to useful chemicals to be a concept of great value toward a goal of reducing our dependence on fossil fuels. Described herein is the culmination of my thesis work toward developing environmentally benign methods for the depolymerization of lignin. We have discovered unique modes of reactivity in photo- and electrochemistry that lead to lignin depolymerization. Additionally, we have developed strategies that utilize redox chemistry to enable lignin valorization under relatively mild reaction conditions. Our goal is to understand the limits to lignin depolymerization better and to use that knowledge to develop catalyst systems that can fragment lignin in a mild and reproducible manner.

Chapter 1 Introduction

1.1 The Case for Photoredox Catalysis

Natural products, chemical substances derived in their natural state from living organisms

(e.g., plants, animals, microbes), have been used to treat human disease since the dawn of

medicine.[1] Roughly half of the new chemical entities introduced between 1981 and 2002 were

natural products, semi-synthetic natural product analogs, or synthetic products that were inspired

by a natural product. One needs little persuasion to realize the significant impact that natural

products have had on modern day medicine. In the pursuit of achieving synthetic competence that

mirrors the efficiencies found in biological systems, chemists have pursued the constant

development of chemical methods for the synthesis of complex chemical targets. This endeavor

and the rapid ability to communicate and publish scientific articles has led to a misconception that

the field of total synthesis is mature and that further exploration is no longer necessary.[2] The

antithesis to this misconception lies in the idea that molecular complexity is time-dependent, and

through innovation, synthetic chemistry is made simpler.[3] A large driver of innovation in synthetic

methodology is the academia-industry relationship.[4] Industry is continuously in need of accessing

novel intermediates in a manner that is cost-efficient and safe, helping to identify real-world targets

and enlist academic groups to deliver new methods and structural motifs. Even in the midst of

rapid publication and the expedient communication of chemical data and structure, there appears

to be a lack of new methods and reactions making their way into industrial settings in a meaningful

manner. A specific example that highlights the lack of new reactions in industrial settings is found

in a study published in 2014. This study analyzed the most used chemical reactions in medicinal chemistry and natural product total synthesis in 2014 versus those conducted in 1984.[5] The analysis showed that of the most used synthetic reactions, none of them were discovered in the past twenty years and only two were discovered in the 1980s and 1990s. This analysis shows that the integration of new and modern methods has yet to make a profound impact in industry, so the impetus for exploring new modes of reactivity still exists.

In the search for new reaction strategies, free radical chemistry has sparked a remarkable intrigue in chemists for the many decades since Professor Moses Gomberg's seminal report of the existence of carbon-centered free radicals.[6] Radicals have been heavily studied for new methodologies and in applications to natural product total synthesis, mainly due to the exquisite reactivity and unique bond connections that can be formed. In many cases, radical reactivity allows the formation of new bonds that are otherwise inaccessible through polar, two-electron processes.[7] The synthesis of remarkably complex natural products has been achieved with the aid of photochemical steps that generate radical intermediates, such as ingenol, ginkgolide B, α-cedrene, and many more.[8,9,10] Despite the distinctive modes of reactivity for free radicals, they are often considered difficult to control. Historically, radical generation has been initiated either thermally or chemically.

A common strategy for generating open-shell, free radical intermediates outside of chemical initiation is through photochemical means. Traditional organic photochemistry has been well studied and implemented, and it is dependent on organic molecules absorbing ultraviolet (UV) light (Table 1).[11,12] Students and practitioners of chemical studies have probably noticed that most salts and even organic materials are often colorless. This is likely a direct result of that molecule's lack of visible-light absorbance, which is the light that is most abundantly produced by household

2

lamps and lighting fixtures, as well as from the sun. UV light is a wavelength that is also provided by the sun and is not detectable by the human eye. Most organic molecules absorb light in the UV wavelengths, and as a result, UV light is often used for photochemically-induced reactions.[13] If centuries of work have previously enabled photochemical methods for accessing complex intermediates, what is the necessity for more innovation in the way we utilize light sources to access radical intermediates? Ultimately, two immediate issues come to mind: (1) UV light reactions are recalcitrant to scale-up operations, expensive, and require the implementation of additional safety precautions, and (2) UV light can promote uncontrollable side reactions due to the indiscriminate photoexcitation of functional groups found in a molecule.

Table 1. Relationship between energy, wavelength, and frequency.

Type of radiation	Wavelength (λ = nm)	Energy (kcal-mol^{-1})	Frequency (n = Hz = s^{-1})
ultraviolet	200–400	140–70	1.5×10^{15}–7.5×10^{14}
violet	~400	70	7.50×10^{14}
green	~500	60	6.0×10^{14}
red	~700	40	5.0×10^{14}
Near-infrared (NIR)	~1000	30	3.0×10^{14}

Insofar, chemical and photochemical methods for radical generation have been discussed. With chemically induced radical generation comes the cost of toxic or explosive chemicals–alongside their toxic byproduct counterparts–that pose challenges for waste management. Environmental considerations have also impacted how chemists design reactions to avoid excessive amounts of waste that is harmful to human health and the environment. In the wake of a green chemistry renaissance, photoredox catalysis has risen to widespread popularity in the

modern-day radical chemistry literature. Photoredox catalysis has sparked the design of new approaches to generating and controlling redox chemistry in organic molecules.

<p style="text-align:center">1.2 The Principles of Design and Strategy for Photocatalysis</p>

Photoredox is a colloquially but academically accepted term that combines the root word photo- (meaning light) and the suffix redox (relating to the movement of electrons) to describe the type of reactivity resulting from the photochemical manipulations of the redox potentials of a catalyst to effect the movement of electrons between catalyst and substrate. The prevailing thought was that if a catalyst can be designed to absorb visible-light, instead of UV light, one could *selectively photoexcite the catalyst in the presence of a substrate chemical, solvent, and other additives*. This concept laid the groundwork for the advent of modern-day photoredox catalysis. Photoactive catalysts have been known to engage in single-electron-transfer (SET) processes, typically organic dyes, but it was the realization that ruthenium- and iridium-based photosensitizers could be used due to some unique properties exhibited by these photocatalysts. The utilization of Ru- and Ir-based photocatalysts is common in photoredox catalysis due to their ability to absorb visible-light, their long-lived excited state lifetimes (τ), ability to engage in SET redox events through outer sphere electron transfer, and the dual nature of the photocatalyst to act as an oxidant or as a reductant.[14,15,16] The seminal findings for the photochemical and electrochemical behaviors of $Ru(bpy)_3^{2+}$ were reported in the 1970s and 80s, well before the current explosion in methods for photoredox reactions, and the culmination of this work has been summarized in a review.[17] The general scheme for photoredox reactions is depicted in Figure 1. Upon irradiation of a photocatalyst with visible-light, the photocatalyst can enter a photoexcited state. The Ir- and Ru-based photocatalysts have a particularly long photoexcited state lifetime (e.g.,

<p style="text-align:center">4</p>

Ru(bpy)$_3^{2+}$ = 1100 ns; *fac*-Ir(ppy)$_3$ = 1900 ns). In the event of a photochemical excitation event, the photocatalyst undergoes a metal-to-ligand charge transfer (MLCT) and subsequent intersystem crossing (ISC) event. The ISC enables the transition of an electron to another orbital with a concomitant spin-flip, which results in the electronic configuration where relaxation of the electron is now spin-forbidden. This ISC process ultimately results in the long-lived excited state lifetimes of Ru- and Ir-based photocatalysts. The MLCT process effectively results in single electron oxidation of the metal center from M^n to M^{n+1} while reducing one of the ligands, thus resulting in a radical anion ligand intermediate. The MLCT is responsible for the dual nature of the photocatalyst to act as an oxidant or a reductant (Figure 2). For the remainder of the text, oxidation potential (E_{ox}) refers to the required applied potential of a substance to remove an electron, and the reduction potential (E_{red}) is the required applied potential of a substance to add an electron.

The ground state redox potentials of photocatalysts can be easily obtained using electrochemical measurements. The ground state potentials can then be used with photophysical data to obtain the excited state potentials. This is a useful, predictive method to anticipate photocatalyst SET processes. A remarkable property of photocatalysts is that their redox properties are always enhanced, i.e., the reduction or oxidation becomes more energetically favored. This concept of enhanced redox potentials is described in Figure 1.a, where photoexcitation of an electron leads to the ground state electron affinity (EA(R)) becoming a more negative value (*EA(*R)), which results in a more oxidizing intermediate. Likewise, the ground state ionization potential (IP(R)) becoming a more positive value (*IP(R)) that increases the reducing power of the intermediate. Typically, the oxidation of a substance requires a positive potential, and the reduction of a substance requires a negative potential, but these numbers are always relative to a certain electrochemical standard. In organic chemistry, the best practice is to use organic solvents with a

quasi-reference electrode using the same solvent. This operation is easily performed using a piece

of conductive metal as the reference electrode, and then referencing the potentials to ferrocene

after a control oxidation sweep has been done on the ferrocene. Converting ferrocene to a more

standard reference that is used in organic chemistry, such as the standard calomel electrode (SCE),

is simply done by taking the potential vs. Fc^+/Fc and adding +0.38 V (Figure 2.a). A thorough

examination of relevant oxidation potentials for common organic molecules has previously been

reported by Nicewicz and co-workers.[18]
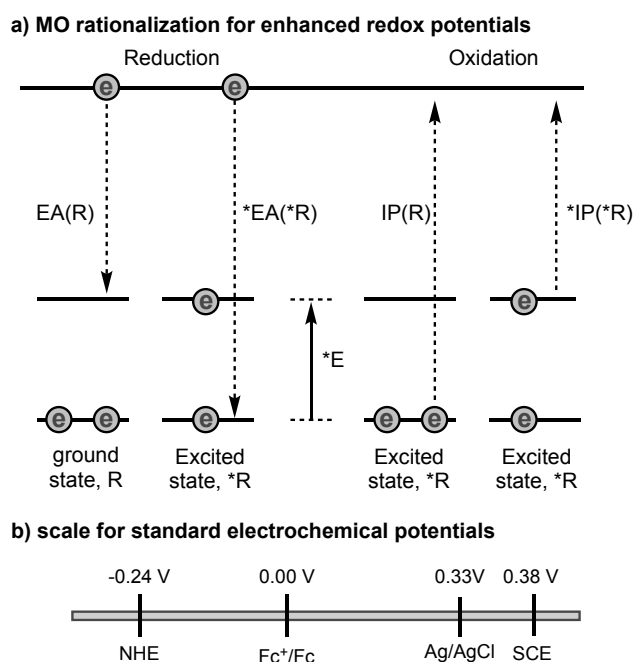
Figure 1. (a) representative MO diagram of excited state redox potentials (b) relative standard electrochemical potentials.

The dramatic effect on the ground-state potentials upon excitation of an electron that

undergoes MLCT and ISC affords the redox-active photocatalyst. It is this enhancement in redox

potentials that imparts the unique reactivity of photoexcited catalysts. If one knows the redox

potentials of the photocatalyst and the desired organic substrate for manipulation, one can predict

whether photoinduced electron transfer (PET) will occur. In one mechanistic manifold of PET, the

photocatalyst can undergo a reduction to arrive at a reduced $PC^{\bullet-}$ intermediate (Figure 2). For the catalyst to turnover, it must encounter an oxidant to which it can transfer its extra electron. This sequence is known as a reductive quenching cycle. Alternatively, the oxidative quenching pathway can ensue in the presence of an oxidant that can quench excited state photocatalyst to $PC^{\bullet+}$. Once a photocatalyst has been excited with light, other processes can quench the photocatalyst that are not direct electron transfer processes. Commonly encountered quenching processes include non-radiative quenching process (i.e., ISC or triplet reaction) or the radiative process of phosphorescence, which can lead to non-productive pathways. Figure 2 further highlights the electrochemical potentials of commonly employed photocatalysts that should enable the reader of this text to understand the proceeding work in this document better, and for referencing the photocatalysts to their assigned labels (**Ir.1 – Ir.4**). The redox potentials listed emphasize the simplicity in being able to selectively evaluate photocatalysts based on their ability to oxidize or reduce a chemical reagent. Triplet-energy transfer has recently been developed into a useful reaction manifold that induces reactivity through triplet sensitization instead of electron transfer. This type of reactivity will not be further described in this writing, but the reader is pointed to many examples of triplet-energy transfer reactivity referenced herein.[19,20,21,22,23,24,25,26] More detailed reading in singlet and triplet energy values as well as triplet-triplet annihilation have been referenced.[27,28,29,30]

The mechanistic considerations discussed heretofore have positioned the field of photoredox catalysis for optimal success in academic and industrial processes. Photoredox catalysis is arguably one the sub-branches of chemistry to be most quickly adapted in an industrial setting as illustrated by multiple reports of photoredox catalysis methods coming out of industrial research labs, as well as industry-academia collaborative projects (Figure 3).[31,32,33,34,35,36,37]
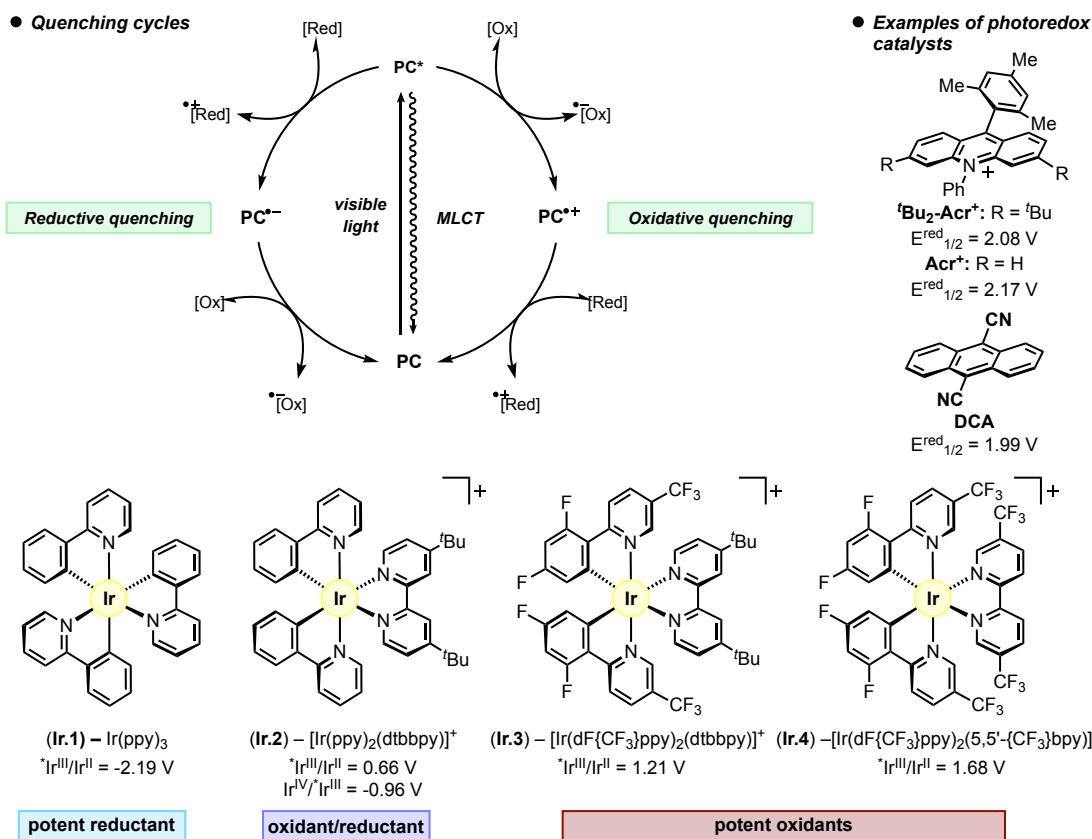
Figure 2. A representative quenching cycle for a photocatalyst is depicted, along with a number of different photocatalysts and their relevant redox potentials (vs. SCE). See ref 59 for a note on the potential for DCA.

The Stephenson group has identified photoredox as an innovative strategy for reaction development to modernize the chemist's perspective on forming and controlling free radical intermediates. With the plethora of bond disconnections that can be envisioned using photoredox catalysis, the Stephenson group has leveraged the ability to harness visible-light to create methods that are operationally simple and environmentally benign compared to their UV-mediated counterparts.
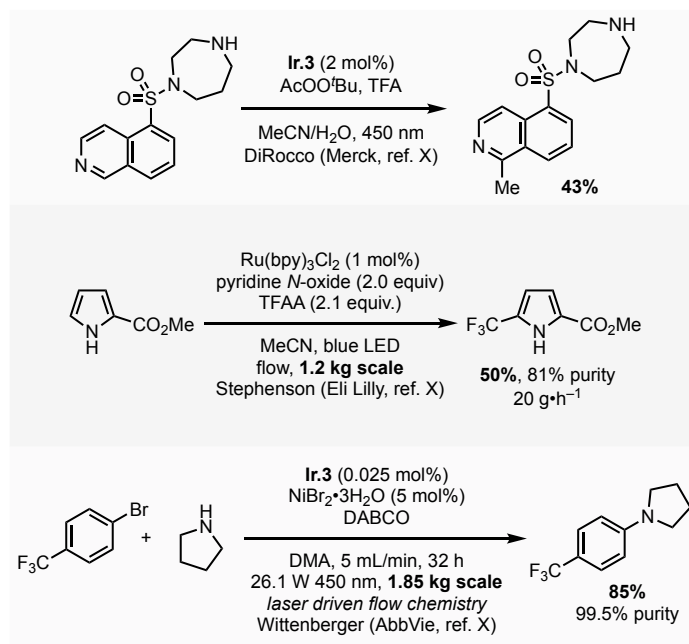
Figure 3. Examples of photoredox catalysis being applied in industrial and academic settings.

1.3 Introduction to Lignin and the Prospects of Biomass Conversion

The depletion of fossil fuel sources has prompted urgent efforts in developing technologies to convert renewable sources into products typically derived from crude oil processing.[38] The bedrock of these efforts relies on identifying an appropriate, renewable source that is sustainable in a long-term operation to produce useful chemicals and macromolecules. Modern day society is intimately tied to its energy usage with an ever-increasing demand that has mostly been met by the processing and consumption of fossil fuels. Amid a green chemistry revolution, the increased demand for energy has also brought about the heightened awareness of the importance of technologies that harness renewable sources for energy and chemicals. Investments in renewable energy technology have allowed the U.S. to experience its first sustained period of rapid reductions in greenhouse gas emissions and simultaneous economic growth since 2008; however, comparatively little investment in research has been directed toward identifying renewable sources

for commodity chemicals.[39] Impressively, renewable energy contributions in the U.S. increased from 6.5% to 11.3% between the years 2007 and 2017.[3]

The term "commodity chemicals" is not clearly defined in the academic or industrial literature. Some reports regard commodity chemicals as chemicals that sell for less than 1 USD/lb, but this measure will drastically vary with the shrinkage and expansion of global markets and economies.[40] Additionally, some reports have defined commodity chemicals as chemicals that are produced on a scale greater than one million tons/year.[41] For the remainder of this writing, the reader should merely consider commodity chemicals as chemicals that are produced on a very large scale to satisfy global markets. These chemicals are often used as the solvents in numerous industrial processes, building blocks for complex molecule synthesis, or monomers for polymer synthesis. When considering the sourcing of commodity chemicals from renewable carbon sources, one should remember the two renewable sources of carbon: biomass and atmospheric CO_2. Biomass, the largest source of renewable energy accounting for 5% of total consumption energy in the U.S.,[42] has been considered an alternative to fossil fuels for the production of ethanol, biofuels, and small molecule feedstocks, but technologies for generating commodity chemicals from non-food woody biomass are still in their adolescence. Biomass consists mainly of three distinct polymeric material. First, and the most abundant, is cellulose–a polymer of glucose. The second most abundant polymer comprising biomass is lignin, a polymer synthesized by plants from phenylpropanoid monomers. The third most abundant portion of biomass is hemicellulose, which is a polymer mostly made from xylose, as well as other sugar monomers. Paper and pulping processes often seek to utilize the cellulose portion of biomass and regard the lignin portion as waste. Due to its unique chemical structure, lignin has attracted the attention of many scientists looking to harness a renewable source for producing useful commodity chemicals. Lignin is the

second most abundant biopolymer on the planet, and the DOE has estimated the sustainable biomass potential in the U.S. to be 1.2 billion tons per year, a target that is reachable within 35 years.[43] This increased number, compared to the current 190 million tons of biomass used per year for electricity and biofuel generation, has generated the impetus in research across the globe to convert biomass (including lignin) into useful, value-added chemicals.

1.4 The Biosynthesis of Lignin and its Structure

The first documented description of lignin in 1838 attracted the attention of a considerable number of curious chemical researchers.[44] Chemists and plant physiologists sought to elucidate lignin's structure and to help explain its purpose, bond connectivity, and to understand the potential for its upgrading to valuable chemicals further. Lignocellulosic biomass is an intricate and recalcitrant polymeric material that is a renewable carbon source, and lignin serves as the main component in plants that impart structural rigidity. The ideal utilization of lignocellulose biomass would be through a so-called biorefinery.[45,46] The International Energy Agency (IEA) Bioenergy, an international agency created to improve the exchange of information related to bioenergy and biofuel production, defined the biorefinery as "*the sustainable processing of biomass into a spectrum of marketable products and energy*".[47] Lignin is the second most abundant biopolymer on the planet, only behind cellulose, found in most terrestrial plants and it is the only renewable source of aromatic carbons, making it an ideal candidate for conversion to value-added products through a biorefinery.[48]
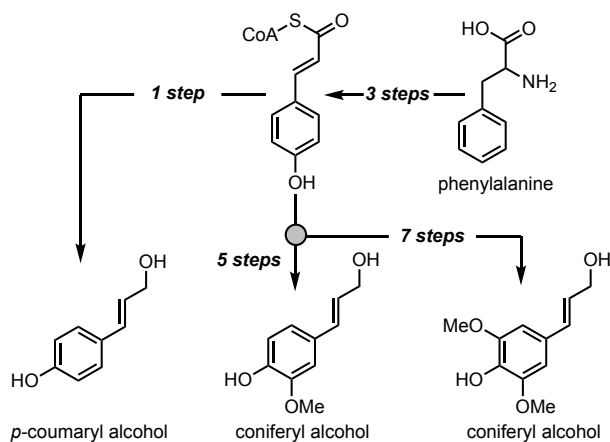
Figure 4. An abbreviated scheme for the biosynthesis of the monolignols

Lignin is a biopolymer synthesized by plants from three monomer units known as monolignols. The three monolignols are termed *p*-coumaryl alcohol, coniferyl alcohol, and sinapyl alcohol (Figure 4). The monolignols originate from phenylalanine, which gets converted to *p*-coumaric acid. Further elaboration to a Co-A intermediate is the first intermediate where the enzymatic process branches. One more reductive, enzymatic step affords *p*-coumaryl alcohol, and several additional steps eventually results in the synthesis of coniferyl and sinapyl alcohol. The three monolignols vary by the methoxy-substitution on the aromatic rings, which has a direct impact on the available connections that are possible in the synthesis of the lignin polymer. Once the monolignols are synthesized, they are transported to the cell wall and soon thereafter undergo polymerization that affords the primary lignin polymer (Figure 5.a; lignin is found in nature attached to cellulose and hemicellulose, the constituents of which are represented in Figure 5.b). Polymerization begins with a net deprotonation and single-electron oxidation from the phenol, which leads to several possible resonance structures (Figure 5.c). Figure 5.c shows the corresponding bond formations via radical coupling that results in the synthesis of the β-O-4, dihydrobenzofuran, and β-β linkage motifs. These three linkage motifs are among the most common, accounting for approximately 45–60%, 10%, and 10% of the total linkage motifs,

respectively, depending on the plant species and external variables. Several other linkage motifs occur less frequently, such as the 4-O-5 (Figure 5.a) and 5-5, that are rarely targeted for lignin depolymerization strategies.
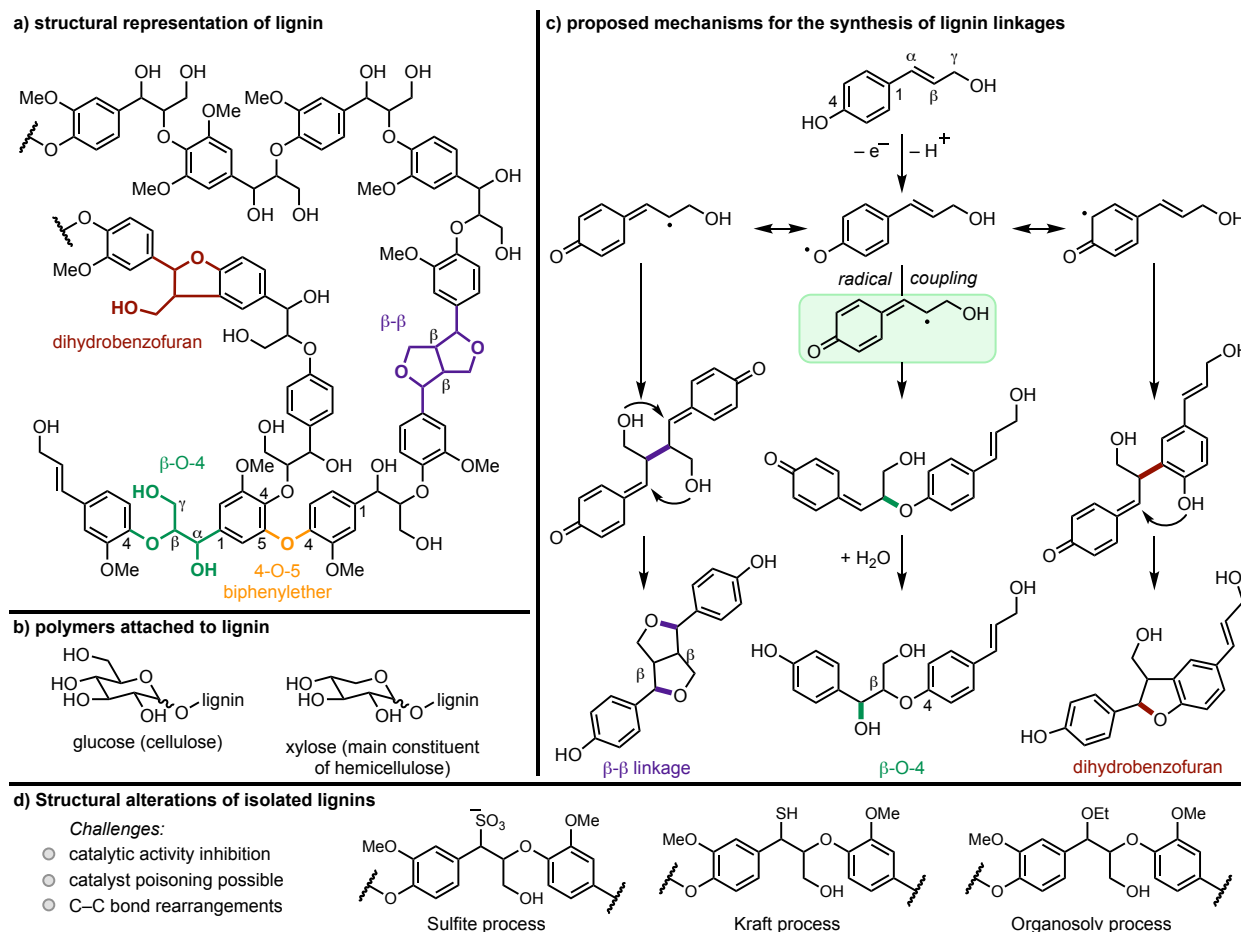
Figure 5. (a) representative structure of a lignin polymer (b) constituents of the polymers found attached to lignin (c) a proposed mechanistic pathway for linkage synthesis (d) representative structural alterations of isolated lignins.

Other critical structural notes on lignin include the fact that lignin is optically inactive, and that it is a mostly linear polymer with minimal branching points.[49,50] Additionally, the structure of native lignin depicted in Figure 5.a is often not the structure of lignin that is actually isolated from conventional separation techniques. Several extraction methods are used in industrial processes to separate lignin from the principal components of the lignocellulosic biomass that often alter the chemical structure and bond connectivities of the lignin (Figure 5.d).[46,51] It is essential to recognize

that the structure of the isolated lignin depends on the separation technique. Chemists should consider these structural alterations and the current state-of-the-art technologies to acquire a lignin before developing fragmentation strategies. The two most commonly used techniques in the paper and pulp industries are the Kraft and lignosulfonate extraction methods.[52] However, these methods can replace the benzylic hydroxyl groups in lignin with thiol groups and sulfonate groups, respectively, among other chemical transformations (e.g., dehydration, oxidation). Organosolv methods have been developed to help retain the structure of native lignin, but acidic extraction conditions cause the formation of interunit C–C and C–O bonds that are less reactive to catalytic depolymerization protocols.

1.5 Conclusion

This chapter has sought to establish the conceptual groundwork for the proceeding work contained in this document. The maturation of the field of synthetic methods to-date has enabled remarkable achievements, but the production of new methods for bond formation continually identifies areas of improvement. Although the initial reports for the use of photoredox catalysis go back to 1978, it was not until the late 2000's that an exponential growth in photoredox methods occurred (

Figure 6).[53] Research in photoredox catalysis has brought about a new and straightforward way to achieve desirable reactions in a very easy-to-use manner. Realization of the potential doors that photoredox catalysis could open led to its rapid expansion, and, ultimately, our group's entry into this field of research. Photoredox catalysis has reinvigorated old schools of thought that are now being used in ways that achieve efficiencies never matched before. My work described herein

14

seeks to establish new photochemical and electrochemical methods that simplify the valorization of biomass to allow for simple and efficient methods for lignin valorization on a meaningful scale.
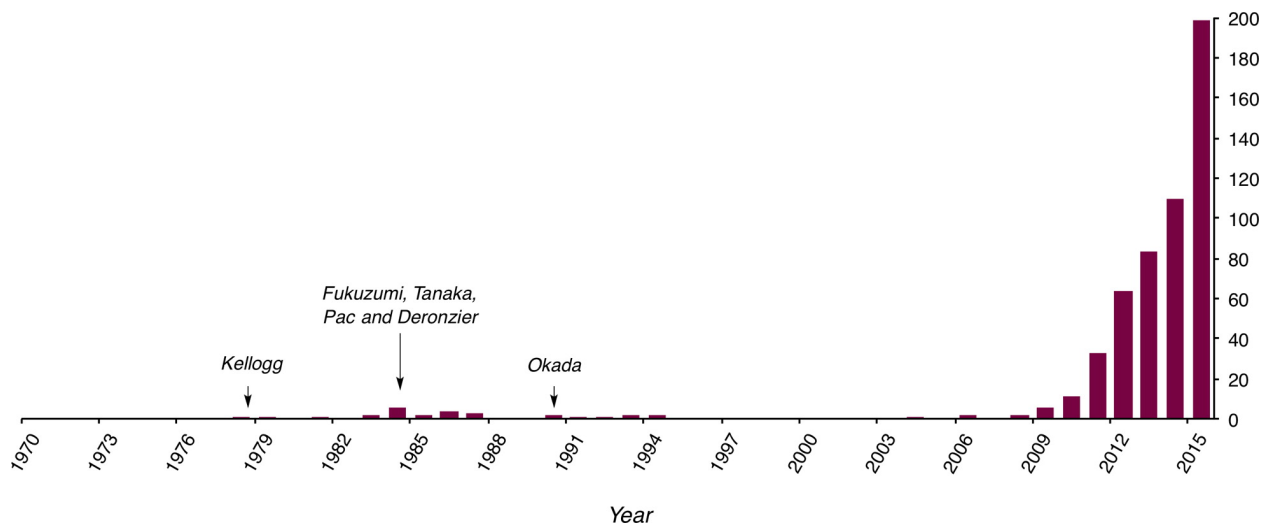
Figure 6 A bar chart representing the yearly published papers in the field of organic photoredox catalysis. Reprinted with permission from J. Org. Chem. 2016, 81, 6898–6926. https://pubs.acs.org/doi/10.1021/acs.joc.6b01449 © 2016 American Chemical Society.

Chapter 2 Development of a Photochemical Strategy for Cleaving C–O, C–S, and C–N Bonds

2.1 Introduction: From Seminal Reports to Modern Methods

Initial lignin depolymerization studies were primarily focused on elucidating the structure of lignin and attempting to replicate the depolymerization mechanism purported by lignases found in white rot fungi. Adkins and co-workers sought to apply reducing conditions that were able to selectively reduce esters in the presence of alkenes, which required more forceful conditions compared to commonly employed alkene hydrogenation conditions.[54] In accord, they found the using a Cu-Cr oxo-catalyst could be reacted with hardwood lignin under high hydrogen pressures to afford a mixture of hydroxy cycloalkanes and methanol (Figure 7). Additionally, Hibbert and co-workers were able to find that varied conditions when reacting maple woodmeal with Raney-Ni under high temperatures could also afford small molecule products while maintaining the aromaticity of the original lignin polymer (Figure 7).[55] These reports represent some of the first experiments that helped to confirm that the monomer unit that is the building block for lignin synthesis.

In an attempt to further replicate nature's method of lignin depolymerization, chemists have pursued oxidative processes for lignin depolymerization. It is largely believed that enzyme degrading catalysts, such as those found in *Phanerochaete chrysosporium,* initiate the lignin depolymerization sequence by single electron oxidation of lignin that then induces C–C bond fragmentation of the lignin backbone.[56,57] Some early approaches adopted a biomimetic approach
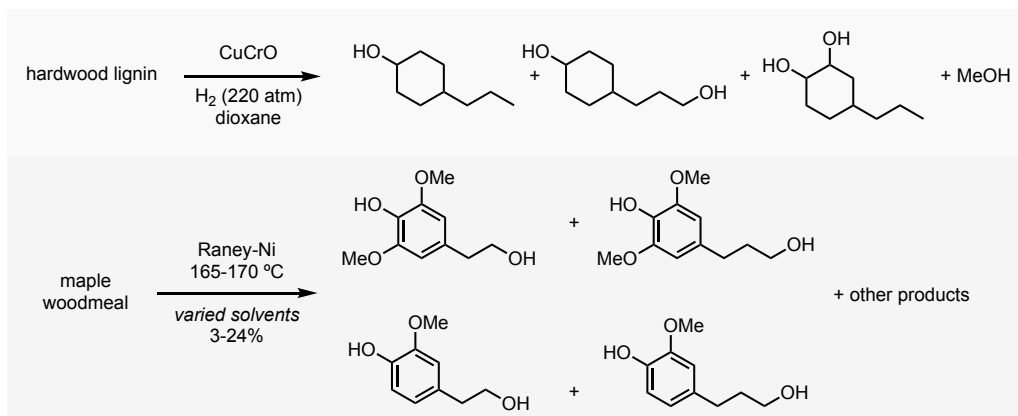
Figure 7 Early examples of lignin depolymerization for understanding the chemical structure of lignin.

by using a heme-model catalyst (Fe(TPP)Cl) in the presence of peroxide to effect lignin oxidation

or fragmentation on a lignin model substrate (**1**, Figure 8). A notable number of products were

isolated and identified. Firstly, the benzylic oxidation product **2** was observed in a minimal 3%

yield, whereas the oxidative fragmentation product **3**, resulting from C_α–C_β bond fragmentation,

was isolated as the major product in 54% yield. Additionally, C_β-O-4 fragmentation products, **4**

and **5**, were isolated as the oxidized product and the non-oxidized product, in 25% and 3% yield

respectively. This was a significant result that helped lend support to the biochemical mechanism

for lignin depolymerization in plants, as well as the ability to induce lignin backbone fragmentation

under oxidative conditions.
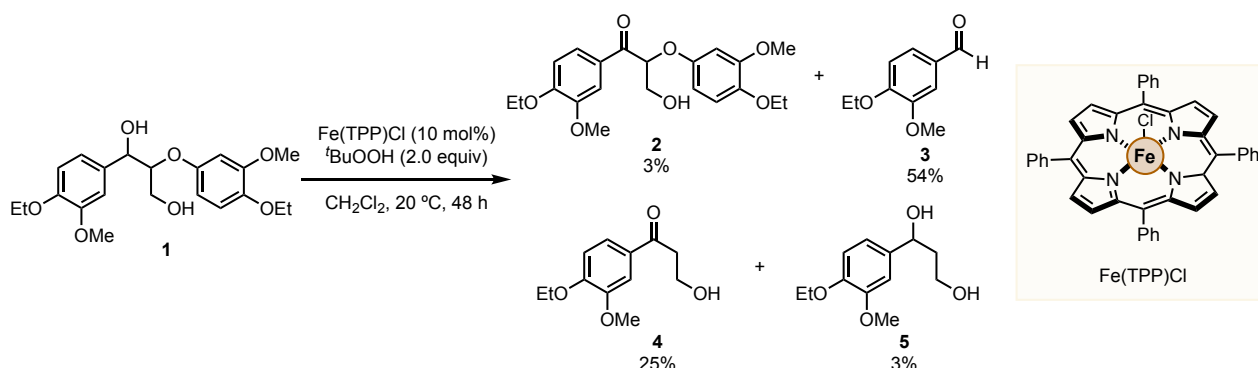
Figure 8 Heme-inspired fragmentation of a β-O-4 lignin model substrate.

In terms of photochemical methods for lignin depolymerization, some initial studies were reported by DiCosimo and co-workers in 1988, wherein combinations of Mn and Co salts were used to mediate thermally-driven single-electron oxidation of lignin substrates.[58] Photochemical strategies represent an exciting strategy toward lignin depolymerization owing to the many arene units, alcohol functional groups, and particularly weak C–O bonds. Certain redox-active photocatalysts might be able to be tuned for selective fragmentation of lignin. More recently, Mariano and co-workers reported that DCA could be photoexcited to produce a highly oxidizing photoactive state.[59] As previously noted, oxidative methods are attractive considering the aromatic units on lignin are relatively electron-rich due to the donation of electron density coming from the phenol and methoxyl groups. It was envisioned that a potent oxidant could oxidize a lignin substrate by a single electron, which would precede a C_α–C_β bond fragmentation (Figure 9).[60,61] Accordingly, Mariano and co-workers found that irradiation of DCA with UV-light in an oxygen-saturated solution of 5% aqueous MeCN with model substrate would afford the fragmentation products as a result of C_α–C_β bond fragmentation (Figure 9). Interestingly, an appreciable increase in yield of fragmentation was noticed when the reaction was performed on a β-1 model (96%) compared to the β-O-4 model (55%).

Mariano's example of oxidative fragmentation is one of the earlier reports of a photoredox catalyst being used for lignin fragmentation. This chemistry, among others, has served as a major source of inspiration for the strategies developed in our group. One of our greatest sources of inspiration for lignin depolymerization comes from work reported by the Toste group. Toste and
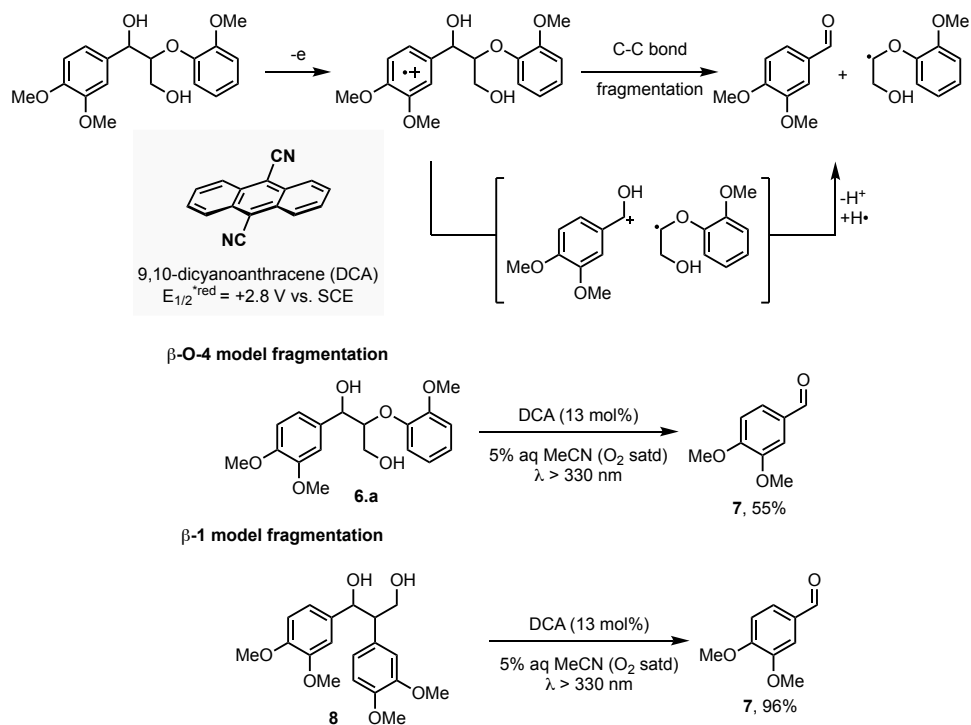
Figure 9 Photoredox-based methods for oxidative fragmentation of lignin substrates.

co-workers have reported the use of a vanadium-Schiff base catalyst that was able to fragment lignin β-O-4 model systems, as well as native lignin (Figure 10).[62,63] The authors proposed a mechanism in which a ketyl radical-like intermediate that is bonded to a vanadium species undergoes C–O bond homolysis to afford an enolate intermediate, that would then further convert to products. We saw the ketyl radical intermediate as a prime intermediate to engage using photoredox catalysis. We soon embarked on reaction exploration and system optimization to reduce this concept to practice.
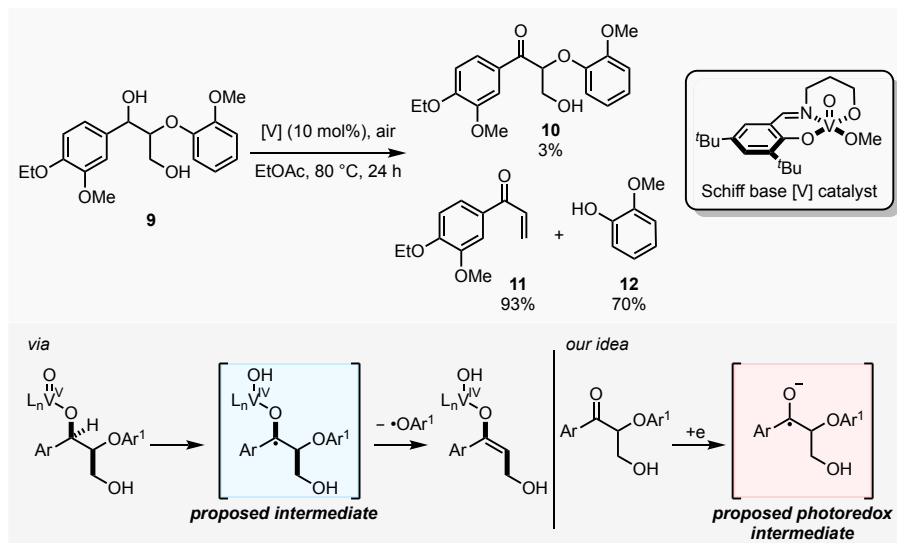
Figure 10 The Toste group's method for lignin depolymerization as a source of inspiration.

2.2 Ketyl Radical Chemistry Accessed by Photoredox Catalysis

Our group has relied on the principles of photoredox catalysis to develop useful and interesting reactions that allow us to achieve rapid access to complex scaffolds and key intermediates.[64] Our group's first publication in photoredox catalysis disclosed the tin-free method for reductive dehalogenation of activated alkyl-bromides.[65] We later showed unactivated C–I bonds and C–Br bonds could be reduced under the appropriate conditions.[66,67] These reports helped lay the foundation on which much of our current research efforts are focused. Since these reports, our group has utilized photoredox catalysis to access immediately relevant pharmaceutical scaffolds and to carry out bi-functionalization reactions of styrenyl anisole starting materials to synthesize medicinally relevant phenethylamines (Figure 11).[68,69]
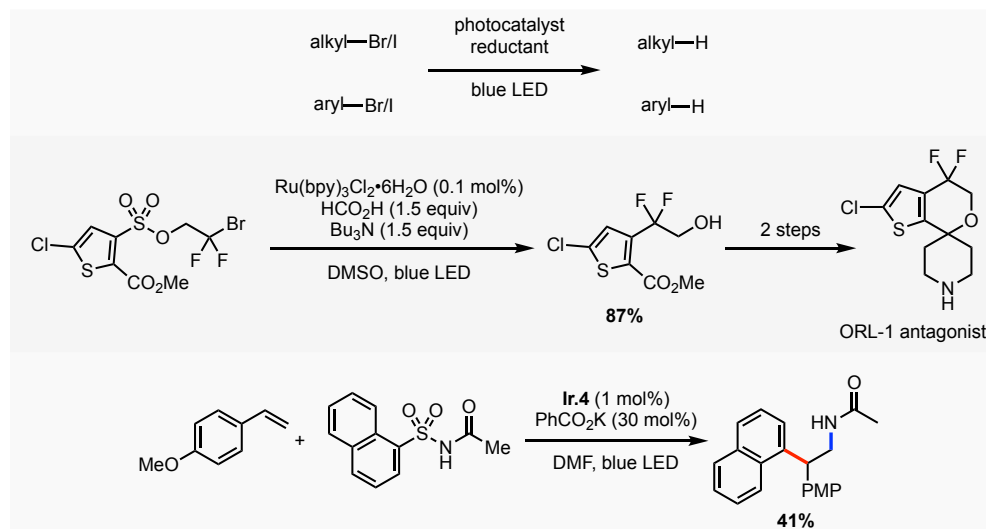
Figure 11 A representation of important photoredox-based methods reported from the Stephenson group.

With regards to lignin depolymerization, we envisioned that the β-O-4 linkage would be the best linkage to target since it is the most studied and also the most repeated linkage in lignin. Oxidation of the β-O-4 linkage would afford a ketone that can be targeted by photoredox catalysis for single electron reduction to a ketyl radical intermediate. There is a plethora of literature that suggested the feasibility of lignin backbone fragmentation through a ketyl radical intermediate. Firstly, the C_β–O bond found in the β-O-4 linkage has a relatively weak BDE of ~69 kcal/mol (computed with DFT, Figure 12).[70]
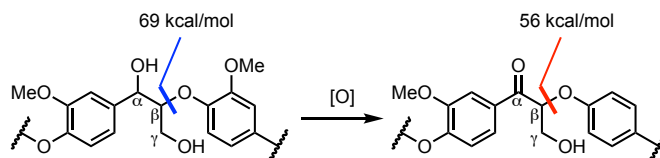
Figure 12 Decrease in BDE upon alcohol oxidation.

It was also calculated that the BDE of that same C–O bond decreased by about 13 kcal/mol (~56 kcal/mol) upon oxidation of either the α- or γ-hydroxyl group. The benefits of this oxidation are two-fold: (1) the weakened BDE allows for milder reaction conditions to be used for the C–O fragmentation, and (2) the ketone product (the oxidation product) can act as a functional handle

for targeting with photoredox catalysis, specifically for accessing a ketyl radical anion intermediate.

Our group has learned much from previous studies that guided us in developing photochemical strategies for lignin depolymerization. We have leveraged the dramatic effect felt by C–H and C–C bonds adjacent to nitrogen atoms upon single electron oxidation. Specifically, the pK_a and BDE of the α-C–H bond in triethylamine decrease significantly upon single electron oxidation, making the amine radical cation intermediate a highly reactive intermediate that is prone to further reaction (e.g., deprotonation, HAT, Figure 13).[71] This type of reactivity was leveraged in our group's report of a photoredox enabled aza-Henry reaction (Figure 13).[72] Inducing C–C bond homolysis is more challenging, but our group found that only 4.2 kcal/mol of ring strain was necessary to break C–C bonds in our efforts to convert catharanthine into *Aspidosperma* and *Iboga* alkaloids.[73] More recently, our group demonstrated the utility in oxidizing aminocyclopropanes to induce C–C homolysis to generate a distonic amine radical cation (β-iminium radical) that could undergo serial 6-exo and 5-exo cyclizations to afford the formal [3+2] cycloaddition product (Figure 13).[74]

The profound effects of redox manipulations on certain functional groups support the concept of using ketyl radical intermediates to fragment the backbone of lignin. Literature precedent that is more relevant to our initial strategy for lignin β-O-4 is found in the use of photoredox catalysis for the fragmentation of C–O and C–N bonds of keto-epoxide and keto-aziridine substrates.[75,76] These reports showed that reduction of ketones that are adjacent to strained rings
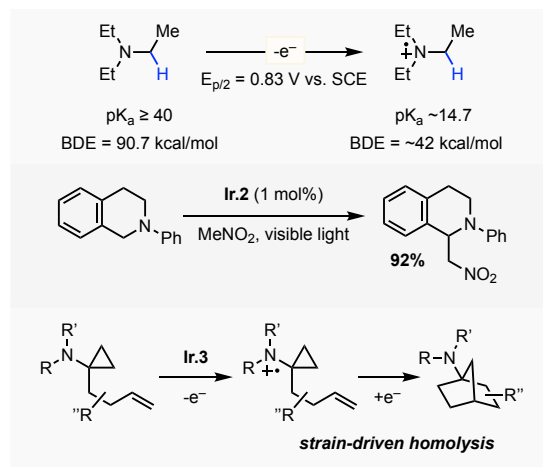
Figure 13 The effects imparted by single electron oxidation of alkyl amines.

can be reduced under photochemical conditions with a photocatalyst and subsequently induce the homolysis of the adjacent C–X bond (X = N or O). These encouraging reports helped guide our group's development of a photochemical strategy for the fragmentation of β-O-4 lignin model systems.[77] Our initial strategy for lignin model substrate fragmentation was developed to take advantage of the bond-weakening event upon oxidation of the benzylic alcohol found in the β-O-4. It was found that the selective oxidation of the benzylic alcohol could proceed with high yield and high selectivity using a stoichiometric oxoammonium salt known as Bobbit's salt (Figure 14). Following oxidation, the oxidation product could be fragmented using **Ir.2** in the presence of *N,N*-diisopropylethylamine as a sacrificial reductant. Formic acid was found to decrease reaction times and increase overall yields, most likely acting as a proton or hydrogen atom source. This two-step sequence required a simple filtration from the oxidation step to afford analytically pure oxidation product, which could then be directly subjected to the photochemical fragmentation conditions. The reaction proved to be useful on several lignin model substrates with varying methoxy substitution as well as substrates with and without the extra γ-hydroxyl group (Figure 14.a). A notable achievement in this report was the adaptation of the photochemical fragmentation into a flow system. When comparing a batch reactor system to a flow system, it was found that the

throughput of product could be increased from 0.05 mmol/h to 1.8 mmol/h (Figure 14.b). Flow chemistry provides a significant advantage for photoredox catalysis since it allows for better light penetration through the reaction solution, whereas batch reactors typically limit light penetration to the very outer outside edge of the reactor. A question that had yet to be addressed was regarding how the color of lignin, typically a very dark color, would affect the photochemical reaction. To shed some light on this question, two separate photochemical fragmentation reactions were run in the presence of commercially available lignosulfonate. This experiment was carried out to determine whether the lignosulfonate would shut down reactivity or if the darkening of the reaction solution would inhibit photocatalyst excitation. Interestingly, the reaction in a batch reaction showed no product formation, whereas the flow reaction showed 90% and 92% yield of the fragmentation products, on-par with the expected yields under normal reaction conditions (Figure 14).

Ultimately, our group's first report on lignin model oxidation and photochemical fragmentation laid the groundwork for future work on lignin model systems as well as native lignin. The applications of these strategies are being made increasingly affordable by developing techniques that use catalysts, green reagents, and operate under ambient conditions. My first endeavor in lignin chemistry was concerned with expanding the scope of the ketyl radical-induced fragmentation while trying to improve the overall atom economy.
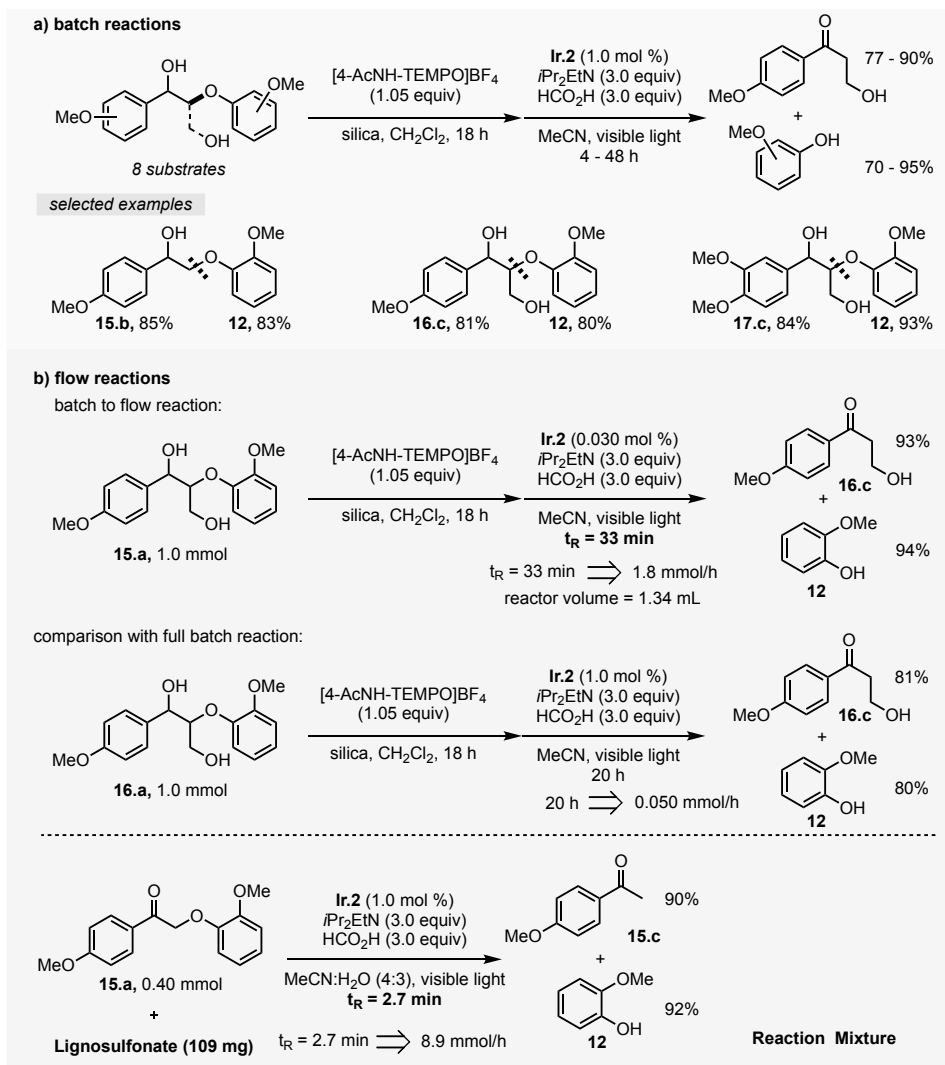
Figure 14 Our group's previous work in photochemical strategies for lignin depolymerization.

2.3 Reaction Development and Results

Following the publication of our photochemical fragmentation of lignin models,[77] we generated the following hypothesis: if we can use these conditions to fragment C–O bonds, then we can adapt the conditions to fragment C–N and C–S bonds. Not only did we wish to expand the scope of the fragmentation reaction, we also wanted to explore reaction conditions that would allow us to reduce the stoichiometry of the additive reagents, ^{i}Pr$_2$EtN and HCO$_2$H, as a means to improve the cost and atom economy of the reaction. We mostly thought that formic acid was useful

for providing a proton and electron source (or a hydrogen atom). If this is true, then lowering the formic acid stoichiometry should be viable when using a protic solvent instead of MeCN, as the protic solvent can act as a proton or electron source. We decided to commence with reaction exploration by applying a benchmark reaction to consider the viability of switching solvents and decreasing the amounts of additives.
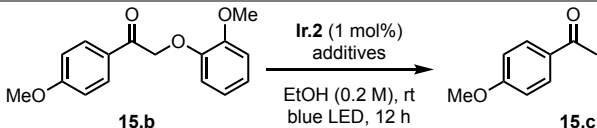
First, we decided to evaluate the efficiency of the reductive dehalogenation of diethylbromomalonate in different solvents with **Ir.2**.[78] This set of experiments sought to identify a solvent that could act as a capable H-atom donor (Table 2).

Table 2 Efficiency of reductive dehalogenation in different solvents.

EtO$_2$C—CO$_2$Et   **Ir.2** (1 mol%)   EtO$_2$C—CO$_2$Et
| |
Br   solvent, rt   H
13   blue LED, 12 h   **14**

solvent	conversion
MeOH	5%
EtOH	67%
^{i}PrOH	46%
THF	57%

We targeted simple alcohols (methanol, ethanol, and isopropanol) as well as THF since α-C–H bonds have been known as rather labile C–H bonds for HAT chemistry.[79] The results showed that EtOH was the best solvent for this transformation. After identifying EtOH as a competent solvent for reductive dehalogenation, we focused on adapting the EtOH solvent to the reaction conditions for lignin model fragmentation. We carried out a small evaluation of additive effects on the fragmentation of lignin model **13** in EtOH as the solvent. It was known that ^{i}Pr$_2$EtN and HCO$_2$H were essential additives for lignin model fragmentation base on our previous reports.[77] Accordingly, we looked at how the presence and absence of additives would affect the yield of the fragmentation reaction (Table 3).

Table 3 Optimization of additive stoichiometry.

additive	conversion	additive	conversion
none	0%	guaiacol (1 mol%)	0%
^{i}Pr$_2$EtN (0.5 equiv)	37%	guaiacol (1.0 equiv)	0%
^{i}Pr$_2$EtN (1.0 equiv)	50%	No photocatalyst	0%
^{i}Pr$_2$EtN (2.0 equiv)	82%	No light	0%
^{i}Pr$_2$EtN (2.0 equiv) + HCO$_2$H (1.0 equiv)	100%		

It was readily apparent that the absence of any additives was detrimental to the overall reaction progress. The lack of conversion in the absence of additives also supports the idea that the photocatalyst is not directly quenched by substrate **15.b**. Increasing amounts of ^{i}Pr$_2$EtN led to higher yields, and the addition of formic acid led to the best yield. Based on previously proposed mechanisms, we thought the amine was acting as a sacrificial electron donor. We also considered that the phenol product (guaiacol) that was a product from the fragmentation could serve as an electron source, and thus act as a quencher for the photocatalyst. Additionally, we considered the possibility of guaiacol acting as an acid catalyst which would play the same role as the formic acid. When we used guaiacol as an additive, we saw no conversion. Increasing the amount of guaiacol to a full stoichiometric equivalent still led to no conversion. Running the reaction without any photocatalyst or light also resulted in no conversion. We finally settled on conditions optimized in EtOH with 2.0 equivalents of ^{i}Pr$_2$EtN and 1.0 equivalent of HCO$_2$H, an improvement from 3.0 equivalents of both reagents from our previous reports.

Aryl ketone substrates were first explored, including β-O-4 lignin model systems (Figure 15). Increasing methoxy substitution was tolerated (**15.b-18.b**), with the highest yield substrate obtained from a model system without the γ-hydroxy group (**15.b**). The aldehyde substrate **19.b**
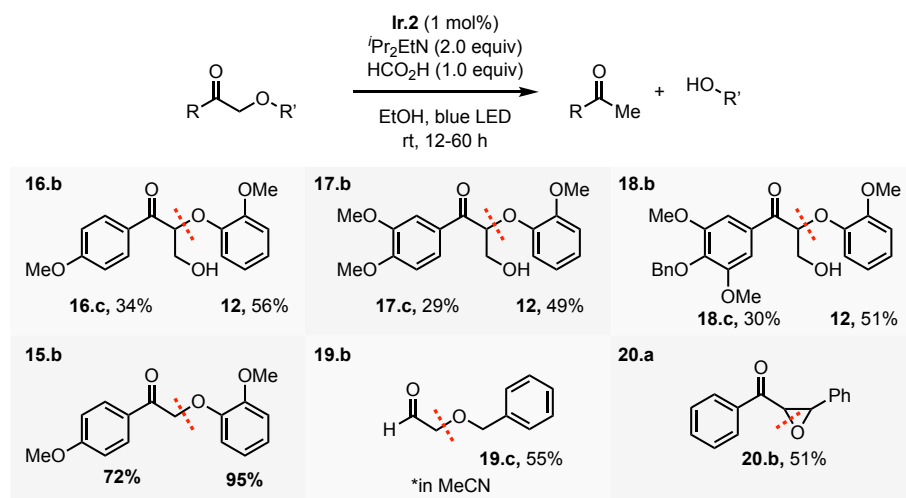
Figure 15 Scope for C–O bond fragmentation.

failed to convert in EtOH, most likely due to in-situ acetal protection of the aldehyde. The reaction converted to afford benzyl alcohol as product in 55% yield when MeCN was used as solvent. Additionally, the keto-epoxide substrate **20.a** afforded the β-hydroxyketone product in 51% yield.

In accordance with our goal to further expand the scope of this photoredox method, we applied the reaction to C–N and C–S bonds (Figure 16). We found that amine substrates, both protected and unprotected, afforded the fragmentations products in good yields (**21.a-24.a**). The morpholine substrate provided the acetophenone product, but no morpholine product was able to be isolated. Sulfide substrates were also compatible for fragmentation with the established reaction conditions, showing great flexibility in arene substitution and ring structure (**28.a-35.a**). In addition to the fragmentation of C–X bonds, some substrates did not fragment, but they formed pinacol coupling products instead (Figure 17).
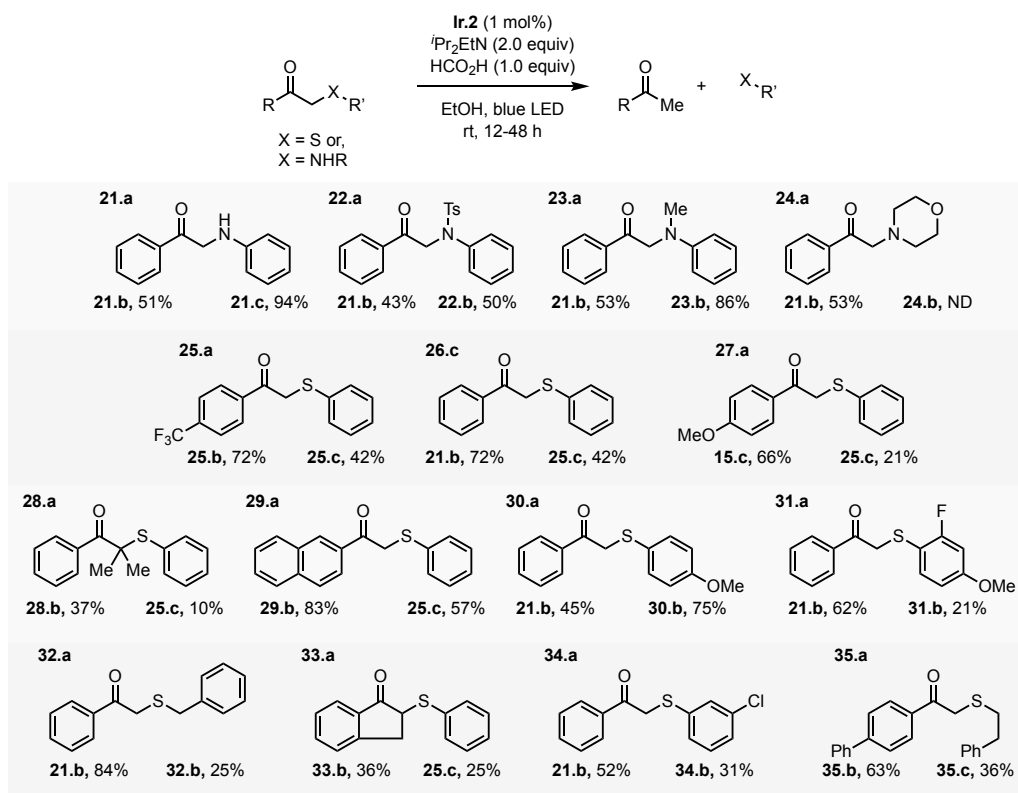
Figure 16 Reaction scope for C–N and C–S bond fragmentation.

We attribute this phenomenon to a slow fragmentation step upon the formation of the ketyl radical anion intermediate. Overall, this method enabled us to explore conditions using a greener solvent for carrying out carbon-heteroatom bond fragmentations that are paramount to our group's mission in developing lignin depolymerization strategies. We envision the expansion of the scope of this reaction will better inform the biomass and photoredox community for future strategy developments in methodology and synthesis.
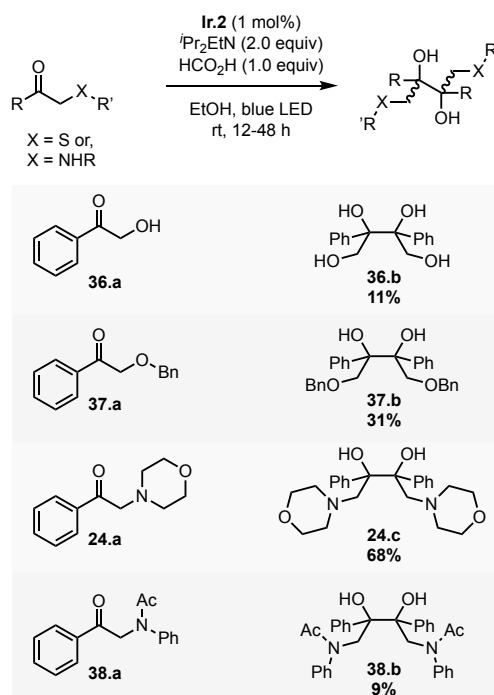
Figure 17 Scope of substrates that fragmented and proceeded to form radical coupling products.

2.4 Conclusions

We strongly believe that the continued development of methodologies for selective C–X bond fragmentation will benefit future endeavors in natural product and drug molecule synthesis, as well as other active areas of research in polymers and biomass conversion. This chapter represents some of our group's initial explorations into the use of Ir-based photocatalysts for the reduction of unstrained α-keto-ethers, amines, and sulfides using decreased amounts of additives. We also found how ketone reduction could occur in a manner that led to C–C bond formation instead of C–X bond fragmentation, for which the selectivity was largely influenced by substrate electronics and reaction conditions. These results have helped lay the groundwork for the remaining content that is discussed in this document.

Chapter 3 Two-step strategies for lignin depolymerization

*Portions of this chapter have been published in Bosque, I.; Magallanes, G.; Rigoulet, M.; Kärkäs, M. D.; Stephenson, C. R. J. Redox Catalysis Facilitates Lignin Depolymerization. *ACS Cent. Sci* **2017**, 621; Magallanes, G.; Kärkäs, M. D.; Bosque, I.; Lee, S.; Maldonado, S.; Stephenson, C. R. J. Selective C–O Bond Cleavage of Lignin Systems and Polymers Enabled by Sequential Palladium-Catalyzed Aerobic Oxidation and Visible-Light Photoredox Catalysis. *ACS Catalysis* **2019**, *9*, 2252.

3.1 Introduction

As mentioned in Chapter 2, our lab has generally taken a two-step approach toward lignin depolymerization. There have been numerous studies regarding reductive,[80,81] oxidative,[82,83,84,85] and redox-neutral fragmentations.[77,86,87,88] The oxidation of the lignin β-O-4 allows us to take advantage of the ketone functional group as well as the weakened C_β–O bond (Figure 12). Two of the most prominent examples of two-step strategies have been reported by the Stahl group and the Westwood group (Figure 18).

Stahl and co-workers first developed a catalytic aerobic oxidation by using AcNH-TEMPO to carry out a completely selective benzylic oxidation of lignin model compounds as well as native lignin.[89] This oxidation was used in their later report where they oxidized lignin and subsequently depolymerized it by boiling the oxidized lignin in formic acid with sodium formate as an additive (Figure 18).[85] Stahl and co-workers, in a collaborative effort with various departments and research centers, further elaborated their work to expand the oxidation and fragmentation to lignins isolated by different techniques (e.g., enzymatic, mild acidolysis-HCl/dioxane, copper-alkaline hydrogen peroxide) from various wood sources (i.e., poplar, maize, maple).[90] Their best results were

obtained by lignin that was isolated by enzymatic extraction from poplar wood samples.
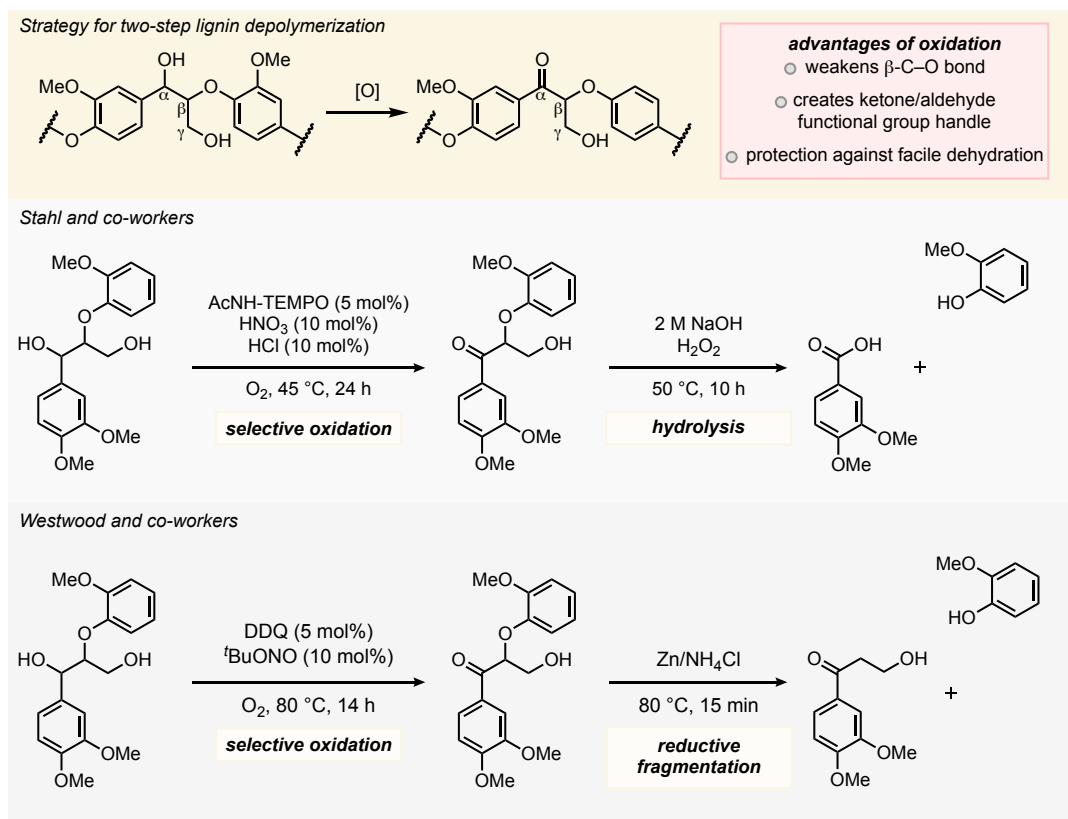
Figure 18 Summary of two-step approaches to lignin depolymerization.

The success of the fragmentation by hydrolysis depends on the oxidation, probably due to the C_β–O bond weakening but the oxidation also probably helps to reduce alcohol elimination. Also problematic is the inter- and intramolecular condensations that are acid catalyzed and have detrimental effects on lignin depolymerization protocols. Additionally, Westwood and co-workers developed a catalytic aerobic oxidation utilizing a nitrite salt and DDQ as a catalyst system that can be turned over by oxygen.[86] The oxidation protocol worked well on lignin model systems as well as native lignin. They then developed reductive conditions using Zn metal to target the β-O-4 bond fragmentation to afford monomer products from native lignin.[86] These two reports resemble the strategy that our group has employed. Our initial efforts employed a stoichiometric oxidant to achieve the selective oxidation of the benzylic alcohol.[66] We later reported a dual-catalytic strategy

using Pd and Ir to photochemically oxidize lignin models (Figure 19).[91] We found that efficient oxidation using catalytically competent amounts of Pd and Ir necessitated sodium persulfate ($Na_2S_2O_8$) as a stoichiometric oxidant. The reaction worked on lignin model systems to afford oxidation products in good yield; however, model systems that had the γ-hydroxy moiety would afford mixtures of benzylic ketone product and aldehyde product. We attributed the aldehyde product formation to the primary alcohol oxidation event, which nicely sets up the aldehyde intermediate (39) for a retro-aldol reaction. Although the undesired primary alcohol oxidation still fragments the β-O-4, which would result in lignin backbone fragmentation, the conditions were not amenable to native lignin systems.
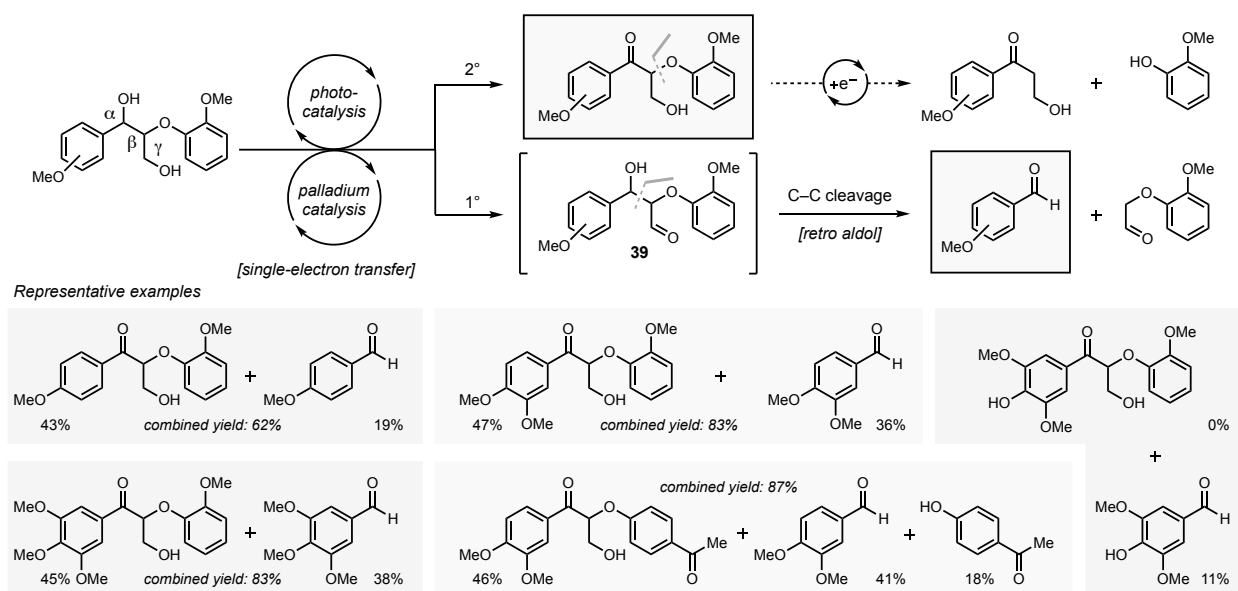
Figure 19 Scope and mechanistic aspects of Pd/Ir dual catalysis strategy for lignin depolymerization

Moving forward, we have envisioned many different strategies to employ electrocatalysis, organic dyes, and different methods to streamline the process for lignin depolymerization. The research efforts described herein represent our efforts in attempting to streamline the two-step process while making it more cost-effective. This objective aligns with our group's overall goal to develop meaningful and scalable chemistry.

3.2 Sequential Palladium-Catalyzed Aerobic Oxidation and Visible-light Photoredox Catalysis

for Lignin System Fragmentations

In line with our goal to develop useful reactions for lignin depolymerization, we sought to find oxidation conditions that could easily translate to reductive fragmentation conditions. Our previously discussed oxidations were either wasteful (stoichiometric oxidants) or were cost-prohibitive (Pd and Ir). Accordingly, we recognized that O_2 was a desirable terminal oxidant for large-scale applications. Nature uses tailored metalloenzymes to activate molecular oxygen (O_2) for performing catalytic oxidations.[92,93,94] Industrial and academic research programs are also interested in the use of O_2 in chemical synthesis instead of chemical oxidant additives since it is abundant and highly atom-economical.[95,96,97] Thus, we considered the use of a Pd-catalyzed aerobic oxidation that could avoid the requirement for redox-active co-catalysts as an attractive entry for enabling dioxygen-coupled turnover of Pd. We saw great potential in the Pd(OAc)$_2$/DMSO catalyst system that was independently developed by the groups of Larock and Hiemstra in the 1990s.[98,99] It was expected that DMSO serves to stabilize reduced Pd (Pd^0, also known as "palladium black") and promote redox cycling with O_2. Aerobic oxidations have long been considered for process scale chemistry, but a recent report from GlaxoSmithKline's API Chemistry team highlights the challenges and desires for oxidation chemistry. They reported the use of a high-boiling solvent (sulfolane, bp = 285 ºC) with heat and bubbling air to oxidize 400 g of material.[100] The products were isolated in high purity after distillation. Based on this precedent, we sought to develop Pd-mediated aerobic oxidation conditions that would allow for efficient scalability with important implications for future scale-up processes.

Initial studies were focused on using air or an O_2 atmosphere for effective conversion of alcohol to ketone product. We started with a solution of **15.a** in DMSO with 10 mol% Pd(OAc)$_2$

at 65 ºC under an oxygen atmosphere that afforded the ketone product **15.b** in >95% yield (NMR).

Gratifyingly, we were able to reduce the loading of Pd(OAc)$_2$ to 5 mol% and still afford **15.b** in

97% isolated yield (Figure 20). Additionally, were were able to get equally good results using air

as the oxygen source. We then moved to examine the generality of this reaction with a number of

different lignin model substrates. Lignin model systems bearing the γ-alcohol or the free phenol

functionality have proven to be challenging substrates for transition metal-based systems.[84,101] We

were pleased to see that those classes of substrates (**16.a, 17.a, 45.a,** and **46.a,** respectively)

displayed the desired reactivity when subjected to our optimized reaction conditions. Expectedly

so, the simpler single-hydroxy model substrates afforded the ketone oxidation products in good

yields (**15.a** and **40.a**). Substrates that contained a phenoxy-subunit different from the 2-

methoxyphenol subunit also showed good yields for oxidation (**41.a-43.a**).
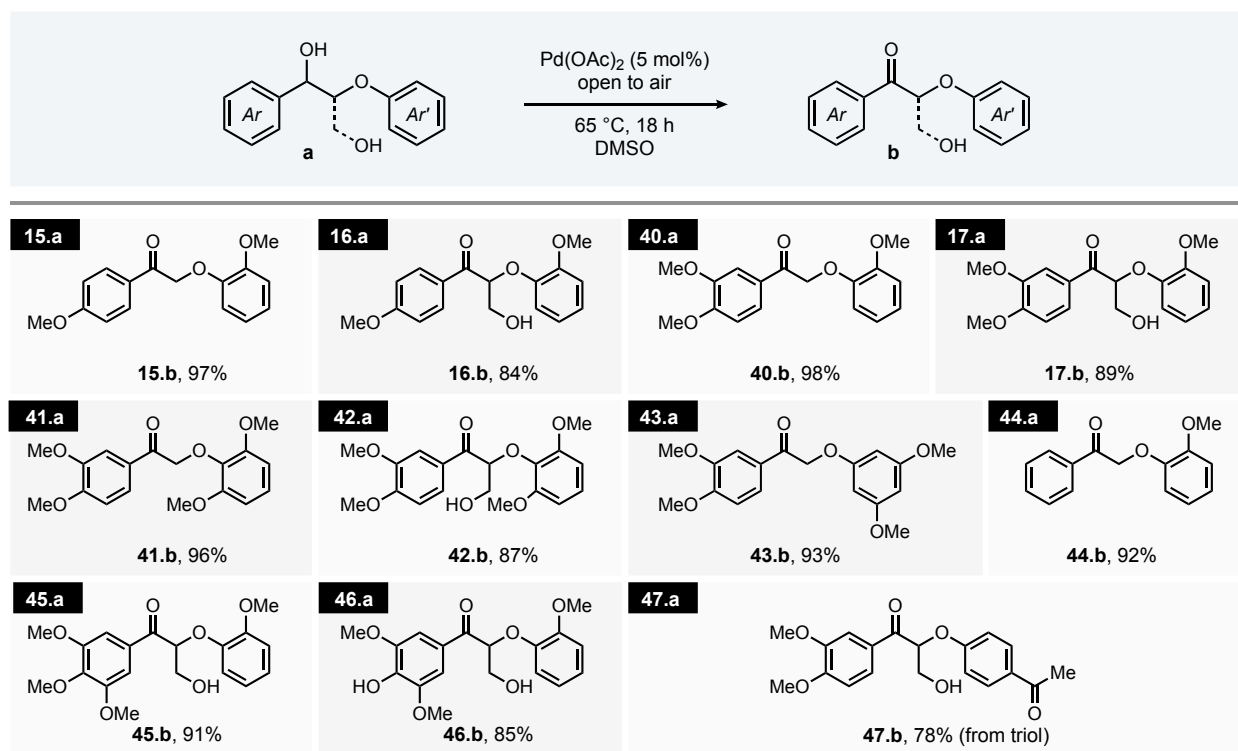
Figure 20 Scope of the Pd-mediated aerobic oxidation of lignin model substrates

Additionally, we designed the triol-substrated **47.a** to probe the reactivity for the oxidation of multiple benzylic alcohols. Gratifyingly, the triol substrate afforded the diketone product **47.b** in 78% yield. Also of note is substrate **44.a**, which often lacks significant reactivity under oxidation conditions, afforded the ketone product **44.b** in 92% yield, further exemplifying the remarkable selectivity and reactivity of our oxidation system.

After we established the operationally simple aerobic oxidation conditions for bezylic alcohol oxidation of β-O-4 model substrates, we sought to establish a reliable method for the selective C–O bond cleavage of the oxidized β-O-4 model substrates. We envisaged that our previously reported photochemical methods for lignin model substrate fragmentation could be easily adapted for a more streamlined two-step process with our oxidation protocol. We started by subjecting **15.b** to the aerobic oxidation conditions, then subsequently subjecting that crude product material to the photochemical fragmentation conditions including **Ir.2** (1 mol%), ^{i}Pr$_2$EtN (3.0 equiv), and HCO$_2$H (1.0 equiv) for 12 h. The reaction showed good conversion, but we decided to rerun the reaction with a lower loading of **Ir.2** (0.03 mol%) as well as lowering the stoichiometric equivalents of ^{i}Pr$_2$EtN (1.2 equiv), and HCO$_2$H (0.1 equiv) while extending the reaction time to 36 h. After purification, the fragmentation products **15.c** and **12** were isolated in 94% and 92%, respectively (Figure 21). Extensive investigation into a one-pot process where the reagents for the photochemical fragmentation were added directly to the reaction mixture at the end of the oxidation reaction never showed fruitful results. The optimal process necessitated aqueous work-up between the oxidation step and the C–O fragmentation step as well as different solvents for each step; however, no intermediate purification was required between the steps. Various substrates afforded products in good yield, that is, aerobic oxidation and subsequent C–O bond fragmentation. Coumaryl substrates **15.a** and **16.a** converted nicely to afford **15.c** and **16.c**

in 94% and 83%, respectively. Coniferyl substrates **40.a** and **17.a** also showed good conversion to

40.c and **12** in 95% and 91% yield and **17.c** and **12** in 86 % and 87%, respectively. Sinapyl substrate

45.a with the highest methoxy substitution showed good conversion in the two-step sequence to

afford the desired products. **42.a** converted nicely to **17.c** and **41.c** in 84% and 82%, respectively.

Finally, the triol model substrate, **3.5.c**, was subjected to the two-step sequence to afford the

coniferyl based fragment, **17.c**, and the coumaryl based fragment, **47.d**, in a respective 76% and

78% yield.
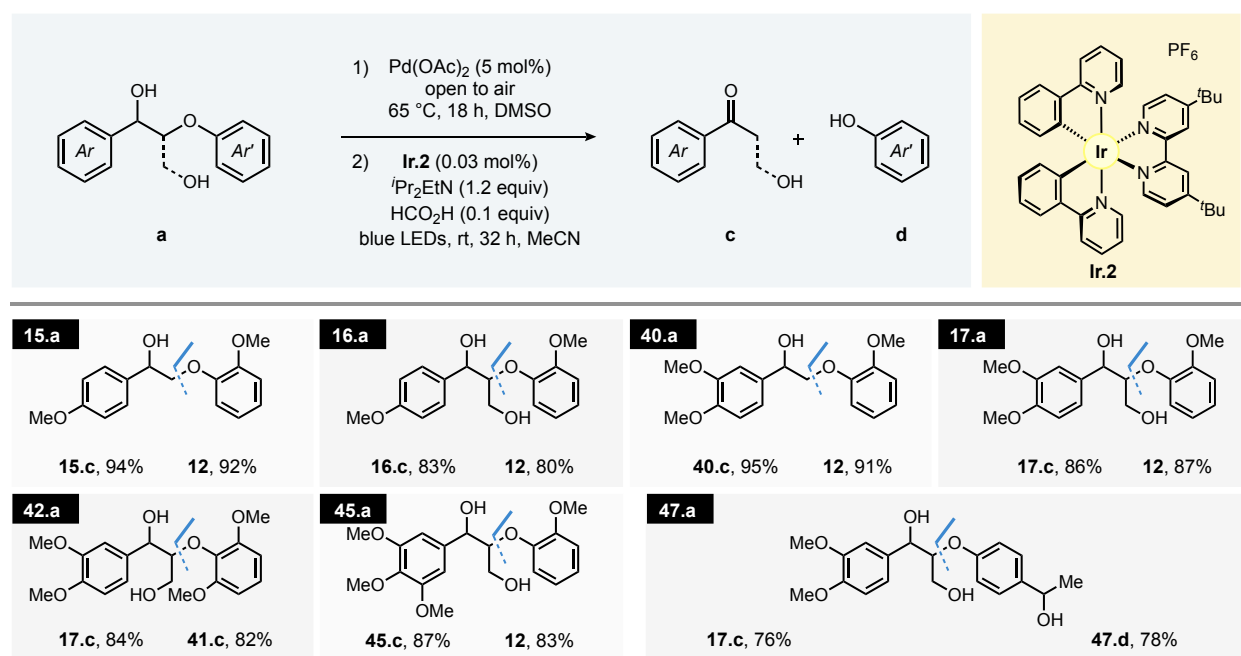
Figure 21 Scope of the two-step sequence for lignin model substrate fragmentation

Following the successful merger of our aerobic oxidation and photochemically enabled C–

O fragmentation, we sought to increase further the prospects of our reactions to be integrated into

a larger scale, high throughput process. For this reason, we looked to flow chemistry. Flow

chemistry has been extensively utilized and reviewed in the past decade and shows promising

results for its ability to enable process scale photocatalysis.[102,103,104,105] Common advantages of

flow photochemistry compared to batch photochemistry are decreased reaction times, lower

catalyst loadings, increased throughput, and better heat dissipation. We were able to modify an in-house built flow system to achieve our goal of effectively adapting the fragmentation to a flow reactor. Using transparent tubing with an inner diameter of 0.762 mm and a residence time of 150 minutes, we were able to convert **15.b** to the fragmentation product **15.c** in 79% yield (Figure 22). The γ-hydroxylated substrate **16.b** was converted to fragmentation product **16.c** in 77% yield. The guaiacol fragment **12** was isolated in 63% and 66% yield, respectively. These results correspond to an increase in substrate consumption from 0.013 mmol h^{-1} in batch to 0.4 mmol h^{-1} in flow, thus highlighting the potential for future scale-up processes in flow.
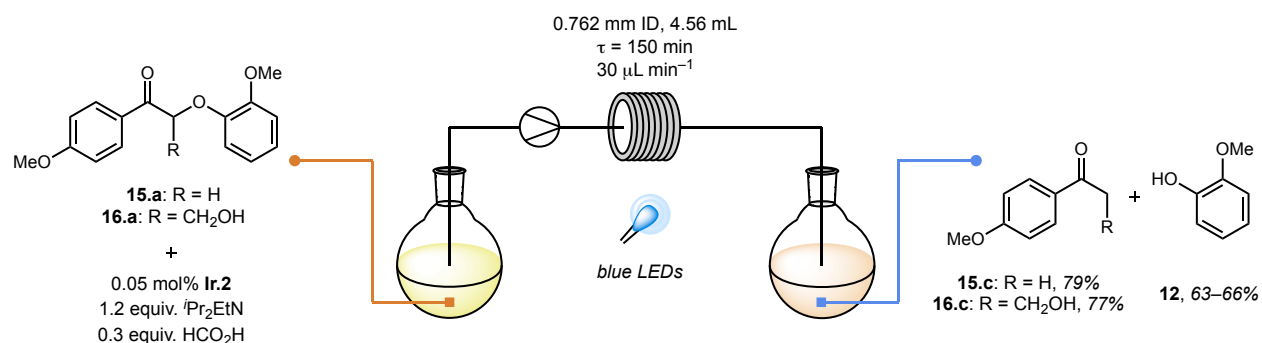
Figure 22 Photochemical C–O fragmentation in flow

One characteristic of lignin that poses a challenge for photochemical methods is its dark color. When in solution, lignin is a very dark brown or black solution, which can inhibit a photocatalyst's ability to absorb light. Another major problem is the lack of solubility of lignin in common organic solvents. We wondered whether these common attributes of lignin would be detrimental to our photochemical fragmentation strategy. To probe the efficacy of our method, we synthesized three model polymer substrates that contain the β-O-4 linkage motif (**48-50**). Subjecting these polymers to similar reaction conditions with an extended reaction time (48 h) afforded the fragmentation products (**47.d, 49.b,** and **50.b**) in 97%, 80%, and 88% yield, respectively (

Figure 23).
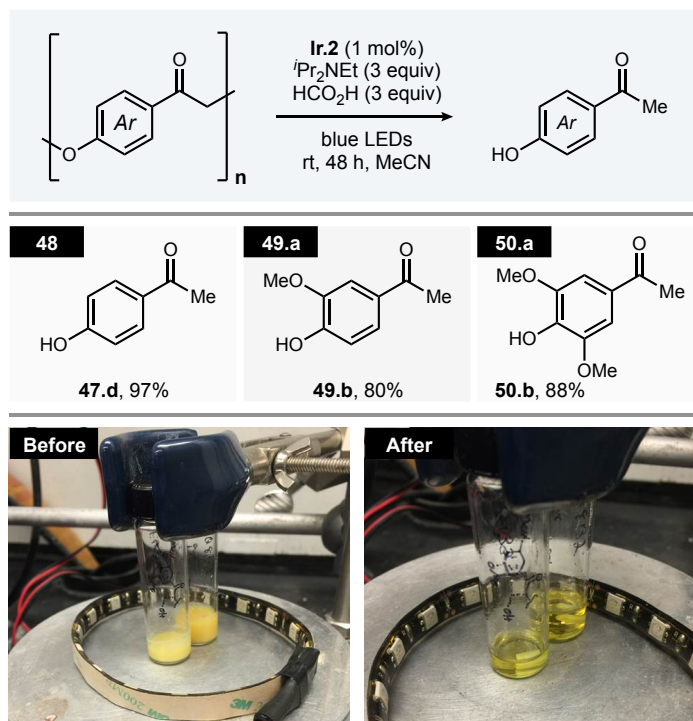
Figure 23 Depolymerization of heterogeneous lignin model polymer substrates

The products contain unprotected phenol moieties that do not inhibit reactivity or cause deleterious side reactions to occur. As we expected, the polymers were highly insoluble, making the starting reactions a heterogeneous mixture as shown in

Figure 23. Remarkably, the reaction becomes homogeneous with time as a result of the polymer fragmenting into its small molecule products. To further replicate the structure of a native lignin polymer, polymers **48-OH**, **49.a-OH**, and **50.a-OH** were subjected to hydroxymethylation conditions to add the γ-hydroxy functional group. Because the polymer substrates were not completely soluble under the hydroxymethylation conditions, they were only partially hydroxymethylated. The amount of hydroxymethylation was measurable by ^{1}HNMR and was reported for each polymer as shown in Figure 24. Subjecting each of those polymers to the fragmentation conditions afforded the mixtures of products from the respective starting polymers.

Polymers **48-OH**, **49.a-OH**, and **50.a-OH** converted in overall yields of 79%, 86%, and 74%, respectively (Figure 24).
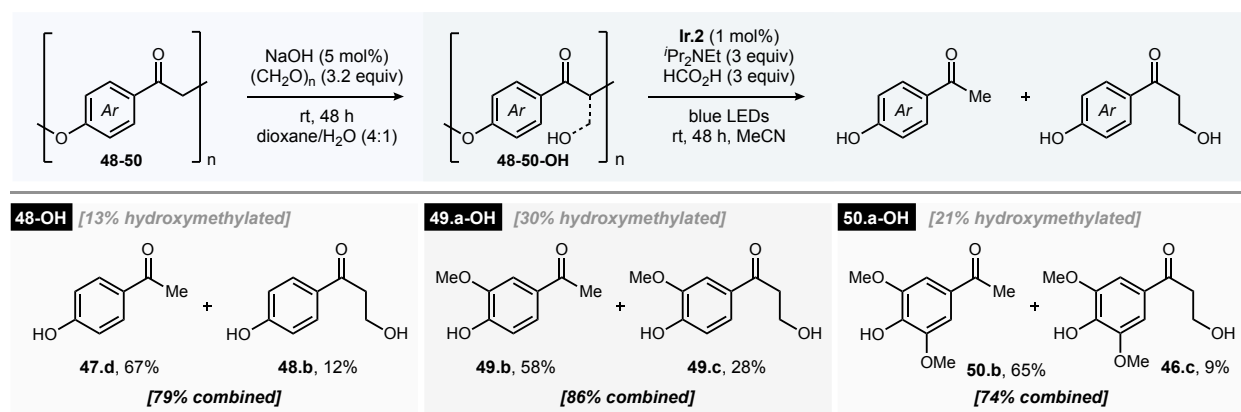
Figure 24 Hydroxymethylation and depolymerization of model polymer substrates

After the success of the depolymerization of our polymer model substrates, we still explored two more experiments to understand the efficacy of our reaction better. First, a mixed polymer was synthesized (**51**) that incorporated equimolar amounts of monomer units that represent the arene groups of the coumaryl, coniferyl, and sinapyl subunits. This mixed polymer was subjected to our reaction conditions for C–O bond fragmentation to afford 40% overall yield, with 70% based on returned starting material (BRSM) (Figure 25). The reaction did not fully solubilize, a likely explanation for the comparatively lower yield. Finally, we were curious to compare our standard fragmentation conditions using blue LEDs to a reaction run in the presence of sunlight. Using polymer **48** and running a blue LED reaction and a Michigan sunlight reaction for 8 h, product **47.d** was isolated in 49% and 45% yield, respectively. These results show that this reaction can be solar powered and has promising implications for the adaptation of photoredox reactions to solar-driven processes.
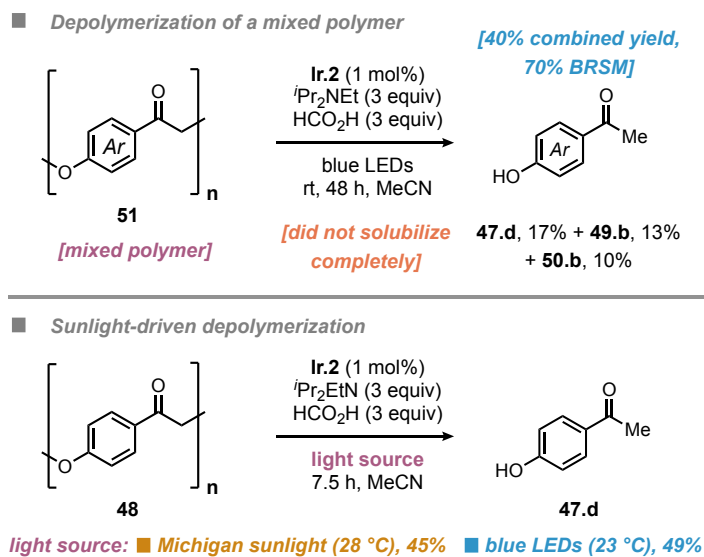
Figure 25 Mixed polymer and sunlight depolymerization reactions

Lastly, we carried out several experiments to interrogate the mechanism of the photochemical C–O fragmentation reaction. We performed quenching experiments using Stern-Volmer analyses, which is a common technique for elucidating photoredox reaction mechanisms.[106] We first determined that neither HCO_2H nor ketone substrate **15.b** showed an ability to decrease the photoluminescence of photocatalyst **Ir.2**. We did observe that $^iPr_2EtN$ has a significant quenching effect of the excited state photocatalyst (**Ir.2***), with a quenching rate (k_q) of 1.33×10^8 M^{-1} s^{-1}.[107] We also found that a combination of **15.b** and HCO_2H did not quench **Ir.2**; meanwhile, a three-component mixture consisting of **15.b**, HCO_2H, and $^iPr_2EtN$ produced a similar quenching rate, 1.31×10^8 M^{-1} s^{-1}, to that of $^iPr_2EtN$ alone.[107] The observed quenching data suggest two critical aspects of the reaction (i) $^iPr_2EtN$ quenches **Ir.2**, and (ii) the presence of the other additives do not significantly alter the quenching of **Ir.2** by $^iPr_2EtN$. These conclusions suggest that HCO_2H does not have anything to do with the quenching process, instead it acts as a proton source for activation of the ketone functional group.[108] Electrochemical analysis was performed on **Ir.2** in MeCN and revealed an irreversible reduction event ($E_{pc}(Ir^{III}/Ir^{II}) = -1.53$ V) and a reversible oxidation event ($E_{1/2} = +1.18$ V). The redox potentials were then used to estimate

the excited-state redox potentials of **Ir.2**, providing E_{ox} (Ir^{IV}/Ir^{III*}) as -1.31 V and E_{red} (Ir^{III*}/Ir^{II}) as $+0.96$ V.[109] These redox potentials are in agreement with a reductive quenching mechanism, in which photo-excited **Ir.2** is quenched by a SET by the amine to generate an Ir^{II} intermediate that can do a single electron reduction of ketone substrate **15.b** to regenerate the starting Ir^{III} photocatalyst and a ketyl radical intermediate **15.b'** (Figure 26). This ketyl radical anion intermediate undergoes C–O bond cleavage to afford product **15.c** after HAT. The phenoxide fragment (**12'**) is protonated to afford the phenol product (**12**).
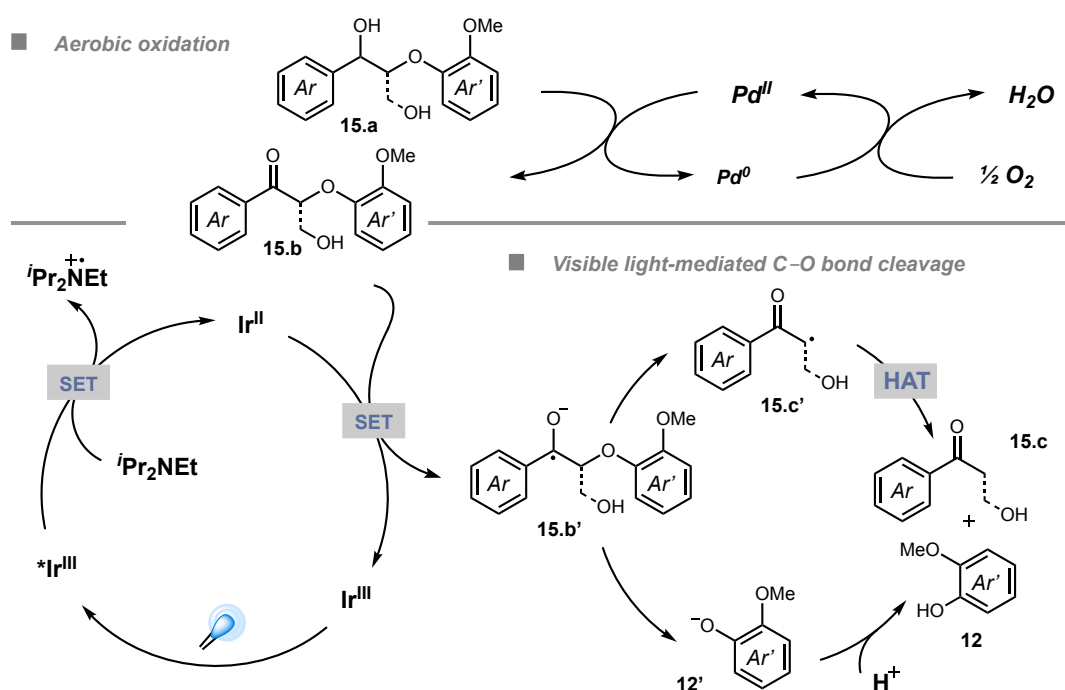
Figure 26 Mechanistic hypothesis for photochemical fragmentation of lignin substrates.

Our data comprising reaction efficiency and scope, adaptation to flow, and mechanistic studies describe an effective method for oxidizing and fragmenting β-O-4 lignin model systems. We also showcased the implications for future adaptations of photoredox catalysis for the programmable deconstruction of synthetic and natural polymers. Ultimately, we were not able to adapt the Pd aerobic oxidation to native organosolv lignin, which shows some limitations on that catalytic system. We believe that the results reported in this chapter will better inform our future

endeavors and the endeavors of other lignin scientists on limitations associated with lignin oxidation and depolymerization. Our group is focused on developing solutions to lignin depolymerization through mechanism-based investigations, and we will be furthering this objective in future work.

3.3 Redox Catalysis Facilitates Lignin Depolymerization

The previous chapter highlighted some of the challenges associated with oxidation reactions of lignin and lignin model substrates, but it also highlighted the robust nature of our photochemical β-O-4 fragmentation. A significant problem that was posed to our Pd-mediated aerobic oxidation and photochemical fragmentation sequence was the requirement for a solvent swap. Methods for lignin depolymerization on large-scale would ideally avoid the need for a solvent swap or purification. This in mind, we envisioned coupling our photochemical C–O bond fragmentation method with an oxidation method that would require no intermediate purification or isolation. This required an oxidation method in which chemical reagents for oxidation would not interfere with or inhibit the photochemical fragmentation step. This was seen as a formidable challenge since an oxidation reaction is inherently enabled by some redox-active reagent, which would likely be reactive in a photoredox mechanism. Ultimately, we decided on pursuing an electrochemical method for the oxidation. Aspects of electrochemistry confer exquisite control in selectively oxidizing or reducing reagents since one can control the exact potential (E) or current (i) that goes through the system. Additionally, electrochemical oxidations have been well studied and are considered a green alternative to chemical reagent-mediated oxidations (Figure 27.a).[110,111] The ability to utilize electrical current or even oxygen as a terminal oxidant should allow oxidation to occur with minimal additive reagents.

a. Chemical oxidation

- generally homogeneous reactions
- stoichometric oxidants (PCC, CrO₃, MnO₂) or catalytic inorganic oxidants (HNO₃/HCl)
- generally metal-based catalysts (Pd(II), Cu (II))

1 or 2 e⁻ oxidation

b. Direct electrooxidation

- high applied potentials
- lower selectivity
- over-oxidation
- expensive electrodes

1 e⁻ oxidation

less control and formation of *oxidation* and *degradation* products

c. Electrocatalytic oxidation via HAT

- predictability of the reaction behavior (CV)
- lower applied potentials
- O₂ is the terminal oxidant
- metal-free catalysts

1 e⁻ oxidation

controlled **oxidation** and **high selectivity**

d. *Stephenson group lignin depolymerization approaches*

this approach | intermediates not isolated one-pot process

Figure 27 Differences in lignin oxidation strategies.

Before we embarked on reaction exploration, we considered the existing literature on lignin valorization using electrochemistry. When considering electrochemical reactions, there are two primary mechanistic manifolds. One is direct electrolysis where an electrode needs to come in contact with a substrate molecule to do a SET event (Figure 27.b). This type of mechanism is limited in what is being oxidized and often can lack selectivity due to overoxidation. Another mechanistic manifold is that in which a chemical mediator is used to help mediate the desired chemical reaction (Figure 27.c). A method for direct electrochemical reduction of the lignin backbone has been reported but was poorly efficient and gave complex product mixtures.[112] Similarly, direct electrochemical oxidation to induce fragmentation of lignin has been done but has proven rather difficult, often requiring high oxidation potentials,[110] or requiring expensive and

toxic electrodes (i.e., IrO_2,[113] Pt,[114] Ru/V oxides,[115] Au,[114] or Pb[116]). The requirements for a direct reaction between the substrate and electrode are often plagued by back electron transfer processes and overly high potentials that can lead to degradation. These drawbacks can be overcome by the application of a chemical mediator, allowing the reaction to operate under milder conditions that can increase efficiency and selectivity. We saw an opportunity for the use of a mediator that can facilitate a HAT process since the benzylic hydrogen atom of the β-O-4 is relatively activated, ultimately leading to benzylic alcohol oxidation. Mediators in electrochemical settings have found widespread use in many applications,[117,118] but applications in the valorization of lignin are scarce.[119,120,121]

Before we initiated any experiments, we considered the physical properties of HAT catalyst candidates. TEMPO has previously been used for alcohol oxidation,[122,123,124] but was found to be too weak for a HAT catalyst ($BDE_{TEMPO–H} = 71$ kcal mol^{-1})[123] to abstract benzylic hydrogen atoms in lignin alcohols ($BDE_{C–H} = 84$ kcal mol^{-1}). We identified NHPI as a precursor to the *in situ* generation of the phthalimide *N*-oxyl (PINO) radical, which has an appropriate O–H bond strength ($BDE_{NHPI} = 86$ kcal mol^{-1}).[124] We started to investigate potential HAT catalysts using CV (cyclic voltammetry) analysis.[125] Cyclic voltammetry is an electrochemical technique that continuously scans potential in a specified direction (positive or negative) set by the user that measures current as the output. For the remainder of this text, all electrochemical data are represented in IUPAC convention (i.e., from left to right on the x-axis represents increasing potential, and from bottom to top on the y-axis represents rising current). In general, any measurable current is equivalent to reactivity (i.e., electron transfer). Cyclic voltammetry is commonly employed to investigate redox potentials of many chemicals, and it can help elucidate the mechanistic underpinnings of electron transfer-initiated chemical reactions.[126] When a CV of NHPI was taken by scanning in the positive

direction first, we observed a reversible oxidation event with $E_{1/2}$ = 1.36 V (Figure 28.a). Interestingly, when 2,6-lutidine was added, a negative shift of 570 mV in the reversible oxidation event occurred, resulting in an $E_{1/2}$ = 0.79 V. It was also noticed that the ΔE_{p} (peak-to-peak separation) is 82 mV in the NHPI/2,6-lut system compared to 155 mV for the NHPI solution, implying that the addition of 2,6-lutidine increases the chemical and electrochemical reversibility of NHPI.[127] The decrease in the oxidation of NHPI in the presence of 2,6-lutidine is crucial because it allows us to work at lower oxidation potentials, thus avoiding overoxidation of the electron-rich aromatic rings found in lignin (e.g., phenols commonly oxidize between 1.0 and 2.0 V vs. SCE[18]).
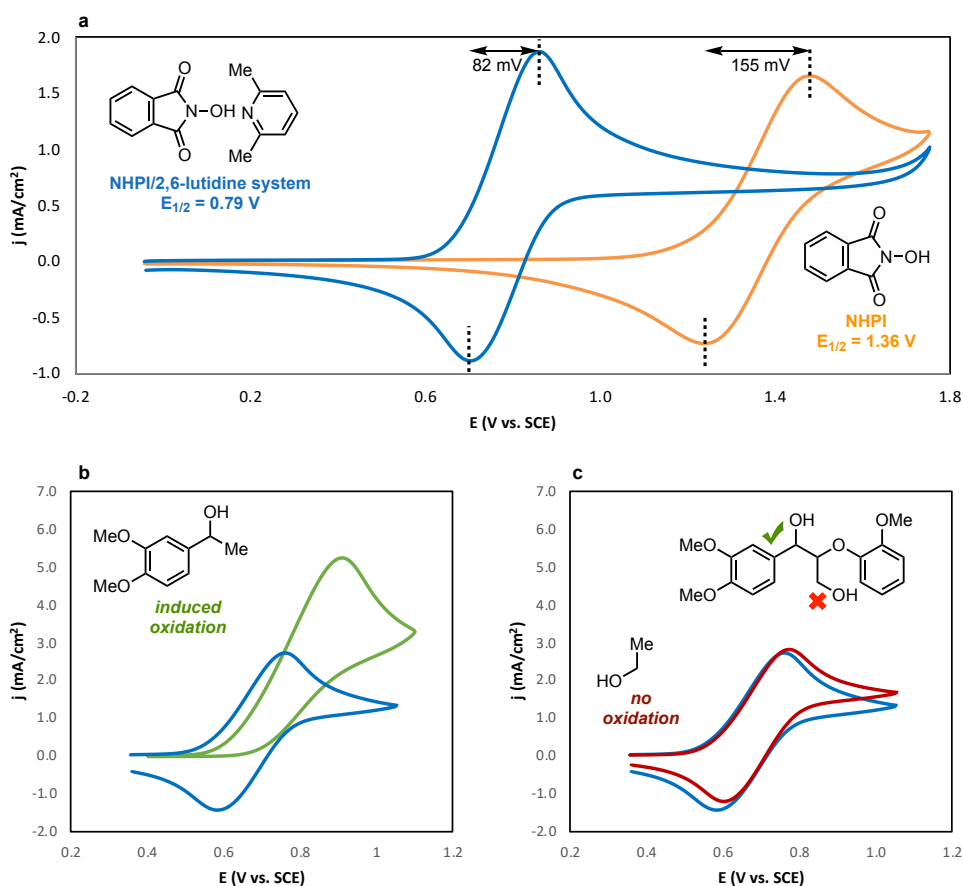
Figure 28 Cyclic voltammetry data for NHPI and 2,6-lutidine.

Using the NHPI/2,6-lutidine system, we performed another CV experiment in the presence of 1-(3,4-dimethoxyphenyl)ethanol since it was a readily available reagent that represents the

benzylic alcohol portion of lignin. The voltammogram showed a unique change in the shape of the curve. As shown in Figure 28.b, where the blue curve represents the CV of NHPI/2,6-lutidine, the curve in the presence of the alcohol shows an increase in the peak current and a loss in the return reduction event (green). This specific change in the curve is representative of an operative catalytic mechanism. To determine if the reaction would specifically target the benzylic alcohol in the presence of the primary alcohol found in β-O-4 linkages, we did the same CV experiment in the presence of ethanol. As shown in Figure 28.c, the voltammogram in the presence of ethanol (red) shows almost no change in the shape of the curve. Based on the data, we hypothesized that if conditions could be developed to carry out oxidation on lignin substrates, then it would be selective for the benzylic alcohol oxidation.

After determining that NHPI could act as a HAT catalyst in the presence of 2,6-lutidine, we sought out experimental conditions for the electrochemical oxidation protocol. Our experimental setup included two electrodes as the working electrode (WE) and the counter electrode (CE), both consisting of RVC (reticulated vitreous carbon), which is a very high surface area composition of graphitic carbon. Additionally, we used an aqueous Ag/AgCl reference electrode with 3 M KCl. We decided to keep the loading of NHPI at 10 mol% and vary other conditions during reaction exploration using a constant potential. As shown in Table 4, we found that bubbling N_2 through the solvent before electrolysis (entries 1 and 2) greatly retarded starting material conversion. Stoichiometric amounts of 2,6-lutidine (entry 3) with oxygen saturated solvent afforded good conversion. Lower loadings and switching to Cl$_4$-NHPI (3,4,5,6-tetrachloro-N-hydroxyphthalimide) for NHPI also afforded good conversion, but a precipitate and color formation occurred when this catalyst was used (entry 4).[128] We also found that 3,5-lutidine was a competent base for the reaction (entry 5), but better conversions were obtained with 2,6-lutidine.

After extending the reaction time to 4 h and switching the electrolyte to KPF_6, an optimal conversion rate of 87% was obtained (entry 7). With optimal conditions, we tried the Cl_4-NHPI reagent as a catalyst again, but the reaction did not show any improvements (entry 8). Finally, control reactions in which base, potential, and NHPI were omitted showed little to no conversion (entries 9-11, respectively).

After optimizing conditions for the electrochemical oxidation of the benzylic alcohol found in the β-O-4 linkages, we ran a series of experiments to determine if the reaction solution after full conversion from the oxidation reaction would prohibit photoredox reactivity. In this vein, we ran fragmentation reactions with the addition of NHPI/2,6-lutidine, KPF_6, with exposure to air, and with the addition of a stoichiometric equivalent of H_2O_2 (Figure 29).

Table 4 Electrochemical oxidation reaction optimization.

entry	2,6-lutidine	electrolyte	time	sparge	^{1}HNMR conversion
1	10 mol%	0.1 M NaClO₄	2 h	N₂	31%
2	1.1 equiv	0.1 M NaClO₄	2 h	N₂	38%
3	1.1 equiv	0.1 M NaClO₄	2 h	O₂	75%
4[c]	10 mol%	0.1 M NaClO₄	2 h	O₂	71%
5	-[a]	0.1 M NaClO₄	2 h	O₂	54%
6	10 mol%[b]	0.1 M NaClO₄	2 h	O₂	40%
7	**10 mol%**	**0.05 M KPF₆**	**4 h**	**O₂**	**87%**
8[c]	10 mol%	0.05 M KPF₆	4 h	O₂	82%
9	-	0.05 M KPF₆	2 h	O₂	<5%
10	10 mol%	0.05 M KPF₆	2 h	O₂	<5%
11	10 mol%	0.05 M KPF₆	2 h	O₂	<5%

[a]3,5-lutidine (10 mol%); [b]added in two portions; [c]Cl₄NHPI used

We considered the feasibility of the formation of hydrogen peroxide as a byproduct from the oxidation and thus confirmed that H_2O_2 did not inhibit reactivity. These results suggest that the reagents in solution from the electrochemical oxidation should not interfere with the photochemical C–O bond fragmentation reaction.
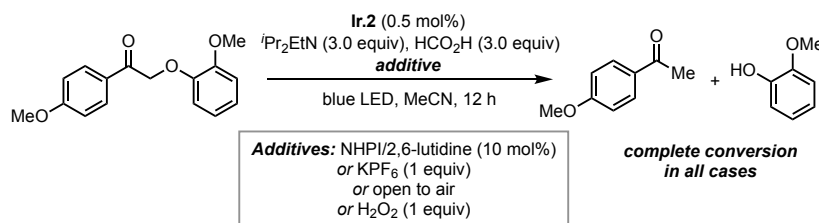
Figure 29 Control reactions of photochemical fragmentation.

With this aggregate data in mind, we embarked on a full scope expansion of electrochemical oxidation followed by direct addition of photocatalyst and other additives to enable the fragmentation (Figure 30). Simple alcohol substrates representing the coumaryl, coniferyl, and sinapyl monomers with the guaiacol-based phenol unit underwent the two-step process to afford the fragmentation products (**15.a**, **40.a**, and **52.a**). Varying the methoxy substitution pattern on the phenol subunit was tolerated (**41.a** and **43.a**), as well as the less-functionalized model (**44.a**). Model substrates with the γ-hydroxy group converted well for the representative monolignols (**16.a**, **17.a**, and **45.a**), and so did the diol model substrates with varied methoxy substitution on the phenol unit (**42.a**, **53.a**, and **54a**). All of the substrates fully converted except for substrate **44.a**.

Moving onward to native lignin, we extracted lignin from pine wood shavings using a modified organosolv isolation technique.[129] The lignin was found to be the most soluble in an acetone/DMSO (98:2) solvent mixture. The solution of lignin was subjected to the electrocatalytic oxidation conditions for 6 h. The reaction was monitored using HSQC spectroscopy as a way to

look for the loss of the α-C–H signal, as well as the shifting of other C–H correlations that would

be expected from an oxidation reaction.
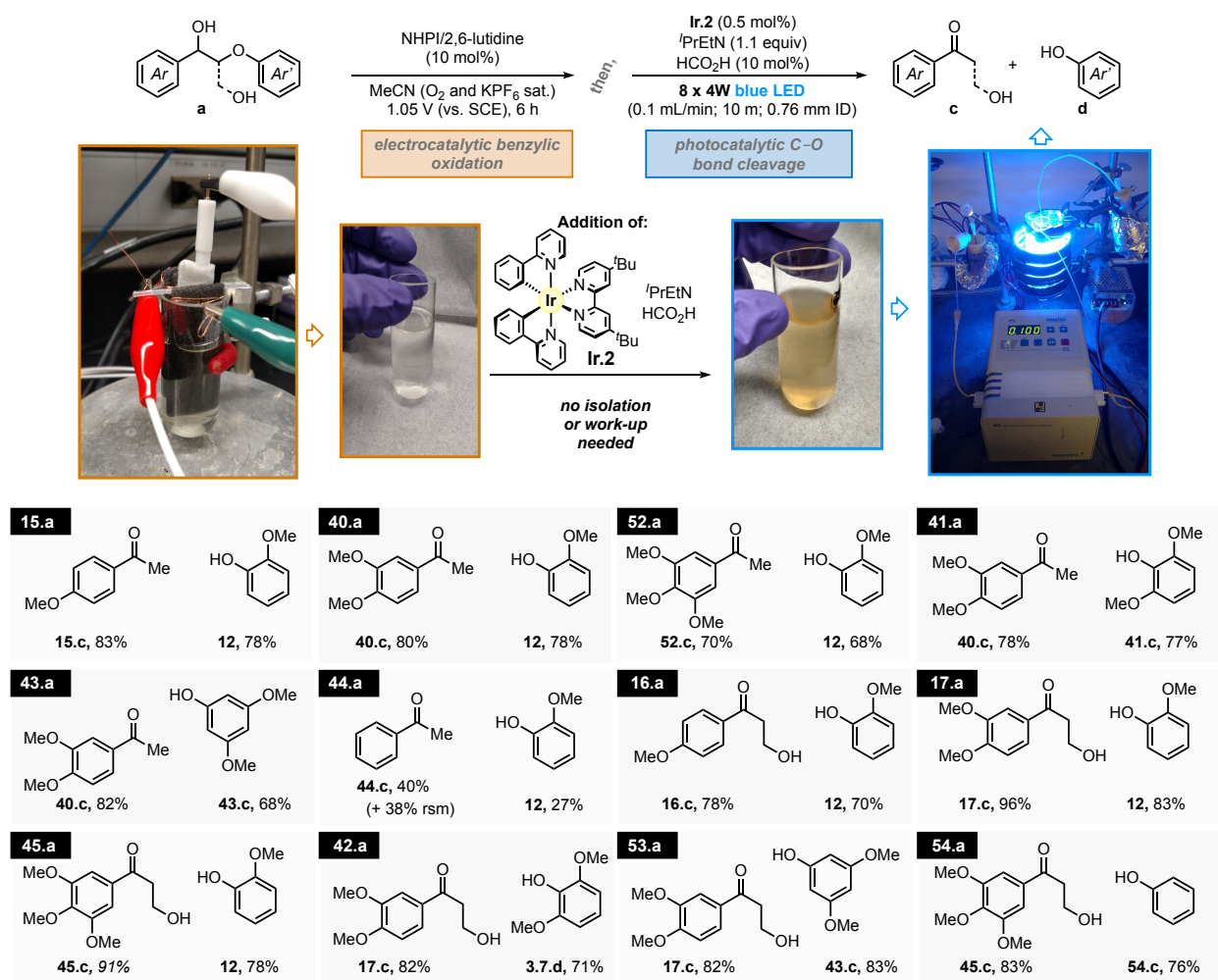
Figure 30 Scope of the electrochemical oxidation and photochemical fragmentation sequence.

As shown in Figure 31, the native lignin (**A**) shows the blue correlations that correspond to the β-

O-4 linkage in lignin. The HSQC analysis after the oxidation of the native lignin showed a

noticeable disappearance of the correlations from **A** and new red signals arising from the oxidized

lignin (**A'**). With the oxidized lignin in hand, we added the photocatalyst and other additives to the

solution and ran it through our photochemical flow setup, after which the HSQC analysis showed

little remaining of lignin polymer and new correlations (purple, **A''**) that correspond to monomer

products. Analysis of the final reaction mixture was performed by GC-MS and GPC. The GPC data, which correlates retention time to polymer size such that larger polymers have a smaller retention time, showed almost no remaining polymer and a large peak corresponding to smaller molecular weight material. Using GC-MS we were able to quantify two products, **I** and **III**, with a total of 2.44 wt% yield by using calibration curves of known standards. Although a seemingly low yield, one should consider that quantifying a monomer product requires two consecutively oxidized β-O-4 units to be fragmented. Thus, these results highlight the remarkable reactivity and selectivity of our photochemical C–O fragmentation reaction. A calculation of an actual isolated yield requires better methods to calculate the theoretical yield of monomer products from β-O-4 fragmentation. This is an active field of study among other quantitative lignin methods for depolymerization, detection, and isolation.
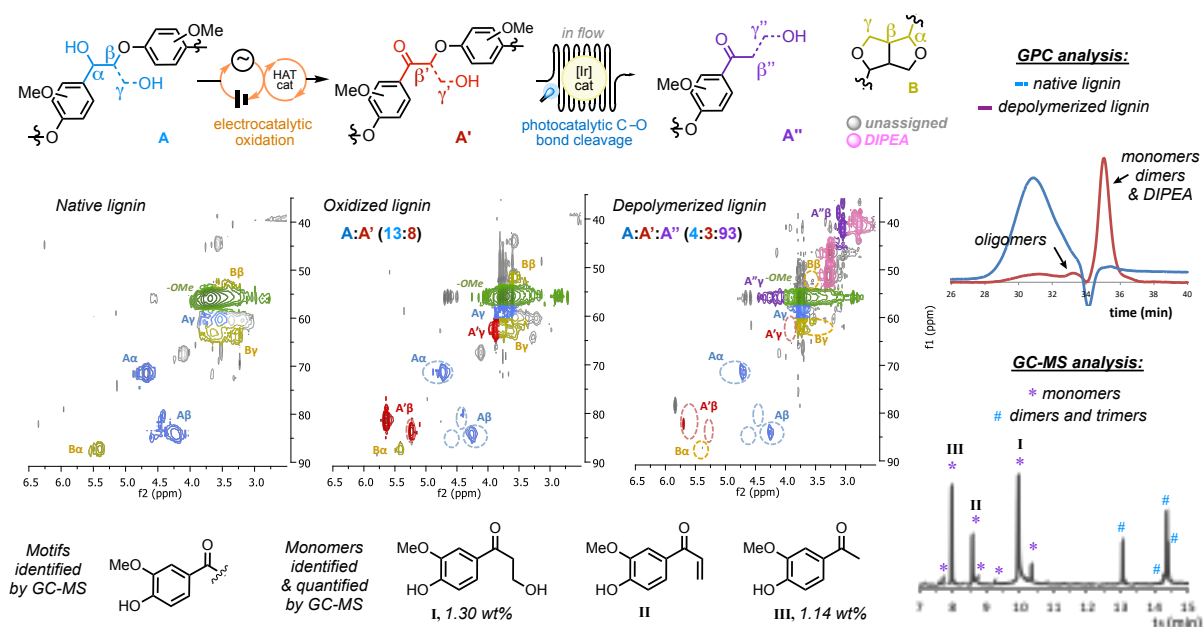
Figure 31 HSQC and fragmentation data for lignin depolymerization.

Having achieved our goal in the development and implementation of a two-step sequence for lignin oxidation and subsequent depolymerization, we sought to understand better the operating

mechanism of the electrochemical reaction (the mechanism for the photochemical C–O cleavage reaction was discussed previously; vide supra). Considering the limited studies on this NHPI/2,6-lutidine system, we began our mechanistic studies by performing KIE experiments.[130,131] We performed an electrochemical oxidation reaction to compare substrate **15.a-H** and **15.a-D** (

Figure 32.a) using either O_2- or N_2-sparged MeCN. We obtained KIE values of 2.3 for the individual runs and 5.6 for the intermolecular competition experiment using O_2-sparged MeCN. These values are indicative of a primary KIE that suggest the abstraction of the benzylic hydrogen atom might be the rate- or turnover determining step.[132] When the same set of experiments were run in N_2-sparged MeCN, similar KIE values of 2.1 and 5.2 were obtained for the individual and intermolecular runs, respectively. Additionally, we calculated the reaction to be first-order in NHPI/2,6-lutidine complex and alcohol.[133] With these data in hand, we proposed the mechanism to begin by anodic oxidation of NHPI to PINO, a process facilitated by 2,6-lutidine via PCET.[134,135,136] PINO can then abstract the benzylic hydrogen atom from **15.a** to form benzylic radical intermediate **15.d**, while regenerating NHPI. From intermediate **15.d**, the ensuing mechanism becomes nebulous. One plausible pathway is a second PCET-based oxidation with either O_2 or the anode as the terminal oxidant to form ketone product **15.b**. Alternatively, O_2 is known to trap α-hydroxy radicals at near
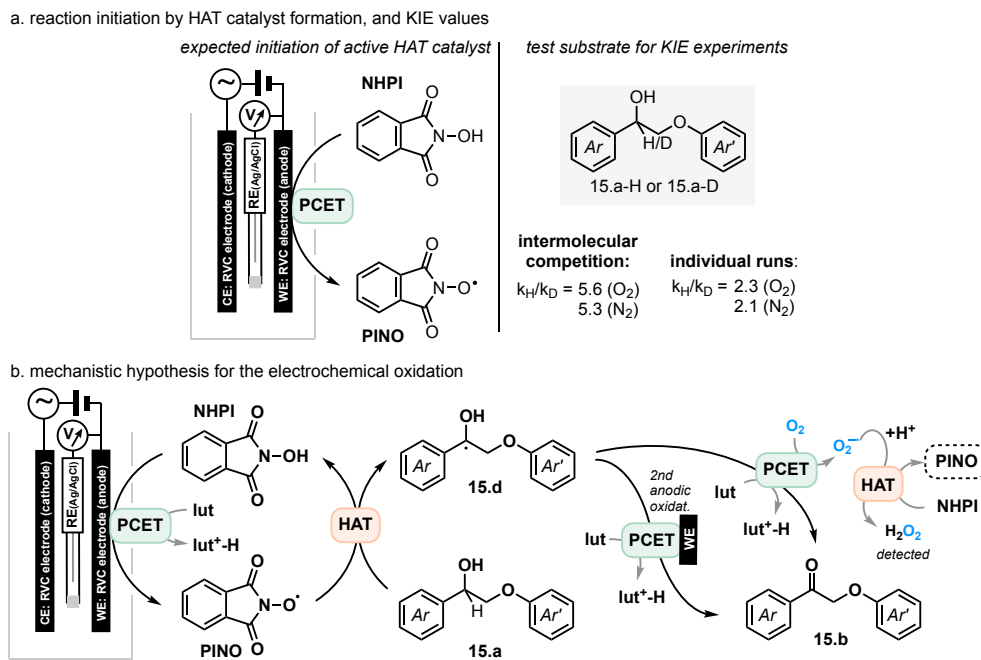
Figure 32 Mechanistic experiments for the electrochemical oxidation reaction.

diffusion-limited rates ($k > 10^9$ M^{-1} s^{-1} in water).[137] These oxidized intermediates are known to

fragment to ketones ($k > 10^6$ M^{-1} s^{-1} in water)[137] in a process that is greatly accelerated by

base.[138,139] This also suggests a PCET-type oxidation of radical intermediate **15.d** by oxygen and

base to afford the ketone product and hydrogen peroxide (H_2O_2). In either of the proposed

mechanisms, H_2O_2 is likely being formed as a by-product. This accounts for the increase in yield

when using O_2-sparged MeCN instead of N_2-sparged MeCN (31% with N_2 and 71% with O_2 under

otherwise identical conditions). Additionally, we performed an electrochemical oxidation reaction

where molecular iodine (I_2) was added to the reaction solution after full conversion. Addition of

iodine caused the formation of a yellow color, indicative of the presence of H_2O_2 (Figure 33).

Addition of H_2O_2 to the reaction solution before electrolysis did not result in a color change.
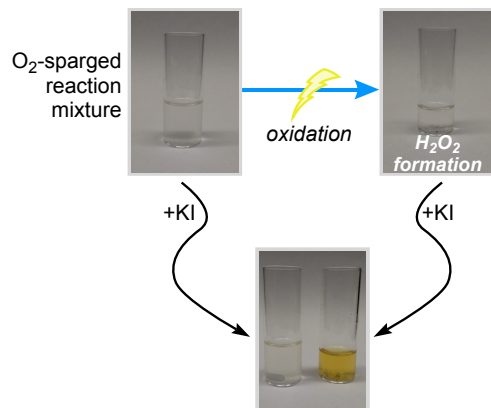
Figure 33 Iodine test for peroxide.

3.4 Metal-free strategies

Our interest in lignin depolymerization, and previous methods that have been hitherto discussed has led us to focus our efforts on developing metal-free methods for lignin depolymerization. Our first reported oxidation method, using an oxoammonium salt, was without metal, but it required a stoichiometric amount of salt that produced stoichiometric amounts of waste byproducts.[77] Our electrochemical oxidation was a metal-free oxidation method that was compatible with our Ir-mediated photoredox method for C–O fragmentation of the lignin β-O-4 linkage, so we set out to find alternatives for Ir.[133] Attributes of precious-metal catalysts–their ability to absorb visible-light, modular synthesis useful for creating libraries of photocatalysts, unique properties that enable MLCT, and long-lived excited state lifetimes–can be difficult to replicate in organic systems. Organic photocatalysts have been referred to as organic dyes, largely due to their ability to easily impart color to organic solutions, but their deep color is often a result of their ability to absorb light, and inherently undergo redox manipulations. Examples of organic dyes include the xanthene dyes (e.g., fluorescein, eosin, and rose bengal). Other organic

photocatalysts have been known when using UV light (e.g., 1,4-dicycanobenzene, benzophenone, fluorenone, quinones, acridiniums, thiazines, pyriliums, and quinoliniums). For further reading, an extensive review of these organic photocatalysts has been published examining their reactivity as photoredox catalysts.[16]

In our search to identify a useful organic photocatalyst for the reductive fragmentation of lignin β-O-4 bonds, we targeted *N*-phenyl phenothiazine (**PhPTH**) as a viable organic photocatalyst. Phenothiazine and its derivatives are electron rich, making them good reducing reagents from the excited state. Their low ground state oxidation potential of +0.68 V vs. SCE in combination with their high-lying singlet and triplet excited states contributes to their strongly reducing potentials.[16] Additionally, the resulting **PhPTH**[•+] is oxidizing enough to be turned over by an electron donor with an oxidation potential less than +0.68 V. We were impressed by the utility of **PhPTH** for a number of different reactions including atom transfer radical polymerizations[140,141,142] and hydrodehalogenation.[143] A notable difference between **PhPTH** and our previously used Ir-based photocatalysts is **PhPTH** mostly absorbs in the UV/near-UV (λ_{max} = 315 nm, Figure 34, 0.00017 M in MeCN). With this in mind, we embarked in applying **PhPTH** to the fragmentation of oxidized β-O-4 models.

We decided to start reaction optimization on substrate **15.a** (

Table 5). Considering the absorbance spectra obtained, we decided to use LED strips for photoactivation that were centered between 390-415 nm. We kept the amount of **PhPTH** constant at 5 mol%, and HCO_2H constant at 1.0 equiv while varying other factors starting with concentration.
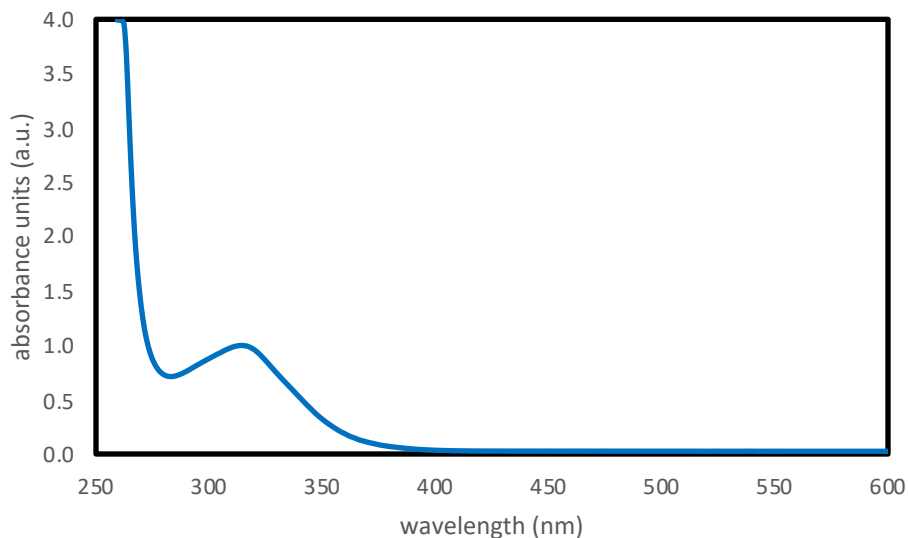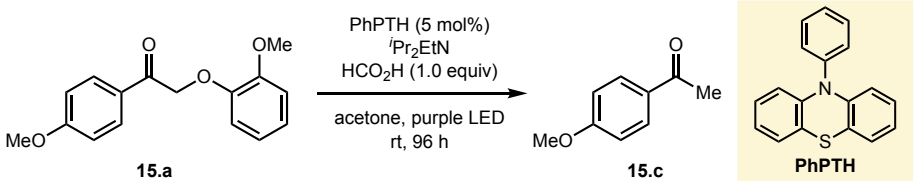
Figure 34 UV-vis absorption spectrum of PhPTH in MeCN.

Going from 0.2 M to 0.05 M showed improved yields (entries 1, 3, and 4). We also found that extending the reaction time could enhance the yield (entry 2). An extended reaction time of 96 h with a reaction solution at 0.05 M led to full conversion of **15.a** (entry 5). Excluding HCO_2H still resulted in good conversion (78%, entry 6), and excluding amine or light afforded <5% conversion (entries 7 and 8). Excluding photocatalyst led to 15% conversion (entry 9). With optimized conditions in hand, we decided to investigate the scope of this reaction; however, there was a reservation with regard to the reaction time. We initially thought the reaction time was long (96 h) due to the comparatively short-lived excited state lifetime of **PhPTH** ($\tau = 0.81$-2.3 ns;[16] for comparison, the τ of **Ir.2** is 557 ns[15]). To our delight, we found the use of a stronger LED light source (40 W, Kessil) with a wavelength emission centered at 390 nm enabled the desired reaction at a significantly reduced reaction time of 3 h. Hence, we explored the substrate scope comparing the LED strips to the Kessil lights (Figure 35).

Table 5 Reaction optimization for PhPTH catalyzed reaction.

entry	LED	solvent (M)	^{i}Pr$_2$EtN (equiv)	time (h)	^{1}HNMR conversion
1	violet	acetone (0.2)	2.0	24	30%
2	violet	acetone (0.2)	2.0	96	60%
3	violet	acetone (0.1)	2.0	24	42%
4	violet	acetone (0.05)	2.0	24	48%
5	**violet**	**acetone (0.05)**	**2.0**	**96**	**>95%**
6[a]	violet	acetone (0.05)	2.0	96	78%
7	violet	acetone (0.05)	-	96	<5%
8	-	acetone (0.05)	2.0	96	<5%
9[b]	violet	acetone (0.05)	2.0	96	15%

[a]no formic acid; [b]no photocatalyst

Overall, the reactions tolerated the varying methoxy substitution patterns on both arene rings. The reaction was also effective on the diketone substrate **47.a**. The Kessil lamp reactions generally show slightly diminished yields. Considering the 15% conversion of **15.b** in the absence of photocatalyst (entry 9,

Table 5), it is possible that there is some side reactivity was ensuing because of the lamp strength and wavelength. Having had success in merging our electrochemical oxidation method with our Ir-based C–O bond fragmentation reaction, we examined the compatibility of the **PhPTH** reaction with other metal-free oxidation methods.
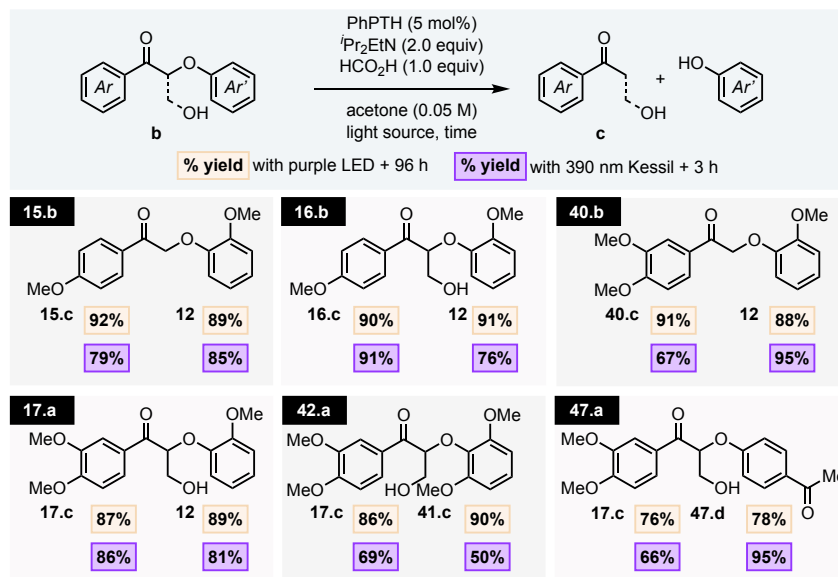
Figure 35 Scope of the PhPTH enabled fragmentation on lignin substrates.

To commence compatibility studies with other methods, we looked to adapt conditions for aerobic oxidation previously reported by Stahl and co-workers.[89] They showed that 4-AcNH-TEMPO, in the presence of HNO_3 and HCl, under an oxygen atmosphere with mild heating (45 ºC) could afford the oxidation products with total selectivity for the benzylic alcohol over the primary alcohol. We found that room temperature conditions under an oxygen atmosphere were sufficient to carry out the oxidation in good yields over 12 h. We removed the organic solvent by vacuum evaporation and directly added the solvent and components for the **PhPTH** fragmentation reaction (purple LED conditions) and found the reactions to be compatible (Figure 36). Testing substrates **15.a**, **16.a**, **40.a**, **17.a**, representative of coumaryl and coniferyl arene units with and without the γ-hydroxy group, represents the ability to easily move from a metal-free oxidation to a metal-free fragmentation strategy.
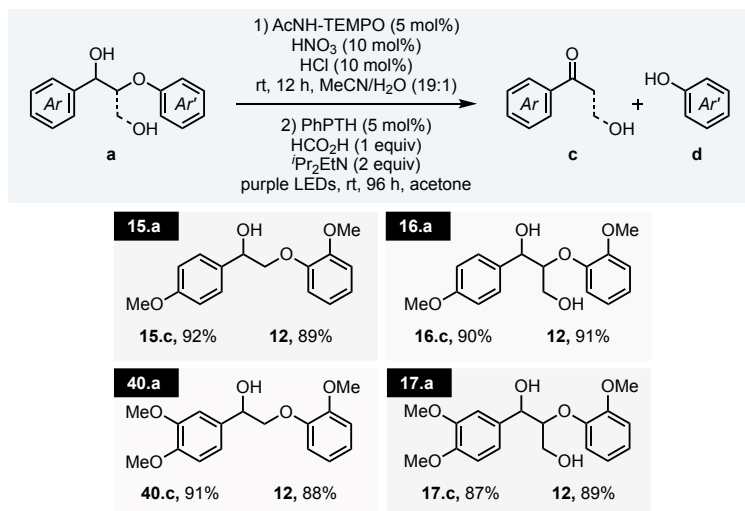
Figure 36 Combined TEMPO oxidation and PhPTH fragmentation.

We also decided to test the compatibility of our **PhPTH** method with our electrochemical oxidation reaction. Subjecting substrates **15.a**, **42.a**, and **45.a** to the electrochemical oxidation conditions was followed by solvent removal by vacuum evaporation and subsequently the addition of the **PhPTH** and the other reagents and solvent to afford the fragmentation products under otherwise standard conditions (with the 390 nm Kessil lamp, Figure 37).
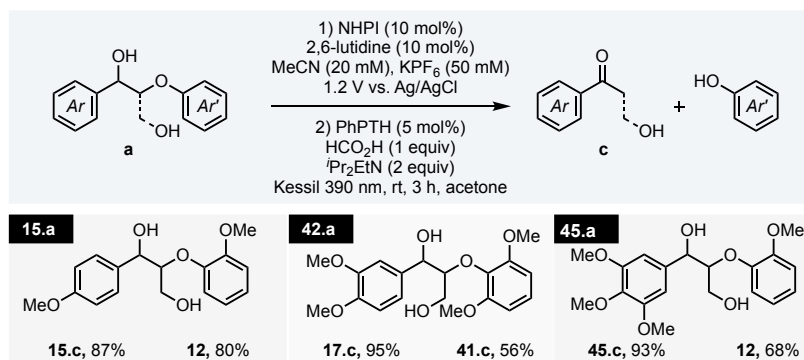
Figure 37 Combined electrochemical oxidation and PhPTH mediated fragmentation.

Overall, we were pleased by the robust nature of the organic photoredox catalyst to mediate C–O bond fragmentation without the need for purification from the oxidation reaction. Our results show that there is room for optimization of light sources, seeing how different lights drastically

changed our reaction time. It is worth noting that the **PhPTH** reaction shows minimal efficiency in MeCN solvent, which is why the switch of solvent was required.

Finally, our pursuit to identify the most efficient and environmentally benign conditions for lignin depolymerization led us to explore an electrochemical reduction of lignin substrates for fragmentation. When designing our electrochemical oxidation reaction, we envisioned an ideal strategy to include a selective oxidation by the anode of an electrochemical cell, followed by the oxidized substrate being reductively cleaved at the cathode. This design strategy exceeds the current understanding of how NHPI/2,6-lutidine reacts in an electrochemical cell and the ability for specific reagents to be reactive or non-reactive at each electrode. For these, and many more reasons, we were never able to identify conditions that would enable the one-pot reaction described. Instead, we decided to study the reductive fragmentation of already oxidized lignin model substrates.

We started reaction screening by applying negative potentials to our electrochemical cell, but only ever saw little to no conversion of the starting material. We eventually found that if ^{i}Pr$_2$EtN was dissolved with the ketone substrate and a strong enough oxidative potential (>0.9 V vs. SCE) was applied to oxidize the amine, then the ketone substrate would be reduced at the cathode and proceed to fragment. We found the typical substrates to react efficiently including those with and without the γ-hydroxy group (Figure 38, note **17.b** and **42.b** are different starting materials due to the varying methoxy substitution on the phenol unit, but afford the same products). Notably, each substrate needs a different time for the reaction to complete and is represented by the listed times for each substrate. Additionally, the phenol fragment does not survive the reaction, most likely due to over-oxidation and decomposition at the anode. We surmise this mode of decomposition is due to the relatively low oxidation potential of 2-methoxyphenol (1.41 V vs.

SCE),[18] which is probably even lower in the presence of stoichiometric amounts of base. To further expand on this notion, we synthesized substrate **55.b** which has an acetyl group on the 4- position of the phenol fragment. We hypothesized that having the acetyl group on the phenol fragment would increase the oxidation potential of that fragment and prevent oxidative decomposition from occurring. When subjecting **55.b** to the fragmentation conditions, we were able to isolate both fragments in 79% and 78% yield for **40.c** and **47.d**, respectively.
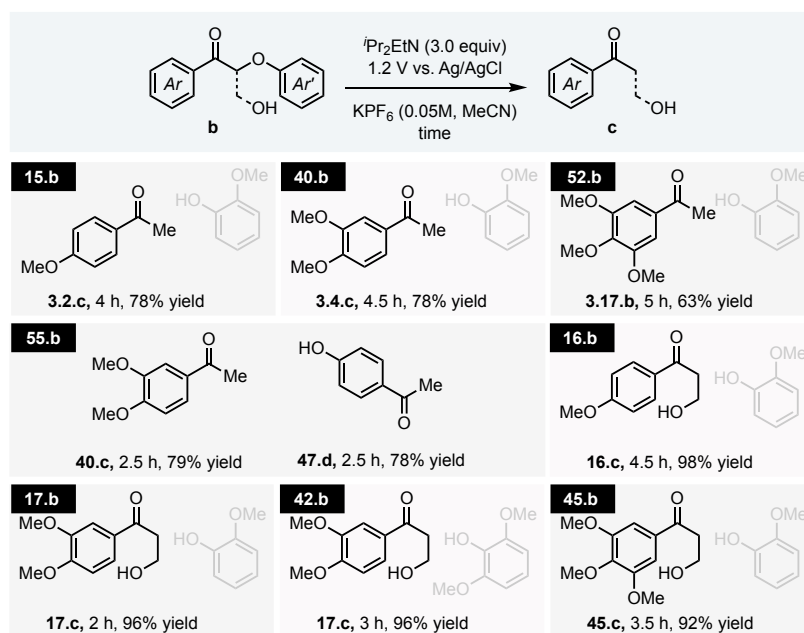
Figure 38 Electrochemical fragmentation of lignin substrates

Interestingly, we found that allowing the reaction to progress beyond the indicated reaction times led to over-reduction of the ketone product to form the pinacol coupling products (Figure 39). With extended reaction times, we were able to isolate the pinacol coupling products for all of the same substrates, representative of the linkages that would be found in native lignin. Subjecting the acetyl substrate, **55.b**, afforded mixed pinacol coupling products as expected.
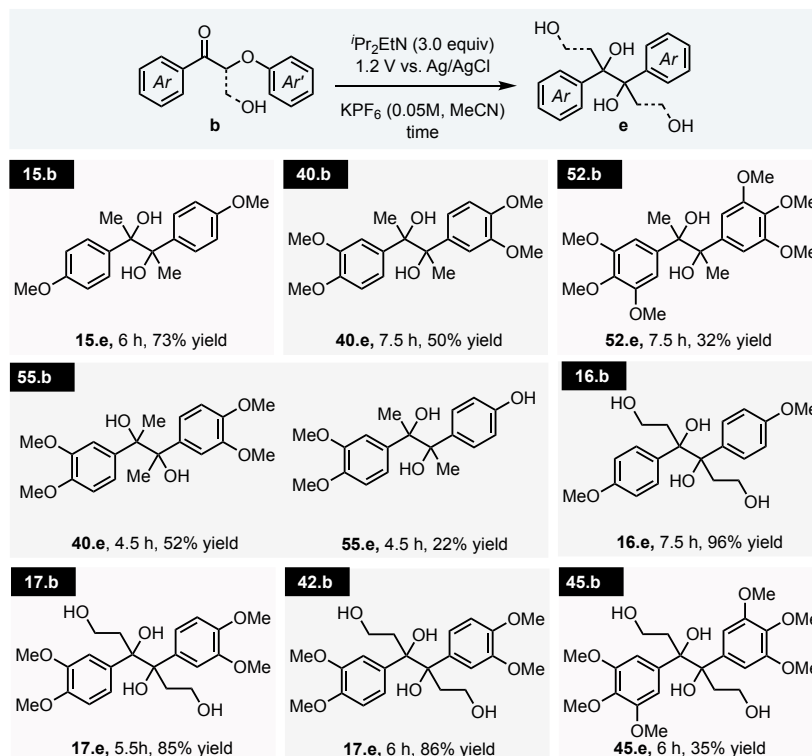
Figure 39 Electrochemical fragmentation and pinacol coupling of lignin substrates.

To explain the results of our fragmentation reaction, we applied simple principles of electrolysis to design an experiment that would give a readout of the potential the cathode is running. The concept lies in the fact that the electrochemical cell needs to complete a full circuit. When a potential of 1.2 V is applied to oxidize the amine, current flows into the anode, thus necessitating that current flows out of the cathode. We took the current readout from one of our constant-potential fragmentation reactions and integrated the area of the curve, which provides the total current that flowed through the system. We were able to obtain fragmentation and pinacol coupling products when setting up the reaction under identical conditions but holding the current constant (with the current calculated from the constant-potential reaction) instead of holding the potential constant. Figure 40 shows the potential readout, as well as the dotted lines that represent the reduction potentials of the oxidized β-O-4 model and the corresponding acetophenone (fragmentation product). This readout of potential explains how the cathode can first reduce the

model system to induce fragmentation, and soon thereafter begin to reduce the acetophenone fragmentation product to afford the pinacol coupling products. Further exploration of the utility and compatibility of this reaction is currently ongoing in our lab.
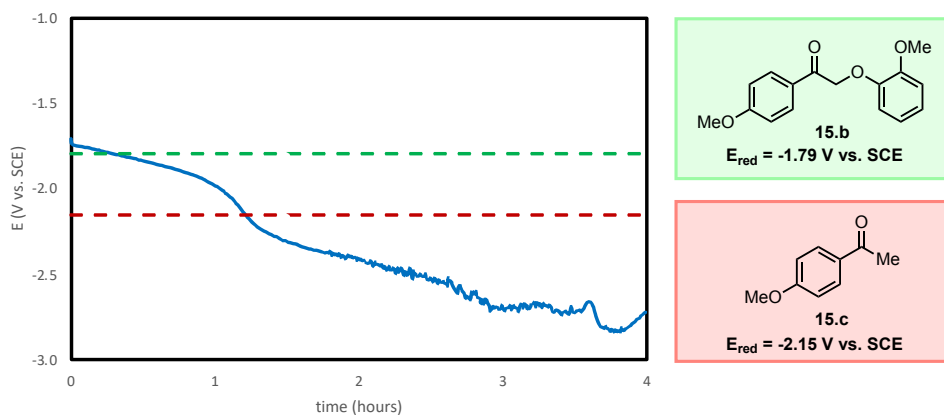
Figure 40 A plot of the potential over time in a current-controlled reaction.

3.5 Conclusions

Lignin depolymerization is a great challenge posed to chemists and engineers alike. The intricacies involved in how reactivity is connected to the isolation of lignin further complicates the difficulty in developing environmentally benign methods for the valorization of lignin. We believe that the solution to the problem should be focused on selectivity, reaction mildness, safety, and effectiveness. Developing two-step processes for lignin model and native lignin fragmentation has allowed us to thoroughly explore our options in designing reaction conditions that meet our high standards of efficiency and safety. We also believe that the utilization of light and electricity are important in order to promote a sustainable future for the field of lignin depolymerization. This chapter has focused on our group's development of two-step processes that we believe will advance the field of lignin depolymerization. Our future goals include the process of translating these reactions to large-scale operations and increasing yields to reduce the proof-of-concept methods to practice.

Chapter 4 One-step Strategies for Lignin Depolymerization

4.1 Introduction

Much of my work on lignin depolymerization has focused on how to marry the two-steps of oxidation and reduction to provide a seamless method that can be scaled up for future use. One embodiment to achieve this goal is the use of a redox-neutral fragmentation strategy. The challenging prospect of a redox-neutral fragmentation is prevalent in the academic literature but is rife with reactivity or translatability issues. Our ideal mechanistic manifold for β-O-4 fragmentation includes the use of a mediator that can shuttle two protons and two electrons from the benzylic alcohol to the C_β–O bond (Figure 41.a). One such example of a redox-neutral fragmentation was reported by Bergman and Ellman (Figure 41.b).[101] This mode of reactivity would deliver depolymerization products from native lignin with high functional group fidelity; however, they were unable to expand the scope to reaction model systems with any extra functionality.
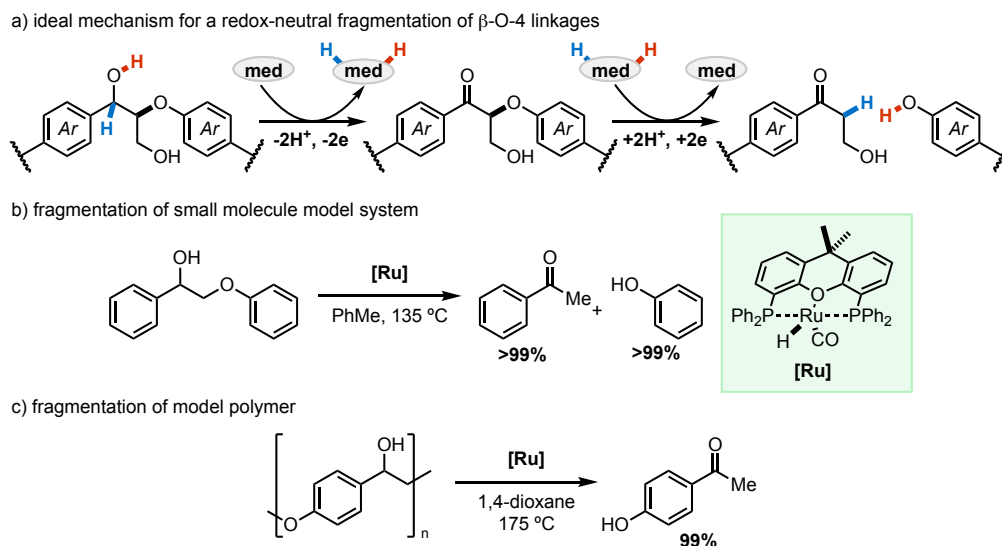
Figure 41 Strategies and examples for redox-neutral fragmentations

The most troublesome challenge to overcome is developing a catalyst system that can offer a high level of functional group selectivity in the presence of the other functional groups present in a lignin polymer. Recently, Knowles and co-workers described a photoredox catalysis-based method to fragment the C_α–C_β bonds of alcohol substrates. They were previously limited to *p*-methoxyphenyl alcohol substrates (Figure 42.a),[144] but have recently expanded the scope to alkyl alcohols as well.[145] Described in their report is the bond cleaving reaction on lignin model substrate **17.a** to afford products **7** and **56** in 89% and 65% yield, respectively (Figure 42.b). This method embodies the principles of a redox-neutral fragmentation, albeit a different bond cleavage than our group has considered.

a) Knowles' PCET-enabled $C_\alpha–C_\beta$ fragmentation of benzylic alcohols
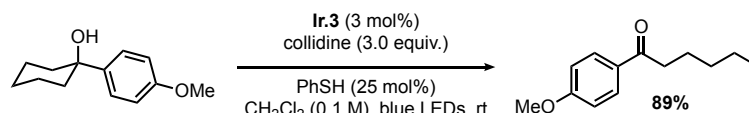
b) Knowles' PCET-enabled $C_\alpha–C_\beta$ fragmentation
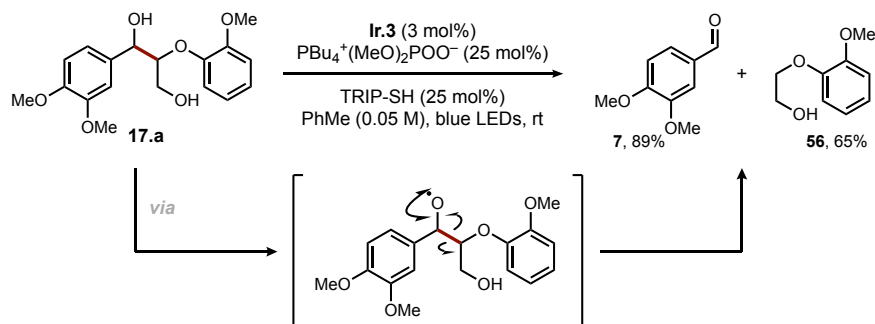
Figure 42 PCET enabled C–C bond fragmentation strategies.

Other strategies for lignin depolymerization in a single step that are not redox-neutral are also commonly encountered in the literature. For example, the Murakami group has reported a method for lignin model fragmentation using an acridinium photocatalyst (**Acr+**) where the photoredox catalysis step is coupled with an oxidative copper catalysis step.[146] The author's goal was to develop copper-based conditions that avoided thermal input as was reported before.[84,147] It was proposed that **Acr+** ($E^{red}_{1/2}$ (**Acr***+/**Acr·**) = 2.17 V vs. SCE) could oxidize a lignin model compound, and in the presence of base and copper it would undergo oxidative fragmentation. The authors were successful when employing **Acr+** with a copper salt, sodium acetate, and blue LED irradiation at room temperature under an air atmosphere (Figure 43). The authors were able to demonstrate the reaction efficacy on many different model substrates that are representative of both the β-O-4 linkage and the β-1 linkage. This is yet another example in which the enhanced redox potentials of excited state photocatalysts can induce a targeted bond fragmentation using visible-light and under ambient conditions.
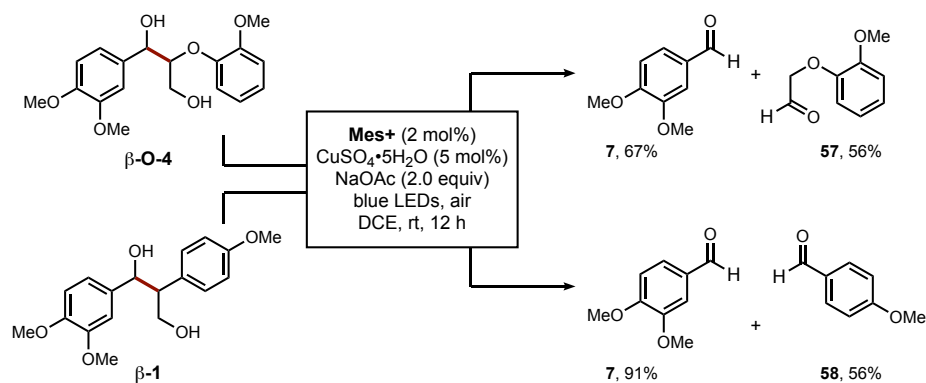
Figure 43 Oxidative, photoredox strategy for lignin substrate fragmentation.

The aforementioned examples represent strategies that our group has embraced in identifying a one-step process for lignin depolymerization. Recently, we independently discovered conditions that lead to a redox-neutral fragmentation of lignin model systems that can either cleave the C_α–C_β bond or the C_β-O-4 bond, and we believe both reaction mechanisms may operate through a PCET mechanism similarly to work reported by the Knowles group. Discussed herein are our initial efforts in developing one-step lignin depolymerization methods using mild reaction conditions and photoredox catalysis.

4.2 Development of a Redox-neutral Fragmentation of a Lignin Model System

I believe that a redox-neutral strategy for lignin fragmentation using photoredox catalysis and PCET-based mechanisms can offer the most efficient route to lignin depolymerization. Our envisioned approach involved a simple reaction sequence involving PCET-enabled oxidation of a lignin model substrate to generate an oxyl-radical intermediate that could go through an immediate C–C bond homolysis (blue line) or a separate hydrogen transfer/proton transfer sequence (red line) to arrive at a different product (Figure 44).
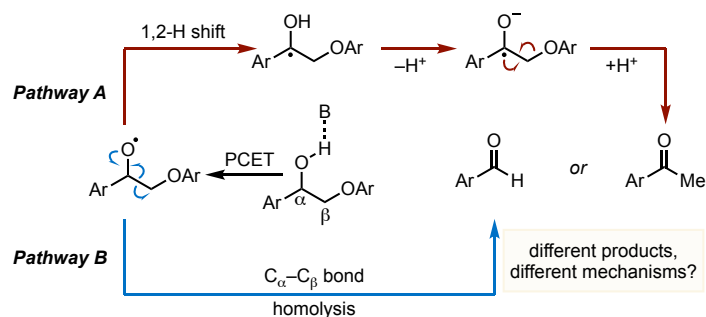
Figure 44 Our envisaged operative mechanistic pathways for redox-neutral fragmentation of lignin β-O-4.

We began our reaction optimization by exploring reaction conditions under more oxidizing conditions. To help enable PCET, we decided to use the phosphate base that has been used by the Knowles group,[148] and a similar base by the MacMillan group,[149] owing to its ability to hydrogen bond and its potent solubility in organic solvents. We used methyl viologen (MV) as an added oxidant in the reaction. We started by looking at photocatalysts with varying oxidizing strengths to identify correlations between the oxidizing potential of a photocatalyst and product formation. Interestingly, there did seem to be a correlation between excited state reduction potentials (E^*_{red}) and conversion of the starting material when using transition-metal based photocatalysts (Table 6). The lone example of an organic photocatalyst (**$^tBu_2$-Acr+**, an acridinium-based photocatalyst) broke apart from the correlation, which points to differences in which SET occurs between an acridinium photocatalyst and a transition-metal based photocatalyst. The use of **Ir.1**, **Ir.2**, and Ru(bpy)$_3$ led to mostly oxidation product (**40.b**), with small amounts of fragmentation product (**40.c**). We noticed a discernible increase in conversion and fragmentation when photocatalysts **Ir.3** and **Ir.4** were used, which are our more oxidizing photocatalysts. Having identified **Ir.4** as the photocatalyst that gave the most conversion of starting material and the highest selectivity for the fragmentation product, we moved on to parse out all of the necessary elements of the reaction (Table 7).

Table 6 Evaluation of photocatalysts for a redox-neutral fragmentation.
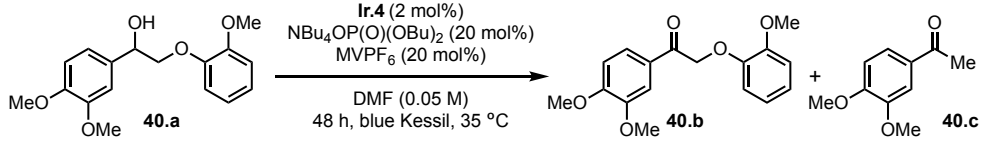
Photocatalyst*	E^*_{red} (vs. SCE)	RSM	oxidation (40.b)	fragmentation (40.c)
Ir(ppy)$_3$ (**Ir.1**)	0.31	93%	<5%	0%
[Ir(ppy)$_2$(dtbbpy)]$^+$ (**Ir.2**)	0.66	68%	31%	11%
Ru(bpy)$_3$(PF$_6$)$_2$	0.77	73%	22%	0%
[Ir(dF{CF$_3$}ppy)$_2$(dtbbpy)]$^+$ (**Ir.3**)	1.21	0%	81%	6%
[Ir(dF{CF$_3$}ppy)$_2$(5,5'-{CF$_3$}bpy)] (**Ir.4**)	1.68	0%	58%	46%
^{t}**Bu$_2$-Acr+**	2.08	90%	10%	0%

*all reactions were bubbled with nitrogen or argon for at least 1 minute before capping and sealing under an inert atmosphere

Firstly, we increased the amount of base from 20 mol% to 50 mol% (entry 1). The increase in base did lead to marginally better selectivity. The omission of the photocatalyst led to 26% conversion and 23% oxidation product (**40.b**). This reactivity is likely a result of the oxidizing nature of MV. When the base was omitted, the conversion was still high, but the selectivity was largely shifted toward the formation of the oxidation product (entry 3). Finally, exclusion of MV led to 82% conversion and 76% **40.c** (with 6% **40.b**, there was perfect mass balance). Mass balance was generally well maintained, and no undesired by-products were ever detected.

Table 7 Reaction component screening.

entry[*]	variation from standard conditions	RSM	oxidation (**40.b**)	fragmentation (**40.c**)
1	50 mol% base	0%	34%	54%
2	no photocatalyst	74%	23%	0%
3	no base	12%	67%	7%
4	no MVPF$_6$	18%	6%	76%

[*]all reactions were bubbled with nitrogen or argon for at least 1 minute before capping and sealing under an inert atmosphere

We further explored reaction conditions with shorter reaction times (48 h to 22 h) in attempts to optimize the redox-neutral reaction (Table 8). We included a new photocatalyst–[Ir(dF{CH$_3$}ppy)$_2$(dtbbpy)]PF$_6$, **Ir.5** that bears structural similarity to the **Ir.3** photocatalyst wherein the phenylpyridine ligand is substituted with -CH$_3$ groups instead of -CF$_3$ groups. Reexamining oxidizing catalysts **Ir.3** and **Ir.4** showed good conversion but poorer yields compared to the 48 h reaction (entries 1-3). Typically, keeping DMF as the solvent and varying the base resulted in poorer conversion and diminished fragmentation yields (entries 4-7). Reexamination of the NBu$_4$OP(O)(OBu)$_2$ base with different solvents (8-11) resulted in varying conversion of **40.a** and yields of **40.c** with no identifiable relationship between solvent and conversion.

Table 8 Reaction optimization on **40.a**.
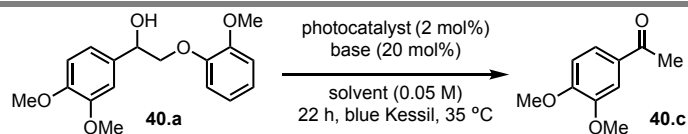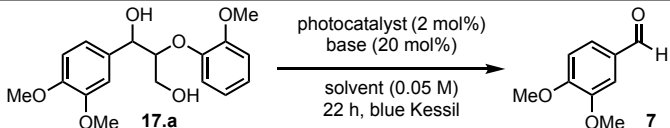
entry	photocatalyst	base	solvent	RSM	yield[a]
1	**Ir.4**	NBu$_4$OP(O)(OBu)$_2$	DMF	54%	21%
2	**Ir.5**	NBu$_4$OP(O)(OBu)$_2$	DMF	31%	39%
3	**Ir.3**	NBu$_4$OP(O)(OBu)$_2$	DMF	30%	50%
4	**Ir.3**	K$_2$HPO$_4$	DMF	62%	18%
5	**Ir.3**	K$_3$PO$_4$	DMF	92%	6%
6	**Ir.3**	NBu$_4$AcO	DMF	52%	6%
7	**Ir.3**	NBu$_4$PhCO$_2$	DMF	48%	10%
8	**Ir.3**	NBu$_4$OP(O)(OBu)$_2$	Acetone	54%	32%
9	**Ir.3**	NBu$_4$OP(O)(OBu)$_2$	MeCN	45%	24%
10	**Ir.3**	NBu$_4$OP(O)(OBu)$_2$	DMA	50%	7%
11	**Ir.3**	NBu$_4$OP(O)(OBu)$_2$	2-butonone	44%	38%

[a]yield determined by ^{1}HNMR using 1,3,5-trimethoxybenzene as the internal standard

Considering the less than fruitful results on model system **40.a**, we decided to explore similar reaction conditions on the diol model substrate **17.a**. Interestingly, we noticed the aldehyde product (**7**) was the major product being formed in the reactions that included photocatalyst and base. Probing this reaction, we looked at our two most oxidizing photocatalysts with different bases (entries 1-4), which showed good conversion but poor yields. We then decided to screen reactions using **Ir.5** looking at a number of different base additives (entries 5-11), which gave variable yields of the aldehyde product. We saw the most consistent results with the inorganic base

K₃PO₄–an oddity considering it is not soluble in the reaction solvent–and proceeded by considering small variations to the reaction conditions. Decreased reaction times (entries 12 and 13), higher concentration (entry 14), as well as deoxygenated solvent (entry 15) all showed similar reactivity without any remarkable improvements.

Table 9 Reaction optimization on **17.a**.

entry	photocatalyst	base	solvent	RSM	yield[a]
1	**Ir.3**	NBu$_4$OP(O)(OBu)$_2$	DMF	26%	14%
2	**Ir.3**	K$_2$HPO$_4$	DMF	40%	13%
3	**Ir.3**	K$_3$PO$_4$	DMF	22%	15%
4	**Ir.4**	NBu$_4$OP(O)(OBu)$_2$	DMF	20%	26%
5	**Ir.5**	NBu$_4$OP(O)(OBu)$_2$	DMF	7%	32%
6	**Ir.5**	K$_2$HPO$_4$	DMF	-	31%
7	**Ir.5**	K$_3$PO$_4$	DMF	-	32%
8	**Ir.5**	NBu$_4$AcO	DMF	-	32%
9	**Ir.5**	NBu$_4$PhCO$_2$	DMF	-	34%
10	**Ir.5**	K$_3$PO$_4$	DMF (O$_2$)	-	32%
11	**Ir.5**	HNC(N(CH$_3$)$_2$)$_2$	DMF	72%	0%
12	**Ir.5**	K$_3$PO$_4$	DMF (6 h)	54%	34%
13	**Ir.5**	K$_3$PO$_4$	DMF (12h)	47%	30%
14	**Ir.5**	K$_3$PO$_4$	DMF (1 M)	42%	30%
15	**Ir.5**	K$_3$PO$_4$	DMF (FPT)	22%	31%

FPT = freeze-pump-thaw; [a]yield determined by ^{1}HNMR using 1,3,5-trimethoxybenzene as the internal standard

The detection of the aldehyde product was a curious finding considering the data from Table 8. We initially hypothesized that PCET-enabled oxidation of the benzylic position could induce C$_\alpha$–C$_\beta$ bond fragmentation or another ensuing mechanism could result in the C–O bond fragmentation (Figure 44). When working with the single alcohol substrate, **40.a**, we consistently

saw C–O bond fragmentation product, likely a result of Pathway A. Alternatively, diol substrate **17.a** showed mostly aldehyde product (only trace amounts of C–O bond fragmentation product were ever detected). Based on our data for substrate **40.a**, we envisioned substrate **17.a** would follow a similar mechanistic pathway. The conversion of **17.a** to **7** lent evidence for a mechanism that goes through primary alcohol oxidation and subsequent retro-aldol. To date, we cannot say with certainty that the operative mechanisms of the fragmentations of **40.a** and **17.a** are mutually exclusive, and this is an ongoing area of research in our lab.

To further exacerbate this observed anomaly of divergent reactivity between model substrates, we looked at subjecting diol substrate **17.a** to reaction conditions with photocatalyst and no added base (Table 10). To our surprise, the C–O bond cleaved product **17.c** was observed. Photocatalysts **Ir.5** and **Ir.4** showed similar yields with varying conversions (entries 1-2), while our less oxidizing photocatalyst **Ir.2** showed effectively no conversion (entry 3). Having obtained the most consistent results with **Ir.3** (entry 4, 35% yield of **17.c**), we evaluated how different solvents would affect the fragmentation results. Polar aprotic solvents (entries 5-9) revealed no significant increase in yield or trend for conversion (17-32% yield). Toluene (entry 10), a solvent with potential reactivity in photoredox reactions because of its labile benzylic hydrogen atoms, gave yields comparable to the other entries. More acid and protic solvents like HFIP (1,1,1,3,3,3-hexafluoroisopropanol) and acetic acid (entries 12-13) lead to decomposition of the starting material with no isolable products. Finally, pyridine as a solvent did show some detectable amounts of product (30%) but did have poor mass balance without any other detectable byproducts.

Table 10 Reaction optimization on **17.a** without base

entry	photocatalyst	solvent	RSM	yield[a]
1	**Ir.5**	DMF	23%	29%
2	**Ir.4**	DMF	60%	30%
3	**Ir.2**	DMF	98%	trace
4	**Ir.3**	DMF	48%	35%
5	**Ir.3**	acetone	23%	32%
6	**Ir.3**	DMA	31%	20%
8	**Ir.3**	THF	49%	17%
9	**Ir.3**	MeCN	57%	30%
10	**Ir.3**	PhMe	56%	20%
12	**Ir.3**	Acetic acid	0%	0%
13	**Ir.3**	HFIP	0%	0%
14	**Ir.3**	pyridine	0%	30%

[a]yield determined by ^{1}HNMR using 1,3,5-trimethoxybenzene as internal standard

These results highlight the intricacies and challenges in developing catalyst systems that attempt to fragment a β-O-4 model in a single step under mild conditions. The Ir-based photocatalysts have been robust in showing that conversion is obtained under a number of different reaction conditions, but there are still many parameters that need to be tuned. There is a clear change in the operative mechanism that depends on the presence or absence of base, and the full

gamut of viable bases has yet to be explored. Additionally, as shown in the report by the Knowles group,[145] we have yet to explore options for including HAT reagents. Moving forward, we plan to examine the operative mechanism for both substrates to understand better what causes the bifurcation in the mechanism between the two model substrates (sterics, intrinsic activation of functional groups, hydrogen bonding capabilities, etc.). Ultimately, we wish to examine the feasibility of an optimized reaction on native lignin. These attempts will likely find more practicality in a flow apparatus to compensate for the dark color of a lignin solution while simultaneously improving the prospects for scaling up. Future work from our lab will be reported in due time.

4.3 Conclusion

Single-step protocols offer several advantages that can be used in catalytic processes to provide a straight forward approach to lignin depolymerization. Described in this chapter was how oxygen can be used for product formation or catalyst turnover. This is advantageous since the use of oxygen is atom-economical and environmentally benign. I also showcased how a redox-neutral mechanism can be used to carry out a series of redox manipulations to arrive at the fragmentation products of lignin β-O-4 model substrates. These recent advances in single-step strategies are helping chemists to understand the chemical limitations for a lignin depolymerization that would satisfy the requirements for green chemistry and for large-scale processing.

One additional aspect of lignin depolymerization chemistry that is critical to the development of single-step strategies is the structure of the lignin upon isolation. I briefly described how common extraction methods can alter the native structure of lignin (Figure 5). Also noted was how organsolv methods can cause undesirable bond formations. These bond formations are often intramolecular bond formations (also referred to as interunit bond formations) that make

more stable bonds that are less reactive to catalysis. This problem is difficult to work around since acid treatment is required to hydrolyze the lignin from the cellulose, but it is the acid that causes the interunit bond formations. A clever solution to this problem has been identified and applied by Professor Jeremy Luterbacher, where they found that adding in a reagent, such as an aldehyde or ketone, during the extraction process to in situ protect the 1,3-diol found in the β-O-4, you can form a protected (i.e., acetal or ketal) 1,3-dioxane β-O-4 linkage that is still susceptible to catalytic hydrogenolysis and largely reduces the amount of interunit bond formations. Luterbacher and co-worker's initial reports showed propionaldehyde as a competent protecting reagent but later described that a number of protecting groups worked well for this reaction sequence (Figure 45).[150,151]
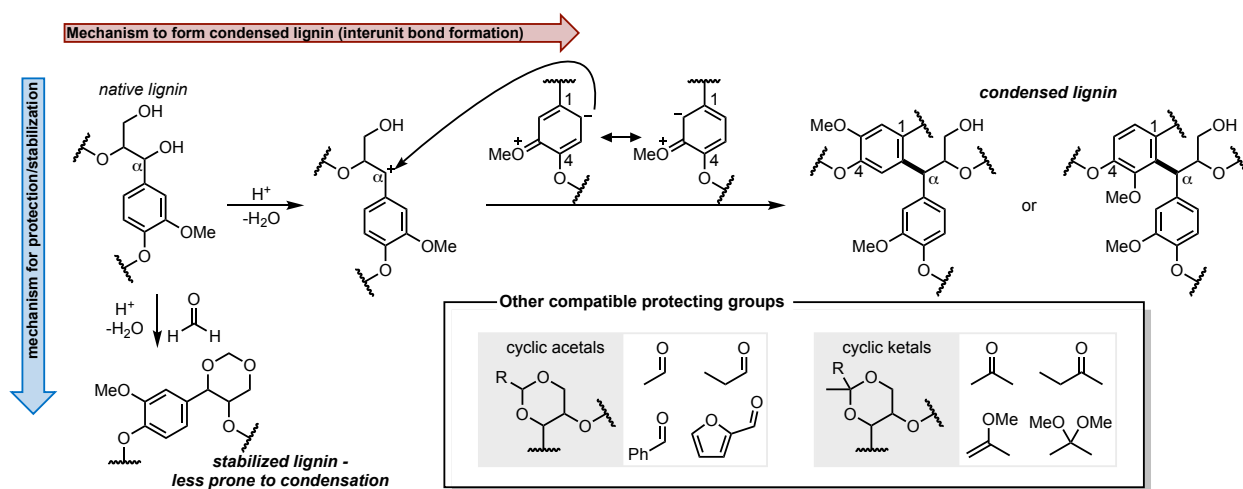
Figure 45 Mechanism for interunit bond formation in lignin, and compatible protecting groups for stabilizing lignin.

This new technology for isolating lignin that depolymerizes at higher yields than traditional organosolv lignin offers chemists new opportunities and insights into how to design catalyst systems for lignin depolymerization. Our group is involved in a collaborative effort with the Luterbacher group to design catalyst systems either photochemically or electrochemically to depolymerize their stabilized lignin.

Appendix

Methods

^{1}H and ^{13}C NMR spectra were recorded at ambient temperature using Varian MR400, Inova 500, Vnmrs 500 and Vnmrs 700 spectrometers operating at 400, 500, or 700 MHz for ^{1}H NMR, and 126 or 176 MHz for ^{13}C NMR using an internal deuterium lock. Chemical shifts (δ) are expressed in parts per million (ppm) and are quoted to two decimal places and a single decimal place for ^{1}H and ^{13}C NMR, respectively, with coupling constants (J) expressed in hertz (Hz) to the nearest 0.1 Hz. ^{1}H chemical shifts are reported relative to the residual protio solvent resonance at δ 7.26 for residual CHCl$_3$ in CDCl$_3$ or using δ 2.05 for the center line of the solvent signal for acetone-d_6. ^{13}C NMR spectra are referenced to the center line of the solvent peak at δ 77.16 for CDCl$_3$ and δ 29.84 for acetone-d_6. NMR data are reported as follows: chemical shift (multiplicity, coupling constants where applicable, number of hydrogens). Multiplicities are reported using the following abbreviations: br = broad, s = singlet, d = doublet, t = triplet, dd = doublet of doublets, ddd = doublet of doublet of doublets, and m = multiplet.

Gel permeation chromatography (GPC) characterization of lignin polymers was performed using THF as the mobile phase using a Shimadzu GPC instrument with a UV diode array detector, and a refractive index detector. The instrument is equipped with three GPC columns connected in series (Waters HT-3, HT-2, and HT-1) and was calibrated with a series of polystyrene standards. High-resolution mass spectra (HRMS) were obtained on an Agilent quadrupole time-of-flight (Q-TOF) mass spectrometer using electrospray ionization (ESI), positive ion mode at the University of Michigan, Ann Arbor, MI, Department of Chemistry instrumentation facility. Infrared spectra

were recorded on a Perkin-Elmer Spectrum BX FT-IR spectrophotometer using an ATR mount with a ZnSe crystal. Absorption bands are expressed in wavenumber (cm^{-1}). UV-vis spectra were recorded on a Shimadzu UV-1601 UV-VIS spectrometer equipped with a Peltier temperature controller. Luminescence quenching experiments were carried out on a Fluoromax-2 fluorimeter equipped with a xenon arc lamp. LED lights and the requisite supplies were purchased from Creative Lighting Solutions (http:/www.creativelightings.com) with the following item codes: CL-FRS5050-12WP-12V (4.4 W blue LED light strip), CL-PS94670-25W (25 W power supply), CL-PC6FT-PCW (power cord), CL-TERMBL-5P (terminal block).
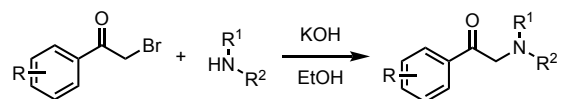
Materials

Unless otherwise stated, all commercially available chemicals were used without further purification. All glassware, including Teflon-coated magnetic stir bars, was dried in an oven overnight at 150 °C or flame dried under vacuum before use. Unless otherwise stated, all reactions were performed under an inert atmosphere of either N_2 or argon. Organic solvents and amine bases were purified prior to use using a Phoenix Solvent Drying System (for organic solvents, available from JC-Meyer Solvent Systems) or PureSolv Micro amine drying columns (for amine bases, available from Innovative Technology), respectively, and maintained under positive argon pressure.

Reactions were monitored by thin-layer chromatography (TLC) using glass-backed plates pre-coated with 230–400 mesh silica gel (250 μm thickness, 60 Å porosity, F-254 indicator). TLC plates were visualized by exposure to a dual short-wave/long-wave UV lamp and staining in ethanolic solutions of *para*-anisaldehyde or potassium permanganate. Flash column chromatography was performed either manually using 43–60 μm (230–400 mesh) silica gel or utilizing Redi*Sep®R*F Gold silica columns with a Teledyne Isco CombiFlash RF automated

purification system. 42 mm (Sartorius Stedim Biotech, Filter Discs, Grade: 292, order number: FT-3-205-042) and 55 mm (Whatman, Qualitative Filter Papers, catalog number: 1001-055) was used for the filtration of polymer precipitates. Volatile solvents were distilled under reduced pressure with a rotary evaporator.

Starting material preparation

*General procedure for the synthesis of amine starting materials*[78]

2-bromoacetophenone (2.0 g, 10.05 mmol) and ethanol (50 mL, 0.2 M in starting material) were added to a dry round bottom flask equipped with a magnetic stir bar. Aniline (1.83 mL, 20.10 mmol, 2 eq.) was added drop-wise, as a white precipitant formed immediately upon addition. This was allowed to stir for 3 hours, upon which the solution was filtered, concentrated *in vacuo*, and recrystallized using ethanol.
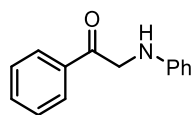
1-phenyl-2-(phenylamino)ethan-1-one (21.a) was synthesized using the general procedure.

|	
TLC (EtOAc/Hex, 7:3), R_f	0.64;
^{1}H NMR (400 MHz, CDCl$_3$) δ:	8.03 (d, J = 7.3 Hz, 2H), 7.65 (t, J = 7.4 Hz, 1H), 7.53 (t, J = 7.7 Hz, 2H), 7.31 – 7.22 (m, 3H), 6.81 (t, J = 7.6 Hz, 3H), 4.67 (s, 2H);
^{13}C NMR (175 MHz, CDCl$_3$) δ:	195.0, 147.0, 134.9, 133.9, 129.4, 128.9, 127.8, 117.9, 113.1, 50.4;
HRMS (ESI):	*m/z* calculated for C$_{14}$H$_{14}$NO [M+H]$^+$: 212.1070, found 212.1070;
FTIR (neat) cm^{-1}:	3410.9, 1686.3, 1601.9, 1508.4, 1444.8, 1356.9, 1321.6, 1261.8, 1219.9, 1178.8, 1147.7, 984,864.4, 743.6, 684.2, 663.5.
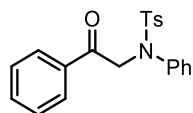
4-methy-N-(2-oxo-2-phenylethyl)-N-phenylbenzenesulfonamide (22.a) was synthesized using the general procedure.

^{1}H NMR (700 MHz, CDCl$_3$) δ:	7.95 (dd, J = 8.2, 1.1 Hz, 2H), 7.60 (d, J = 7.4 Hz, 1H), 7.59 – 7.55 (m, 2H), 7.47 (t, J = 7.8 Hz, 2H), 7.32 – 7.23 (m, 5H (2+3), overlap with CHCl$_3$), 7.18 – 7.14 (m, 2H), 5.05 (s, 2H), 2.44 (s, 3H).
^{13}C NMR (175 MHz, CDCl$_3$) δ:	193.9, 143.9, 139.7, 135.6, 135.1, 133.8, 129.5, 129.2, 128.9, 128.9, 128.4, 128.2, 77.3, 77.0, 57.8, 21.8.
HRMS (ESI):	*m/z* calculated for C$_{21}$H$_{20}$NO$_3$S [M+H]$^+$: 366.1158, found 366.1158
FTIR (neat) cm^{-1}:	3061.9, 2917.1, 1707.2, 1595.3, 1491.8, 1447.4, 1335.1, 1364.6, 1305.8, 1291.6, 1212.6, 1184.4, 1103.8, 1089.9, 1029.7, 1011.6, 1000.4, 980.1, 881.8, 935.3, 912.4, 809.2, 768.2, 755.0, 768.2, 729.9, 667.0, 692.9
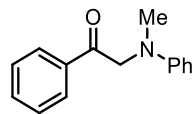
2-(methyl(phenyl)amino)-1-phenylethan-1-one (23.a) was synthesized using the general procedure.

^{1}H NMR (700 MHz, CDCl$_3$) δ:	8.00 (d, J = 7.3 Hz, 2H), 7.62 (t, J = 7.3 Hz, 1H), 7.51 (t, J = 7.8 Hz, 2H), 7.22 (dd, J = 8.4, 7.4 Hz, 2H), 6.74 (t, J = 7.3 Hz, 1H), 6.69 (d, J = 8.6 Hz, 2H), 4.79 (s, 2H), 3.12 (s, 3H);
^{13}C NMR (175 MHz, CDCl$_3$) δ:	195.6, 135.8, 133.5, 128.6, 128.1, 66.7, 53.7.
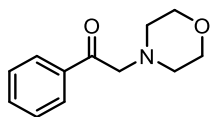
2-morpholino-1-phenylethan-1-one (24.a) was synthesized using the general procedure.

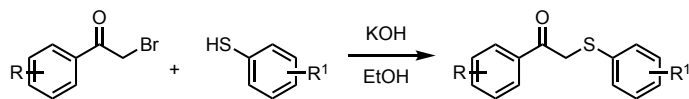^{1}H NMR (400 MHz, CDCl$_3$) δ: 8.01 (d, J = 7.2 Hz, 1H), 7.59 (t, J = 7.4 Hz, 1H), 7.47 (t, J = 7.6 Hz, 1H), 3.83 (s, 1H), 3.81 – 3.74 (m, 2H), 2.69 – 2.58 (m, 2H).

Physical appearance: off-white solid

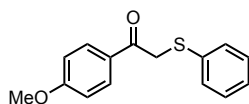## General procedure for phenylethanone sulfides

Prepare a solution of thiol and base ethanol solution, 0.2 M with respect to the thiol. Allow for equilibration and cooling for 30 minutes. Separately, prepare a solution of 2-bromoacetophenone in ethanol, and add slowly to the reaction. Allow appropriate time for reaction. Quench the reaction with an equimolar amount of acid, and then precipitate the product by adding a large excess of water. Crude crystals can be recrystallized in MeOH-H_2O.
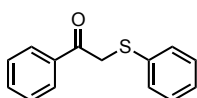
1-phenyl-2-(phenylthio)ethan-1-one (26.a) was prepared using the general procedure for phenylethanone sulfides.

TLC (EtOAc/Hex, 1:5), R_f	0.50;
^{1}H NMR (700 MHz, CDCl$_3$) δ:	7.96 (dd, J = 8.4, 1.2 Hz, 2H), 7.96 (dd, J = 8.4, 1.2 Hz, 2H), 7.60 (ddt, J = 8.6, 7.2, 1.2 Hz, 1H), 7.48 (dd, J = 8.1, 7.4 Hz, 2H), 7.42 –7.38 (m, 2H), 7.32 – 7.28 (m, 2H), 7.26 – 7.21 (m, 1H), 4.29 (s, 2H);
^{13}C NMR (175 MHz, CDCl$_3$) δ:	133.5, 130.5, 129.1, 128.7, 128.7, 127.1, 41.2;
HRMS (ESI):	*m/z* calculated for C$_{14}$H$_{13}$OS [M+H]$^+$: 229.0682, found 229.0682;
FTIR (neat) cm^{-1}:	3074.1, 1668.8, 1596, 1578.4, 1479.2, 1444.9, 1416.1, 1273.2, 1185.8, 1133.9, 1072.5, 1011.2, 941.7, 898, 804.3, 740.5, 722, 66.6, 648.1, 614.1.

1-(4-methoxyphenyl)-2-(phenylthio)ethan-1-one (27.a) was synthesized using the general procedure for phenylethanone sulfides.

TLC (EtOAc/Hex, 1:5), R_f	0.55;
^{1}H NMR (500 MHz, CDCl$_3$) δ:	7.98 – 7.91 (m, 2H), 7.43 – 7.37 (m, 2H), 7.32 – 7.27 (m, 2H), 7.25 – 7.20 (m, 1H), 6.97 – 6.92 (m, 2H), 4.25 (s, 2H), 3.89 (s, 3H);
^{13}C NMR (175 MHz, CDCl$_3$) δ:	192.68, 163.76, 135.03, 131.02, 130.34, 129.00, 128.37, 126.94, 113.83, 55.49, 40.95;
HRMS (ESI):	*m/z* calculated for C$_{15}$H$_{15}$O$_2$S [M+H]$^+$: 259.0787, found 259.0682;
FTIR (neat) cm^{-1}:	1658.2, 1601.4, 1572, 1508.6, 1480.4, 1420.3, 1436.7, 1395.9, 1310.5, 1262.6, 1199.9, 1173.8, 1023.7, 991.6, 817.8, 734.3, 690, 633.1.
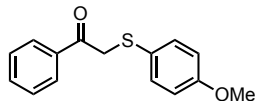
2-((4-methoxyphenyl)thio)-1-phenylethan-1-one (30.a) was synthesized using the general procedure for phenylethanone sulfides.

^{1}H NMR (500 MHz, CDCl$_3$) δ:	7.93 (d, J = 7.8 Hz, 2H), 7.57 (d, J = 7.3 Hz, 1H), 7.47 (t, J = 7.6 Hz, 2H), 7.37 (d, J = 8.6 Hz, 2H), 6.83 (d, J = 8.6 Hz, 2H), 4.14 (s, 2H), 3.80 (s, 3H);
^{13}C NMR (175 MHz, CDCl$_3$) δ:	194.3, 159.7, 135.5, 134.7, 133.3, 132.6, 130.5, 128.9, 128.7, 126.3, 124.5, 114.8, 114.6, 77.2, 77.0, 76.8, 55.3, 42.8;
HRMS (ESI):	*m/z* calculated for C$_{15}$H$_{15}$O$_2$S [M+H]$^+$: 259.0787, found 259.0788;
FTIR (neat) cm^{-1}:	2937.2, 2835.3, 1674.0, 1591.1, 1492.3, 1461.7, 1447.4, 1406.0, 1274.1, 1242.8, 1196.2, 1172.8, 1133.5, 1104.0, 1075.9, 1027.9, 1014.0, 1075.9, 1027.9, 1014.0, 825.8, 798.3, 748.4, 723.8, 686.9.
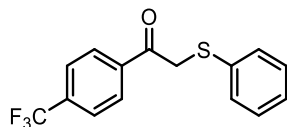
2-(phenylthio)-1-(4-(trifluoromethyl)phenyl)ethan-1-one (25.a) was synthesized using the general procedure for phenylethanone sulfides.

TLC (EtOAc/Hex, 1:9), R_f	0.36 (stains light green in vanillin);
^{1}H NMR (700 MHz, CDCl$_3$) δ:	8.04 (d, J = 8.1 Hz, 15H), 7.74 (d, J = 8.1 Hz, 15H), 7.41 – 7.36 (m, 14H), 7.30 (ddd, J = 6.6, 2.4, 0.8 Hz, 14H), 7.28 (t, J = 1.3 Hz, 3H), 7.27 – 7.25 (m, 4H), 4.26 (s, 16H);
^{13}C NMR (175 MHz, CDCl$_3$) δ:	193.2, 138.2, 135.1, δ 134.8 (q, J = 32.8 Hz), 134.7, 134.5, 134.1, 131.2, 129.4, 129.2, 126.0, 125.9 (q, J = 3.7 Hz), 123.7 (q, J = 272.7 Hz), 121.3, 41.4;
^{19}F NMR (471 MHz, CDCl$_3$) δ:	= –64.17 (s, 3 F);
HRMS (ESI):	m/z calculated for C$_{15}$H$_{12}$F$_3$OS [M+H]$^+$: 297.0555, found 297.055;
FTIR (neat) cm^{-1}:	2896.7, 1679.3, 1580.0, 1511.7, 1482.4, 1438.6, 1409.9, 1393.0, 1326.1, 1311.2, 1311.2, 1285.7, 1195.7, 1162.8, 1111.1, 1065.1, 1026.9, 1015.1, 992.4, 964.0, 900.1, 854.4, 839.0, 825.5, 739.9, 701.1, 689.8.
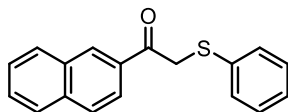
1-(naphthalen-2-yl)-2-(phenylthio)ethan-1-one (29.a) was synthesized using the general procedure for phenylethanone sulfides.

TLC (EtOAc/Hex, 1:9), R_f	0.32

^{1}H NMR (700 MHz, CDCl$_3$) δ: 8.44 (s, 1H), 8.02 (dd, J = 8.6, 1.6 Hz, 1H), 7.96 – 7.86 (m, 3H), 7.63 (t, J = 7.4 Hz, 1H), 7.57 (t, J = 7.5 Hz, 1H), 7.43 (d, J = 7.5 Hz, 2H), 7.30 (t, J = 7.5 Hz, 2H), 7.25 (t, J = 7.3 Hz, 1H), 4.41 (s, 2H);

^{13}C NMR (175 MHz, CDCl$_3$) δ: 194.20, 135.86, 134.95, 132.85, 132.56, 130.87, 130.73, 129.79, 129.25, 128.88, 128.73, 127.94, 127.35, 127.02, 124.36, 41.53;

HRMS (ESI): *m/z* calculated for C$_{18}$H$_{14}$NaOS [M+Na]$^+$: 301.0658, found 301.0658;

FTIR (neat) cm^{-1}: 2896.7, 1679.3, 1580.0, 1511.7, 1482.4, 1438.6, 1409.9, 1393.0, 1326.1, 1311.2, 1311.2, 1285.7, 1195.7, 1162.8, 1111.1, 1065.1, 1026.9, 1015.1, 992.4, 964.0, 900.1, 854.4, 839.0, 825.5, 739.9, 701.1, 689.8.

2-((3-chlorophenyl)thio)-1-phenylethan-1-one (34.a) was synthesized using the general procedure for phenylethanone sulfides.
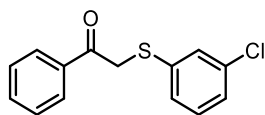
TLC (EtOAc/Hex, 1:9), R_f	0.33

^{1}H NMR (700 MHz, CDCl$_3$) δ: 7.96 (dd, J = 8.4, 1.2 Hz, 1H), 7.61 (ddd, J = 2.4, 1.8, 1.2 Hz, 1H), 7.52 – 7.47 (m, 1H), 7.38 (t, J = 1.6 Hz, 1H), 7.27 (m, 1 H) overlap with chloroform, 7.22 (t, J = 7.5 Hz, 1H), 7.21 – 7.19 (m, 1H), 4.32 (s, 1H);

^{13}C NMR (175 MHz, CDCl$_3$) δ: 193.72, 137.10, 135.41, 133.82, 130.21, 129.80, 128.92, 128.80, 128.16, 127.24, 41.02;

HRMS (ESI): *m/z* calculated for C$_{14}$H$_{12}$ClOS [M+H]$^+$: 263.0292, found 263.0292;

FTIR (neat) cm^{-1}: 3052.3, 2943.0, 2913.8, 1686.2, 1593.2, 1573.4, 1561.6, 1561.6, 1464.3, 1445.8, 1404.1, 1382.3, 1382.3, 1322.5, 1308.1, 1288.9, 1196.9, 1180.2, 1116.2, 1086.1, 1086.1, 1077.5, 1026.0, 999.3, 980.0, 884.0, 884, 871.3, 775.7, 765.0, 751.5, 687.0, 680.2

((2-fluorophenyl)thio)-1-phenylethan-1-one (31.a) was synthesized using the general procedure for phenylethanone sulfides.
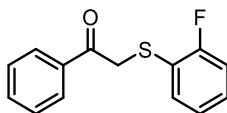
TLC (EtOAc/Hex, 1:9), R_f	0.40

^{1}H NMR (700 MHz, CDCl$_3$) δ: 7.96 (dd, J = 8.4, 1.2 Hz, 1H), 7.61 (tt, J = 7.41, 1.21 Hz, 1H), 7.51 – 7.48 (m, 1H), 7.38 (t, J = 1.6 Hz, 1H), 7.27(dt, J = 7.48,1.57 Hz, 1H overlap with CDCl3), 7.22 (t, J = 7.5 Hz, 1H), 7.21 – 7.19 (m, 1H) , 4.32 (s, 2H);

^{13}C NMR (175 MHz, CDCl$_3$) δ: 193.98 (s) 162.17 (d, J = 246.5 Hz), 135.52 (s), 134.05 (s), 134.04 (s), 133.65 (s), 129.96 (d, J = 8.0 Hz), 128.80 (d, J = 9.5 Hz), 124.74 (d, J = 3.8 Hz), 121.33 (d, J = 17.6 Hz), 116.02 (d, J = 22.5 Hz), 40.51 (s).

^{19}F NMR (471 MHz, CDCl$_3$) δ: -109.06 (ddd, J = 9.4, 7.5, 5.5 Hz);

HRMS (ESI): *m/z* calculated for C$_{14}$H$_{11}$FNaOS [M+H]$^+$: 269.0407, found 269.0407;

FTIR (neat) cm^{-1}: 3070.3, 2947.6, 2911.4, 1679.9, 1593.5, 1578.8, 1565.6, 1465.8, 1445.9, 1397.5, 1317.6, 1284.4, 1261.9, 1220.1, 1191.4, 1180.6, 1160.0, 1123.1, 1070.2, 1031.3, 999.4, 983.7, 927.8, 888.2, 852.9, 826.9, 806.3, 806.3, 743.3, 687.4, 678.4.
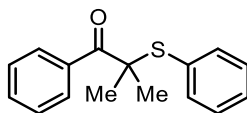
2-methyl-1-phenyl-2-(phenylthio)propan-1-one (28.a) was synthesized using the general procedure for phenylethanone sulfides.

TLC (EtOAc/Hex, 5:95), R_f	0.42

^{1}H NMR (700 MHz, CDCl$_3$) δ: 8.25 (d, J = 8.4 Hz, 2H), 7.54 (td, J = 7.7, 1.0 Hz, 1H), 7.46 (t, J = 7.7 Hz, 2H), 7.38 – 7.32 (m, 3H), 7.32 – 7.24 (m, 2H, overlap with CHCl$_3$), 1.57 (s, 6H);

^{13}C NMR (175 MHz, CDCl$_3$) δ: 201.20 (s), 137.90 (s), 137.16 (s), 132.49 (s), 131.78 (s), 130.48 (s), 130.16 (s), 129.59 (s), 128.84 (s), 55.67 (s), 27.59 (s);

HRMS (ESI): *m/z* calculated for C16H17OS [M+H]$^+$: 257.0995, found 257.0994;

FTIR (neat) cm^{-1}: 3060.3, 2967.4, 2928.0, 1665.8, 1595.6, 1574.2, 1473.5, 1460.9, 1438.7, 1383.5, 1364.5, 1304.0, 1259.7, 1157.3, 1118.8, 1088.3, 1068.0, 1024.9, 1002.0, 975.5, 881.6, 792.4, 750.0, 732.1, 702.2.
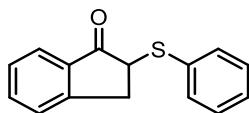
2-(phenylthio)-2,3-dihydro-1*H*-inden-1-one (33.a) was synthesized using the general procedure for phenylethanone sulfides.

TLC (EtOAc/Hex, 1:9), R_f : 0.46

^{1}H NMR (700 MHz, CDCl$_3$) δ: 7.78 (d, J=7.66 Hz, 1 H), 7.54 - 7.67 (m, 1 H), 7.44 - 7.52 (m, 2 H), 7.34 - 7.42 (m, 2 H), 7.21 - 7.30 (m, 3 H), 4.08 (dd, J=7.83, 3.75 Hz, 1 H), 3.63 (dd, J=17.71, 7.66 Hz, 1 H), 3.13 (dd, J=17.54, 3.75 Hz, 1 H);

^{13}C NMR (175 MHz, CDCl$_3$) δ: 34.79, 50.34, 124.58, 126.29, 127.12, 127.46, 127.67, 127.84, 128.95, 132.30, 133.28, 135.26, 135.43, 152.06, 202.23;

HRMS (ESI): *m/z* calculated for C$_{15}$H$_{13}$OS [M+H]$^+$: 241.0682, found 241.0682;

FTIR (neat) cm^{-1}: 3058.7, 2906.7, 1763.5, 1721.7, 1602.1, 1580.3, 1602.1, 1580.3, 1481.7, 1470.7, 1437.9, 1419.7, 1325.4, 1299.4, 1273.8, 1205.8, 1185.6, 1173.6, 1146.0, 1087.8, 1020.8, 1008.1, 957.1, 892.4, 849.7, 792.9, 780.4, 740.6, 729.8, 711.0, 689.5.
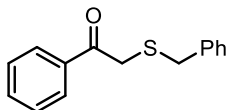
2-(benzylthio)-1-phenylethan-1-one (32.a) was synthesized using the general procedure for phenylethanone sulfides.

¹H NMR (500 MHz, CDCl₃) δ:	7.93 (d, J=8.07 Hz, 2 H), 7.52 - 7.60 (m, 1 H), 7.43 - 7.49 (m, 2 H), 7.34 - 7.38 (m, 2 H), 7.32 (t, J=7.46 Hz, 2 H), 7.17 - 7.28 (m, 2 H), 3.76 (s, 2 H), 3.67 (s, 2 H);
¹³C NMR (175 MHz, CDCl₃) δ:	194.40, 137.26, 135.36, 133.32, 129.26, 128.68, 128.64, 128.52, 127.22, 36.06, 35.82;
HRMS (ESI):	*m/z* calculated for C₁₅H₁₄NaOS [M+Na]⁺: 265.0658, found 265.0658;
FTIR (neat) cm⁻¹:	1670.2, 1595.7, 1449.8, 1394.7, 1292.3, 1197.4, 998.8, 751.1, 685.3, 638.4, 552.6, 536.0, 526.3, 497.6, 480.1, 447.3, 417.9, 412.5.
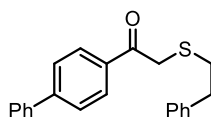
1-([1,1'-biphenyl]-4-yl)-2-(phenethylthio)ethan-1-one (35.a) was synthesized using the general procedure for phenylethanone sulfides.

TLC (EtOAc/Hex, 1:9), R_f	0.55 (brown in anisaldehyde stain)
^{1}H NMR (700 MHz, CDCl$_3$) δ:	8.06 (d, J = 8.4 Hz, 2H), 7.70 (d, J = 8.4 Hz, 2H), 7.64 (dd, J = 8.2, 1.1 Hz, 2H), 7.49 (t, J = 7.7 Hz, 2H), 7.42 (t, J = 7.4 Hz, 1H), 7.30 (dd, J = 9.5, 5.7 Hz, 2H), 7.22 (dd, J = 7.2, 5.3 Hz, 3H), 3.84 (s, 2H), 2.93 (dd, J = 8.9, 6.4 Hz, 2H), 2.89 – 2.83 (m, 2H);
^{13}C NMR (175 MHz, CDCl$_3$) δ:	194.16, 146.22, 140.22, 139.95, 133.96, 129.55, 129.12, 128.73, 128.63, 128.45, 127.48, 127.43, 126.57, 37.20, 35.72, 33.79;
HRMS (ESI):	m/z calculated for C$_{22}$H$_{21}$OS [M+H]$^+$: 333.1308, found 333.1308;
FTIR (neat) cm^{-1}:	2914.2, 2139.9, 2183.1, 2172.7, 2066.2, 1977.0, 1955.0, 1660.3, 1560.5, 1485.1, 1452.8, 1419.8, 1310.9, 1288.9, 1204.5, 1139.5, 1159.9, 1034.3, 1002.6, 927.7 855.8, 845.8, 714.5, 698.5, 988.2, 647.5, 633.9, 620.1, 604.0

General procedure for the synthesis of single-alcohol substrates
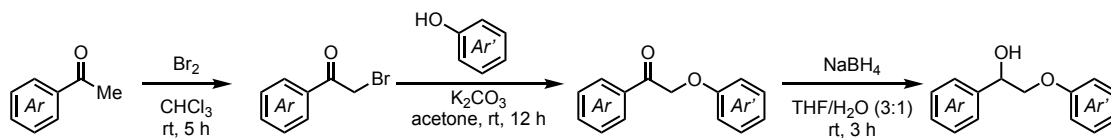
Alcohols were synthetized following a procedure previously reported by us.[133] The corresponding acetophenone (22.2 mmol) was dissolved in $CHCl_3$ (100 mL) under nitrogen atmosphere. A solution of bromine (1.05 equiv) in $CHCl_3$ (80 mL) was added over ca. 5 h in a dropwise manner with an addition funnel under a nitrogen atmosphere. After completion of the addition, the remaining bromine was quenched by adding an aqueous sodium thiosulphate saturated solution and the mixture was let stir until the solution changed from brown to yellow. This mixture was separated, extracted with CH_2Cl_2 and washed with water and brine. The organics were dried over $MgSO_4$, filtered and concentrated under vacuo and the obtained α-bromoacetophenone was recrystallized from EtOH.

α-Bromoacetophenone (12 mmol) was then added to a stirring mixture of K_2CO_3 (1.5 equiv) and the desired phenol (1.1 equiv) in acetone (50 mL) at rt under nitrogen atmosphere and the reaction mixture was allowed to stir for 12 h at rt. After this time, the mixture was filtered, the inorganics were washed with acetone and the filtrate was concentrated. The yellow oil was re-dissolved in warm EtOH and cooled down to 0 ˚C. A precipitate was formed and filtrated with cold EtOH. The product was recrystallized from EtOH to afford pure ketone.

Ketone (10 mmol) was dissolved in a 3:1 mixture of THF/H_2O (15 mL) and cooled down to 0 ºC. $NaBH_4$ (3 equiv) was carefully added and the mixture was allowed to reach rt and stir at this temperature for 2 h. After completion of the reaction (by TLC) water and CH_2Cl_2 were added and the mixture was extracted with CH_2Cl_2 (x3). The organic layer was dried over $MgSO_4$, filtered and concentrated under vacuo to give alcohol products pure enough to be used without further purification.
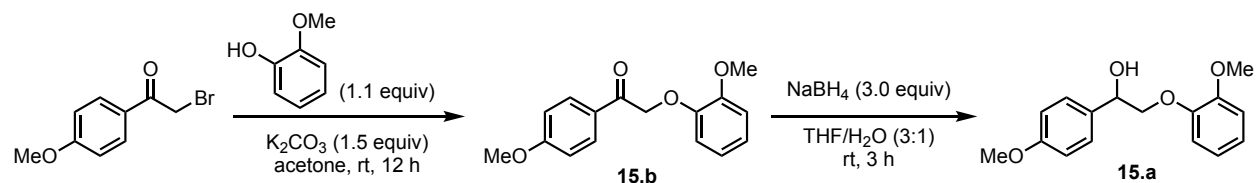
2-(2-methoxyphenoxy)-1-(4-methoxyphenyl)ethan-1-ol (15.a) was synthesized following the general procedure.

TLC (EtOAc/Hex, 1:1), R_f	0.4;
^{1}H NMR (500 MHz, CDCl$_3$) δ:	7.37 (d, J = 8.5 Hz, 2H), 7.04 – 6.97 (m, 1H), 6.97 – 6.87 (m, 5H), 5.07 (dd, J = 9.5, 2.7 Hz, 1H), 4.16 (dd, J = 10.0, 2.8 Hz, 1H), 3.97 (t, J = 9.8 Hz, 1H), 3.90 (s, 3H), 3.82 (s, 3H);
^{13}C NMR (126 MHz, CDCl$_3$) δ:	159.4, 149.9, 148.0, 131.7, 127.5 (2xCH), 122.3, 121.1, 115.5, 113.9 (2xCH), 112.0, 76.0, 71.9, 55.8, 55.3;
Physical appearance:	white solid
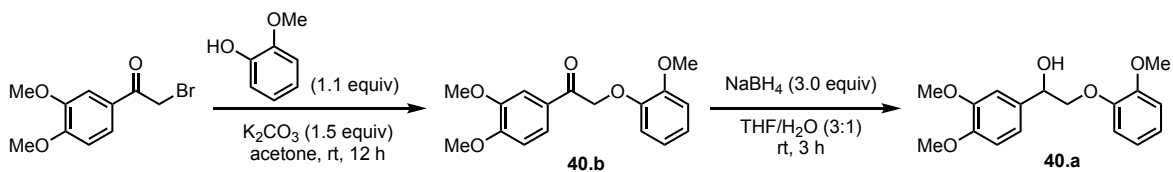
1-(3,4-dimethoxyphenyl)-2-(2-methoxyphenoxy)ethan-1-ol (40.a) was synthesized following the general procedure.

TLC (EtOAc/Hex, 4565), R_f 0.26;

^{1}H NMR (500 MHz, CDCl$_3$) δ: 7.02 – 6.98 (m, 2H), 6.97 – 6.89 (m, 4H), 6.86 (d, J = 8.2 Hz, 1H), 5.05 (d, J = 9.3 Hz, 1H), 4.17 (dd, J = 10.0, 2.9 Hz, 1H), 3.97 (t, J = 9.7 Hz, 1H), 3.90 (s, 3H), 3.89 (s, 3H), 3.88 (s, 3H), 3.40 (d, J = 1.8 Hz, 1H)

^{13}C NMR (176 MHz, CDCl$_3$) δ: 150.1, 149.1, 148.7, 147.9, 132.1, 122.6, 121.1, 118.6, 116.1, 111.9, 111.0, 109.3, 76.4, 72.1, 55.9, 55.9, 55.8.

Physical apperance: white solid.
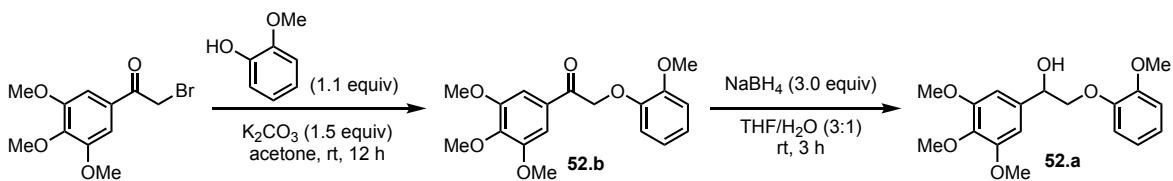
2-(2-methoxyphenoxy)-1-(3,4,5-trimethoxyphenyl)ethan-1-ol (52.a) was synthesized following the general procedure.

Characterization for 52.b

TLC (EtOAc/Hex, 35:65), R_f : 0.30;

^{1}H NMR (500 MHz, CDCl$_3$) δ: 7.31 (s, 2H), 6.97 – 6.92 (m, 1H), 6.89 (d, $J = 7.8$ Hz, 1H), 6.83 (d, $J = 4.0$ Hz, 2H), 5.24 (s, 2H), 3.90 (s, 3H), 3.88 (s, 6H), 3.85 (s, 3H);

^{13}C NMR (126 MHz, CDCl$_3$) δ: 193.8, 153.1 (2xC), 149.7, 147.3, 143.1, 129.8, 122.5, 120.8, 114.6, 112.1, 105.9 (2xCH), 72.4, 61.0, 56.3 (2xCH$_3$), 55.8;

HRMS (ESI): m/z calculated for C$_{18}$H$_{21}$O$_6^+$ [M+H]$^+$: 333.1333, found 333.1333;

Physical appearance: white solid.

Characterization for 52.a

TLC (EtOAc/Hex, 1:1), R_f : 0.22

^{1}H NMR (500 MHz, CDCl$_3$) δ: 7.02 (dd, $J = 17.1$, 9.8 Hz, 1H), 6.98 – 6.89 (m, 3H), 6.66 (s, 2H), 5.03 (dd, $J = 9.2$, 2.6 Hz, 1H), 4.19 (dd, $J = 10.1$, 2.8 Hz, 1H), 3.97 (t, $J = 9.7$ Hz, 1H), 3.90 (s, 3H), 3.87 (s, 6H), 3.84 (s, 3H).

^{13}C NMR (126 MHz, CDCl$_3$) δ: 153.3 (2xC), 150.1, 147.9, 137.5, 135.3, 122.6, 121.1, 116.1, 112.0, 103.2 (2xCH), 76.3, 72.4, 60.8, 56.1 (2xCH$_3$), 55.8;

HRMS (ESI): m/z calculated for C$_{18}$H$_{22}$NaO$_6^+$ [M+Na]$^+$: 357.1309, found 357.1306;

Physical appearance: yellow wax
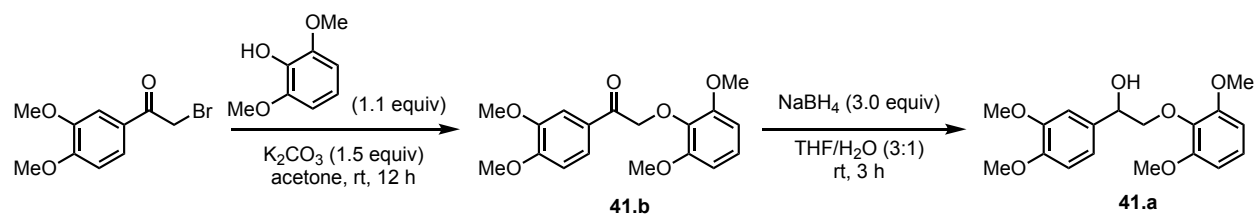
2-(2,6-dimethoxyphenoxy)-1-(3,4-dimethoxyphenyl)ethan-1-ol (41.a) was synthesized following the general procedure.

TLC (EtOAc/Hex, 1:1), R_f	0.38;
^{1}H NMR (500 MHz, CDCl$_3$) δ:	7.06 (t, J = 8.4 Hz, 1H), 6.98 (d, J = 1.5 Hz, 1H), 6.94 – 6.88 (m, 1H), 6.84 (d, J = 8.2 Hz, 1H), 6.63 (d, J = 8.4 Hz, 2H), 4.92 (dd, J = 10.0, 2.4 Hz, 1H), 4.41 (dd, J = 11.0, 2.6 Hz, 1H), 3.90 (s, 9H), 3.87 (s, 3H), 3.71 (t, J = 10.5 Hz, 1H);
^{13}C NMR (126 MHz, CDCl$_3$) δ:	153.2 (2xC), 148.9, 148.5, 136.7, 131.9, 124.0, 118.6, 110.9, 109.3, 105.1 (2xCH), 80.12, 72.18, 56.07, 55.88, 55.84;
HRMS (ESI):	m/z calculated for C$_{18}$H$_{22}$NaO$_6{}^+$ [M+Na]$^+$ 357.1309, found 357.1312;
Physical appearance:	white solid.
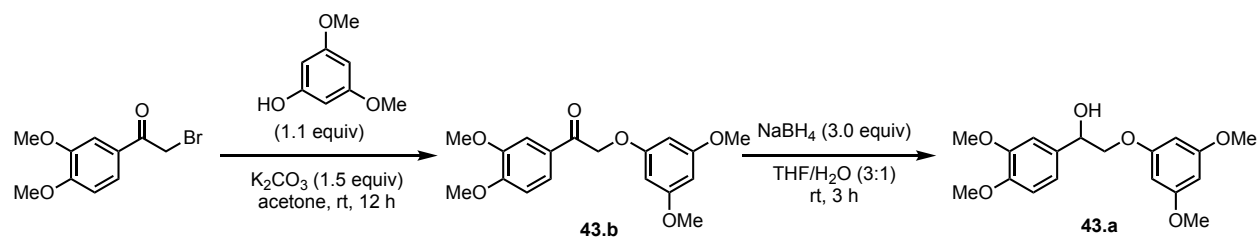
2-(3,5-dimethoxyphenoxy)-1-(3,4-dimethoxyphenyl)ethan-1-ol (43.a) was synthesized following the general procedure.

TLC (EtOAc/Hex, 1:1), R_f	0.44;
^{1}H NMR (500 MHz, CDCl$_3$) δ:	7.02 (d, J = 1.6 Hz, 1H), 6.98 (dd, J = 8.3, 1.5 Hz, 1H), 6.89 (d, J = 8.2 Hz, 1H), 6.12 (s, 3H), 5.07 (dd, J = 8.8, 3.1 Hz, 1H), 4.06 (dd, J = 9.6, 3.2 Hz, 1H), 3.99 (t, J = 9.2 Hz, 1H), 3.92 (s, 3H), 3.90 (s, 3H), 3.77 (s, 6H);
^{13}C NMR (126 MHz, CDCl$_3$) δ:	161.5 (2xC), 160.2, 149.1, 148.9, 132.2, 118.6, 111.1, 109.3, 93.5 (3xCH), 73.4, 72.3, 55.9, 55.9, 55.3 (3xCH$_3$);
HRMS (ESI):	m/z calculated for C$_{18}$H$_{22}$NaO$_6{}^+$ [M+Na]$^+$ 357.1309, found 357.1311;
Physical appearance:	white solid.
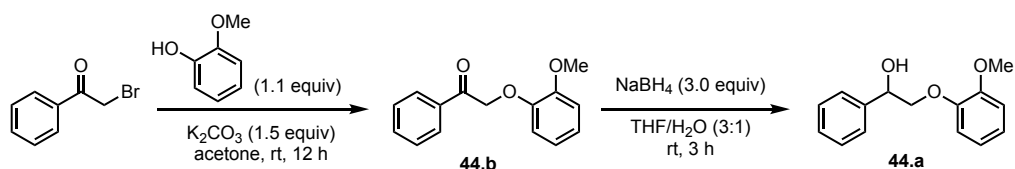
2-(2-methoxyphenoxy)-1-phenylethan-1-ol (44.a) was synthesized following the general procedure.

TLC (EtOAc/Hex, 1:3), R_f : 0.25;

^{1}H NMR (500 MHz, CDCl$_3$) δ: 7.46 (d, J = 7.5 Hz, 2H), 7.39 (t, J = 7.5 Hz, 2H), 7.33 (t, J = 7.2 Hz, 1H), 7.04 – 6.99 (m, 1H), 6.93 (dt, J = 8.1, 4.7 Hz, 3H), 5.13 (d, J = 9.3 Hz, 1H), 4.21 (dd, J = 10.1, 2.8 Hz, 1H), 4.00 (t, J = 9.8 Hz, 1H), 3.91 (s, 3H), 3.48 (br s, 1H);

^{13}C NMR (126 MHz, CDCl$_3$) δ: 150.1, 148.0, 139.5, 128.5 (2xCH), 128.0, 126.3 (2xCH), 122.5, 121.1, 116.0, 112.0, 76.3, 72.3, 55.8.

HRMS (ESI): *m/z* calculated for C$_{16}$H$_{16}$NaO$_3$$^+$ [M+Na]$^+$: 267.0992, found 267.0991;

Physical appearance: colorless oil.

General procedure for the synthesis of diol lignin model substrates

Diols were synthetized following a procedure previously reported by us:[133] ethyl 2-bromoacetate (28.4 mmol) was added to a stirring mixture of the desired phenol derivative (1 equiv) and K_2CO_3 (1 equiv) in acetone (120 mL) under nitrogen atmosphere and the mixture was refluxed overnight. After completion, the mixture was filtered, and the filtrate was concentrated to afford the alkylation products pure enough to be used without further purification.

A solution of acetate alkylation product (13.2 mmol) in THF (5 mL) was slowly added to a solution of LiHMDS (1.1 equiv, 1.0 M in THF) in THF (10 mL) at -78 ˚C under nitrogen atmosphere. Then, a solution of the desired aldehyde (1.0 equiv) in THF (5 mL) was slowly added at -78 ºC and the resulting mixture was stirred for 1 h. A saturated aq. solution of NH_4Cl (10 mL) as added followed by EtOAc (10 mL) and the reaction was let to reach room temperature. The mixture was extracted with EtOAc (x3), and the organics were washed with water and brine, dried over Na_2SO_4, filtered and concentrated. The crude was generally purified by column chromatography (hexanes and EtOAc) to afford pure hydroxyesters.

To a stirring mixture of hydroxyester (5 mmol) in THF/H_2O (3:1, 20 mL) was added $NaBH_4$ (3 equiv) in portions and the mixture was stirred overnight. After completion of the reaction (by TLC) water and CH_2Cl_2 were added and the mixture was extracted with CH_2Cl_2 (x3). The organic layer was dried over $MgSO_4$, filtered and concentrated under vacuo to give diol products, pure enough to be used without further purification.

2-(2-methoxyphenoxy)-1-(4-methoxyphenyl)propane-1,3-diol (16.a) was synthesized following the general procedure.

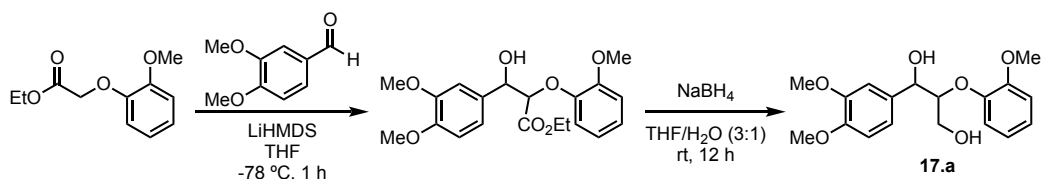|	
TLC (EtOAc/Hex, 1:1), R_f	0.19, 6:4 mixture of diastereomers;
^{1}H NMR (500 MHz, CDCl$_3$) δ:	7.38 (d, J = 8.7 Hz, 2H, major diast.), 7.33 (d, J = 8.6 Hz, 2H, minor diast.), 7.17 – 7.13 (m, 1H, major diast.), 7.11 – 7.04 (m, 1H, major and minor diast.), 7.01 – 6.88 (m, 4H, major diast. and 5 H minor diast.), 5.01 (d, J = 7.2 Hz, 1H, major and 1H minor diast.), 4.17 (dt, J = 5.8, 4.7 Hz, 1H, minor diast.), 4.09 – 3.99 (m, 1H, major diast.), 3.95 (s, 1H, minor diast.), 3.93 (s, 3H, major diast.), 3.90 (s, 3H, minor diast.), 3.82 (s, 3H, major diast.), 3.82 (s, 3H, minor diast.), 3.70 – 3.65 (m, 1H, major diast), 3.63 – 3.59 (m, 1H, major and 1 H minor diast.), 3.47 (ddd, J = 12.4, 8.4, 4.0 Hz, 1H, major diast.), 3.43 (d, J = 3.1 Hz, 1H, minor diast.), 2.75 (dd, J = 7.0, 5.9 Hz, 1H, minor diast.), 2.71 (dd, J = 8.3, 5.1 Hz, 1H, major diast.);
^{13}C NMR (126 MHz, CDCl$_3$) δ:	(126 MHz, CDCl$_3$) δ 159.5/159.1, 151.5/151.2, 147.7/147.0, 132.3/131.8, 128.4/127.4 (2xCH), 124.1/124.0, 121.7/121.60, 120.9/120.7, 114.0/113.8 (2xCH), 112.2/112.2, 89.3/87.1, 73.6/72.7, 61.0/60.8, 55.9/55.9, 55.3/55.3;
Physical appearance:	colorless wax.

1-(3,4-dimethoxyphenyl)-2-(2-methoxyphenoxy)propane-1,3-diol (17.a) was synthesized following the general procedure.

TLC (EtOAc/Hex, 3:1), R_f 0.35, 6:4 mixture of diastereomers;

^{1}H NMR (500 MHz, CDCl$_3$) δ: 7.13 (d, $J = 7.9$ Hz, 1H, minor diast.), 7.07 (d, $J = 3.5$ Hz, 1H, each diast.), 7.02 – 6.87 (m, 6H, major diast and 5H, minor diast.), 6.85 (t, $J = 6.9$ Hz, 1H, each diast.), 4.99 (s, 1H, each diast.), 4.17 (dd, $J = 8.5, 5.2$ Hz, 1H, major diast.), 4.03 (dd, $J = 7.5, 3.6$ Hz, 1H, minor diast.), 3.92 3.90 – 3.87 (m, 10H, major diast. and 9H, minor diast.), 3.71 – 3.60 (m, 1H, major diast. and 2H, minor diast.), 3.53 – 3.46 (m, 1H, minor diast.), 3.45 (t, $J = 5.2$ Hz, 1H, major diast), 2.70 (t, $J = 1.4$ Hz, 1H, each diast.);

^{13}C NMR (126 MHz, CDCl$_3$) δ: 151.3 /151.6, 149.1/149.0, 148.9/148.4, 146.9/147.6, 132.5/132.1, 124.2/124.2, 121.7/121.6, 120.9/121.0, 119.6/118.4, 112.1/112.1, 111.0/111.0, 109.9/109.2, 89.4/87.3, 72.7/72.7, 60.7/60.7, 55.9/55.9 (3xCH$_3$);

Physical appearance: colorless wax.

2-(2-methoxyphenoxy)-1-(3,4,5-trimethoxyphenyl)propane-1,3-diol (45.a) was synthesized following the general procedure.

TLC (EtOAc/Hex, 1:1), R_f	0.08, 4:1 mixture of diastereomers;
^{1}H NMR (500 MHz, CDCl$_3$) δ:	7.07 – 7.00 (m, 1H, each diast.), 6.96 – 6.85 (m, 3H, major diast. and 2H, minor diast.), 6.66 (s, 2H, minor diast.), 6.60 (s, 2H, major diast.), 4.96 (s, 1H, minor diast), 4.94 (d, J = 4.6 Hz, 1H, major diast), 4.15 (dd, J = 8.7, 5.0 Hz, 1H, major diast.), 4.06 – 4.01 (m, 1H, minor diast.), 3.91 (dd, J = 12.1, 5.7 Hz, 1H, each diast.), 3.87 (t, J = 4.9 Hz, 1H, each diast.), 3.86 – 3.83 (m, 4H, each diast.), 3.83 – 3.80 (m, 8H, each diast.), 3.68 (d, J = 13.4 Hz, 1H, each diast.), 3.51 (d, J = 12.0 Hz, 1H, minor diast), 2.96 (br s, 1H, each diast.);
^{13}C NMR (126 MHz, CDCl$_3$) δ:	153.1/153.1 (2xC), 151.3/151.1, 147.3 /146.7, 137.5/137.5, 135.5/135.1, 124.1/124.0, 121.5/121.5, 120.7/120.6, 112.0/103.6, 103.8/102.9 (2xCH), 86.9/89.0, 74.0/72.8, 60.9/60.7, 60.9/60.7, 56.2/56.0 (2xCH$_3$), 56.0/55.7;
Physical appearance:	colorless wax.

2-(2,6-dimethoxyphenoxy)-1-(3,4-dimethoxyphenyl)propane-1,3-diol (42.a) was synthesized following the general procedure.

TLC (EtOAc/Hex, 2:1), R_f	0.33, 85:15 mixture of diastereomers;
^{1}H NMR (500 MHz, CDCl$_3$) δ:	7.10 (t, J = 8.4 Hz, 7H, both diast.), 7.02 (s, 1H, minor diast.), 6.97 (s, 1H, major diast.), 6.84 (s, 2H, each diast.), 6.67 (d, J = 8.4 Hz, 2H, each diast.), 5.08 (d, J = 8.8 Hz, 1H, minor diast.), 5.04 (d, J = 3.6 Hz, 1H, major diast.), 4.21 – 4.14 (m, 1H, major diast.), 3.93 (d, J = 7.3 Hz, 1H, minor diast.), 3.90 (s, 9H, each diast.), 3.88 (s, 3H, each diast.), 3.63 – 3.55 (m, 1H, minor diast.), 3.51 (dd, J = 12.0, 2.6 Hz, 1H, major diast.), 3.32 (d, J = 12.6 Hz, 1H, minor diast.);
^{13}C NMR (126 MHz, CDCl$_3$) δ:	153.5/153.2 (2xC), 148.9/148.9, 148.7/148.1, 135.2/134.9, 132.6/131.9, 124.5/124.5, 119.8/118.1, 110.9/110.2, 108.9/108.9, 105.2/105.2 (2xCH), 89.0/87.0, 74.0/72.4, 60.6/60.4, 56.1/56.1 (2xCH$_2$), 55.9/55.9 (2xCH$_2$);
HRMS (ESI):	m/z calculated for C$_{19}$H$_{24}$NaO$_7^+$ [M+Na]$^+$: 387.1414, found 387.1415
Physical appearance:	colorless wax.

2-(3,5-dimethoxyphenoxy)-1-(3,4-dimethoxyphenyl)propane-1,3-diol (53.a) was synthesized following the general procedure.

TLC (EtOAc/Hex, 3:1), R_f	0.34, 7:3 mixture of diastereomers;
^{1}H NMR (500 MHz, CDCl$_3$) δ:	6.99 (dd, J = 13.3, 9.9 Hz, 2H), 6.87 (dd, J = 8.0, 4.7 Hz, 1H), 6.18 (d, J = 1.8 Hz, 0.7H, major diast.), 6.14 (s, 0.3H, minor diast.), 6.12 – 6.08 (m, 2H), 5.06 (d, J = 4.8 Hz, 0.7H, major diast.), 5.01 (d, J = 6.5 Hz, 0.3H, minor diast.), 4.42 – 4.36 (m, 1H), 3.97 (d, J = 11.9 Hz, 0.7H, major diast.), 3.93 – 3.85 (m, 7H), 3.85 – 3.81 (m, 0.3H, minor diast), 3.80 – 3.75 (m, 5H), 3.74 – 3.67 (m, 0.7H, major diast.), 3.60 (s, 0.3H, minor diast.), 2.74 (s, 0.3H, minor diast.), 2.66 (s, 0.7H, major diast.), 2.12 (s, 0.7H, major diast.), 1.72 (s, 0.3H, minor diast.);
^{13}C NMR (126 MHz, CDCl$_3$) δ:	161.6/161.5 (2xC), 159.8/159.4 (C), 149.1/149.0 (C), 148.9/148.7 (C), 132.8/132.0 (C), 119.3/118.6 (CH), 111.0/110.9 (CH), 109.8/109.3 (CH), 95.2/95.2 (2xCH), 94.0/93.9 (CH), 82.9/81.8 (CH), 73.9/73.7 (CH), 61.4/61.1 (CH$_2$), 55.9/55.9 (2xCH$_3$), 55.4/55.3 (2xCH$_3$);
HRMS (ESI):	m/z calculated for C$_{19}$H$_{24}$NaO$_7^+$ [M+Na]$^+$: 387.1414, found 387.1408
Physical appearance:	colorless wax.

2-phenoxy-1-(3,4,5-trimethoxyphenyl)propane-1,3-diol (54.a) was synthesized following the general procedure.

TLC (EtOAc/Hex, 1:1), R_f

0.19, 7:3 mixture of diastereomers;
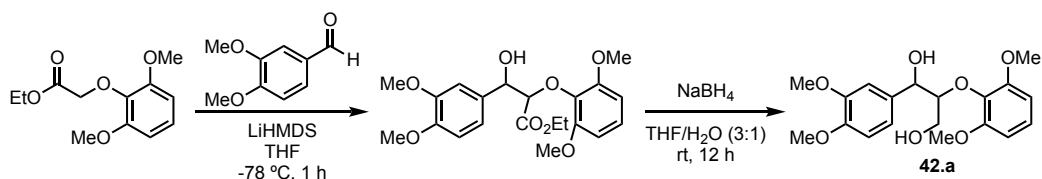
^{1}H NMR (500 MHz, CDCl$_3$) δ:

7.27 – 7.23 (m, 1H, major diast.), 7.21 (t, J = 7.9 Hz, 1H major and 2H minor diast.), 6.99 – 6.90 (m, 1H major and 3H minor diast.), 6.84 (d, J = 8.1 Hz, 2H mjor diast.), 6.64 (s, 2H, minor diast.), 6.60 (s, 2H, major diast.), 4.95 (s, 1H major and 1H minor diast.), 4.39 (dd, J = 9.8, 4.4 Hz, 1H, minor diast.), 4.35 (d, J = 4.3 Hz, 1H, major diast.), 3.97 – 3.91 (m, 1H, major diast.), 3.91 – 3.84 (m, 1H major and 1H minor diast.), 3.80 (s, 3H major and 3H minor diast.), 3.78 (s, 6H major and 6H minor diast.), 3.61 (dt, J = 11.1, 7.8 Hz, 1H, minor diast.), 3.44 (br s, 1H, major diast.), 3.22 (br s, 1H, minor diast.), 2.71 (br s, 1H, major diast.), 2.36 (br s, 1H, minor diast.);

^{13}C NMR (126 MHz, CDCl$_3$) δ:

158.0/157.7, 153.2/153.1 (2xC), 137.6/137.4, 136.3/135.5, 129.7/129.6 (2xCH), 121.9/121.8, 116.5/116.4 (2xCH), 103.8/103.4 (2xCH), 82.5/81.7, 74.2/73.7, 61.6/61.2, 60.8/60.8, 56.1/56.1 (2xCH$_3$);

HRMS (ESI):

m/z calculated for C$_{18}$H$_{22}$NaO$_6^+$ [M+Na]$^+$: 357.1309, found 357.1312

Physical appearance:

white solid.

Synthesis of triol model system (47.a)

Synthesis of 2-(4-acetylphenoxy)-1-(3,4-dimethoxyphenyl)ethan-1-one. A round bottom flask equipped with a reflux condenser and a stir bar was charged with 2-bromo-1-(3,4-dimethoxyphenyl)ethan-1-one (1.00 g, 3.84 mmol), K_2CO_3 (800 mg, 5.79 mmol), 4-hydroxyacetophenone (578 mg, 4.25 mmol), and acetone (10 mL). The resulting suspension was stirred at room temperature for 12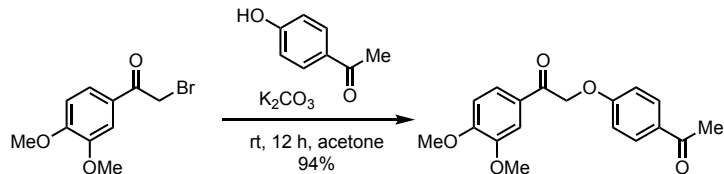 h under a nitrogen atmosphere, and then filtered to remove the inorganics and concentrated *in vacuo*. The resulting solid was purified by column chromatography (hexanes/EtOAc 1:1) to afford the title compound as an off-white solid (1.14 g, 94%). Spectral data are consistent with those reported in the literature.[91]

TLC (EtOAc/Hex, 1:1), R_f	0.31;
^{1}H NMR (500 MHz, CDCl$_3$) δ:	7.91 (d, J = 8.5 Hz, 2H), 7.63 (d, J = 8.4 Hz, 1H), 7.54 (s, 1H), 6.95 (d, J = 8.5 Hz, 2H), 6.91 (d, J = 8.4 Hz, 1H), 5.32 (s, 2H), 3.96 (s, 3H), 3.93 (s, 3H), 2.53 (s, 3H);
^{13}C NMR (126 MHz, CDCl$_3$) δ:	196.8, 192.2, 162.0, 154.2, 149.5, 131.1, 130.7 (2C), 127.5, 122.8, 114.5 (2C), 110.3, 110.2, 70.4, 56.3, 56.2, 26.5.
HRMS (ESI):	*m/z* calculated for $C_{18}H_{19}O_5^+$ [M+H]$^+$: 315.1227, found: 315.1230.

Synthesis of 2-(4-acetylphenoxy)-1-(3,4-dimethoxyphenyl)-3-hydroxypropan-1-one. Substrate (1.07 g, 3.40 mmol) was added to a bottom flask and dissolved in acetone/EtOH (20 mL, 1:1). K_2CO_3 (509 mg, 3.70 mmol) was subsequently added and the mixture was stirred for 5 min. Then, formalin (37 wt%, 400 µL, 5.10 mmol) was added and the reaction mixture was stirred for 2 h. After concentrating the mixture, the crude reaction mixture was extracted with EtOAc (×3), washed with water and brine, dried over Na_2SO_4, filtered and concentrated under reduced pressure. The crude was purified by column chromatography (hexanes/EtOAc 4:1 to 1:1) to afford **2k** as a pale yellow solid (638 mg, 51%). Spectral data are consistent with those reported in the literature.**Error! Bookmark not defined.**

1-(3,4-dimethoxyphenyl)-2-(4-(1-hydroxyethyl)phenoxy)propane-1,3-diol (47.a). 2-(4-Acetylphenoxy)-1-(3,4-dimethoxyphenyl)-3-hydroxypropan-1-one (490 mg, 1.45 mmol) was dissolved in THF/H_2O (4.0 mL, 3:1). The resulting solution was cooled down to 0 °C and $NaBH_4$ (555 mg, 14.5 mmol) was added in small portions over 5 min. After complete addition, the reaction mixture was warmed up to room temperature and stirred for 4 h. Then, additional H_2O was added and the mixture was extracted with CH_2Cl_2 (×3), washed with water (×2) and brine, dried over Na_2SO_4, filtered and concentrated under reduced pressure. The crude mixture was purified by column chromatography (hexanes/EtOAc/EtOH 70:23:7) to afford the product as a mixture of diastereomers (*erythro*:*threo* 5:2) as a pale yellow solid (387 mg, 77%).

Characterization for the major diastereomer
TLC (EtOAc/Hex/EtOH, 23:70:7), 0.25;
R_f

^{1}H NMR (500 MHz, CDCl$_3$) δ:	7.31 (d, J = 8.6 Hz, 2H), 7.01–6.96 (m, 3H), 6.88 (d, J = 8.5 Hz, 1H), 6.86 (d, J = 8.5 Hz, 1H), 5.00 (dd, J = 6.8, 2.9 Hz, 1H), 4.90–4.82 (m, 1H), 4.43–4.38 (m, 1H), 3.88 (s, 6H), 3.84–3.79 (m, 1H), 3.63–3.57 (m, 1H), 2.74 (d, J = 2.9 Hz, 1H), 1.73–1.68 (m, 2H), 1.48 (d, J = 6.6 Hz, 3H);
^{13}C NMR (126 MHz, CDCl$_3$) δ:	157.6, 149.2, 149.0, 139.5, 132.3, 127.0 (2C), 119.4, 116.5 (2C), 111.2, 110.0, 83.2, 73.8, 69.9, 61.3, 56.0 (2C), 25.2;
HRMS (ESI):	*m/z* calculated for $C_{19}H_{24}NaO_6^+$ ([M+Na]$^+$): 371.1465, found: 371.1454.

Reactions for the oxidation of lignin model substrates

General procedure for Pd-mediated oxidation[107]

Under air, a round bottom flask equipped with a stir bar and a reflux condenser was charged with Pd(OAc)$_2$ (0.02 mmol, 4.50 mg, 0.05 equiv), lignin system (0.4 mmol) and DMSO (1.0 mL). The resulting solution was stirred at 65 °C for 18 h under atmospheric air. Upon completion of the reaction, H$_2$O and CH$_2$Cl$_2$ were added to the reaction mixture. The phases were separated, and the aqueous layer was additionally extracted with CH$_2$Cl$_2$ (×3). The combined organic phases were washed with 5% aq. LiCl (×3) and brine (×2), dried over Na$_2$SO$_4$ and filtered. The solvent was removed *in vacuo* to give the crude product as a colorless oil, which was purified by silica gel chromatography (EtOAc/hexanes) to afford the requisite ketone.

15.b

2-(2-methoxyphenoxy)-1-(4-methoxyphenyl)ethan-1-one (15.b) was synthesized following the general procedure for Pd-mediated oxidation, 97%

TLC (EtOAc/Hex, 1:3), R_f 0.20;

^{1}H NMR (500 MHz, CDCl$_3$) δ: 8.01 (d, J = 8.8 Hz, 2H), 6.98 – 6.93 (m, 3H), 6.91 (d, J = 8.0 Hz, 1H), 6.86 – 6.83 (m, 2H), 5.28 (s, 2H), 3.88 (s, 3H), 3.87 (s, 3H);

^{13}C NMR (126 MHz, CDCl$_3$) δ: 193.1, 163.9, 149.7, 147.6, 130.5 (2C), 127.7, 122.3, 120.8, 114.7, 113.9 (2C), 112.2, 72.0, 55.9, 55.5;

HRMS (ESI): m/z calculated for C$_{16}$H$_{16}$NaO$_4^+$ [M+Na]$^+$: 295.0941, found: 295.0934;

Physical appearance: off-white solid.

16.b

3-hydroxy-2-(2-methoxyphenoxy)-1-(4-methoxyphenyl)propan-1-one (16.b) was synthesized following the general procedure for Pd-mediated oxidation, 84%.

TLC (EtOAc/Hex, 1:1), R_f 0.26;

^{1}H NMR (500 MHz, CDCl$_3$) δ: 8.07 (d, J = 8.7 Hz, 2H), 7.01 (t, J = 7.7 Hz, 1H), 6.94 (d, J = 8.7 Hz, 2H), 6.93–6.89 (m, 2H), 6.82 (t, J = 7.7 Hz, 1H), 5.37 (t, J = 5.2 Hz, 1H), 4.06 (d, J = 5.2 Hz, 2H), 3.87 (s, 3H), 3.86 (s, 3H), 2.28 (br, 1H);

^{13}C NMR (126 MHz, CDCl$_3$) δ: 195.1, 164.2, 150.8, 147.2, 131.5 (2C), 128.1, 123.9, 121.3, 119.1, 114.1 (2C), 112.5, 85.0, 63.8, 56.0, 55.7;

HRMS (ESI):   *m/z* calculated for C$_{17}$H$_{19}$O$_5^+$ [M+H]$^+$: 303.1227, found: 303.1238;

Physical appearance: off-white solid.

1-(3,4-dimethoxyphenyl)-2-(2-methoxyphenoxy)ethan-1-one (40.b) was synthesized following the general procedure for Pd-mediated oxidation, 98%.

TLC (EtOAc/Hex, 1:1), R_f 0.48;

^{1}H NMR (500 MHz, CDCl$_3$) δ: 7.68 (dd, J = 8.4, 1.9 Hz, 1H), 7.60 (d, J = 1.9 Hz, 1H), 6.96 (ddd, J = 8.3, 5.8, 3.0 Hz, 1H), 6.92 (dd, J = 8.3, 1.2 Hz, 1H), 6.90 (d, J = 8.4 Hz, 1H), 6.86–6.84 (m, 2H), 5.30 (s, 2H), 3.96 (s, 3H), 3.94 (s, 3H), 3.89 (s, 3H);

^{13}C NMR (126 MHz, CDCl$_3$) δ: 195.1, 164.2, 150.8, 147.2, 131.5 (2C), 128.1, 123.9, 121.3, 119.1, 114.1 (2C), 112.5, 85.0, 63.8, 56.0, 55.7;

HRMS (ESI): m/z calculated for C$_{17}$H$_{18}$NaO$_5^+$ [M+Na]$^+$: 325.1046, found: 325.1042;

Physical appearance: off-white solid.

17.b

1-(3,4-dimethoxyphenyl)-3-hydroxy-2-(2-methoxyphenoxy)propan-1-one (17.b) was synthesized following the general procedure for Pd-mediated oxidation, 89%.

TLC (EtOAc/Hex, 2:1), R_f	0.23;
^{1}H NMR (500 MHz, CDCl$_3$) δ:	7.75 (dd, J = 8.4, 1.9 Hz, 1H), 7.61 (d, J = 1.9 Hz, 1H), 7.01–6.97 (m, 1H), 6.92–6.86 (m, 3H), 6.84–6.79 (m, 1H), 5.40 (t, J = 5.3 Hz, 1H), 4.07 (d, J = 5.3 Hz, 2H), 3.94 (s, 3H), 3.91 (s, 3H), 3.85 (s, 3H), 3.02 (br, 1H);
^{13}C NMR (126 MHz, CDCl$_3$) δ:	195.1, 154.1, 150.6, 149.3, 147.1, 128.2, 123.8, 123.8, 121.3, 118.7, 112.5, 111.1, 110.3, 84.7, 63.9, 56.2, 56.1, 55.9;
HRMS (ESI):	m/z calculated for C$_{18}$H$_{21}$O$_6^+$ [M+H]$^+$: 333.1333, found: 333.1331;
Physical appearance:	off-white solid.

41.b

2-(2,6-dimethoxyphenoxy)-1-(3,4-dimethoxyphenyl)ethan-1-one (41.b) was synthesized following the general procedure of Pd-mediated oxidation, 96%.
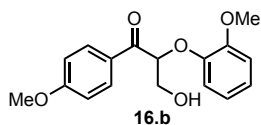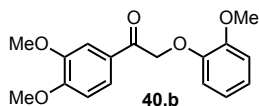
TLC (EtOAc/Hex, 1:1), R_f	0.41;
^{1}H NMR (500 MHz, CDCl$_3$) δ:	7.73 (dd, J = 8.4, 1.9 Hz, 1H), 7.65 (d, J = 1.9 Hz, 1H), 7.01 (t, J = 8.4 Hz, 1H), 6.89 (d, J = 8.4 Hz, 1H), 6.58 (d, J = 8.4 Hz, 2H), 5.15 (s, 2H), 3.95 (s, 3H), 3.94 (s, 3H), 3.81 (s, 6H);
^{13}C NMR (126 MHz, CDCl$_3$) δ:	193.7, 153.4, 153.3 (2C), 149.0, 136.7, 128.4, 124.0, 123.1, 110.7, 110.0, 105.4 (2C), 75.3, 56.1 (2C), 56.0 (2C);
HRMS (ESI):	m/z calculated for C$_{18}$H$_{20}$NaO$_6^+$ [M+Na]$^+$: 355.1152, found: 355.1148;
Physical appearance:	off-white solid.

42.b

2-(2,6-dimethoxyphenoxy)-1-(3,4-dimethoxyphenyl)-3-hydroxypropan-1-one (42.b) was synthesized following the general procedure of Pd-mediated oxidation, 87%.
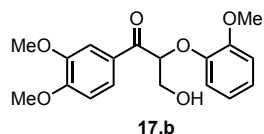
TLC (EtOAc/Hex, 2:1), R_f 0.40;

^{1}H NMR (500 MHz, CDCl$_3$) δ: 7.73 (dd, J = 8.4, 1.9 Hz, 1H), 7.67 (d, J = 1.9 Hz, 1H), 7.02 (t, J = 8.4 Hz, 1H), 6.88 (d, J = 8.4 Hz, 1H), 6.58 (d, J = 8.4 Hz, 2H), 5.09 (dd, J = 7.8, 3.0 Hz, 1H), 4.01 (dd, J = 11.8, 7.8 Hz, 1H), 3.95 (s, 3H), 3.94 (s, 3H), 3.83 (dd, J = 11.8, 3.0 Hz, 1H), 3.73 (s, 6H);

^{13}C NMR (126 MHz, CDCl$_3$) δ: 194.9, 153.4, 152.7 (2C), 149.1, 136.7, 128.7, 124.2, 123.4, 110.9, 110.0, 105.2 (2C), 87.6, 63.7, 56.1, 56.0, 55.9 (2C);

HRMS (ESI): m/z calculated for C$_{19}$H$_{23}$O$_7^+$ [M+H]$^+$: 363.1438, found: 363.1439;

Physical appearance: colorless, sticky oil.

43.b

2-(3,5-dimethoxyphenoxy)-1-(3,4-dimethoxyphenyl)ethan-1-one (43.b) was synthesized following the general procedure for Pd-mediated oxidation, 93%.

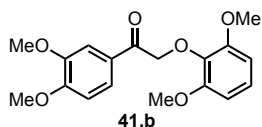|	
TLC (EtOAc/Hex, 1:1), R_f	0.49;
^{1}H NMR (500 MHz, CDCl$_3$) δ:	7.63 (dd, J = 8.4, 1.9 Hz, 1H), 7.55 (d, J = 1.9 Hz, 1H), 6.90 (d, J = 8.4 Hz, 1H), 6.13 (d, J = 2.1 Hz, 2H), 6.11 (t, J = 2.1 Hz, 1H), 5.18 (s, 2H), 3.96 (s, 3H), 3.93 (s, 3H), 3.75 (s, 6H);
^{13}C NMR (126 MHz, CDCl$_3$) δ:	192.7, 161.5 (2C), 159.9, 153.9, 149.3, 127.7, 122.7, 110.3, 110.1, 93.8 (2C), 93.7, 70.6, 56.1, 56.0, 55.4 (2C);
HRMS (ESI):	m/z calculated for C$_{18}$H$_{21}$O$_6{}^+$ [M+H]$^+$: 333.1333, found: 333.1325
Physical appearance:	off-white solid.

44.b

2-(2-methoxyphenoxy)-1-phenylethan-1-one (44.b) was synthesized following the general procedure for Pd-mediated oxidation, 92%.

TLC (EtOAc/Hex, 1:2), R_f　　　　0.54;

^{1}H NMR (500 MHz, CDCl$_3$) δ:　　8.01 (d, J = 7.5 Hz, 2H), 7.60 (t, J = 7.5 Hz, 1H), 7.49 (t, J = 7.5 Hz, 2H), 6.99 – 6.95 (m, 1H), 6.92 (d, J = 8.0 Hz, 1H), 6.85 (d, J = 4.4 Hz, 2H), 5.34 (s, 2H), 3.88 (s, 3H);

^{13}C NMR (126 MHz, CDCl$_3$) δ:　　194.6, 149.8, 147.5, 134.7, 133.7, 128.8 (2C), 128.1 (2C), 122.5, 120.8, 115.0, 112.2, 72.2, 55.9;

HRMS (ESI):　　　　*m/z* calculated for C$_{15}$H$_{14}$NaO$_3$$^+$ [M+Na]$^+$: 265.0835, found: 265.0831;

Physical appearance:　　　　white solid.
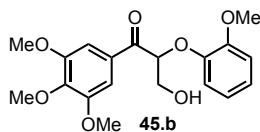
3-hydroxy-2-(2-methoxyphenoxy)-1-(3,4,5-trimethoxyphenyl)propan-1-one (45.b) was synthesized following the general procedure for Pd-mediated oxidation, 91%.
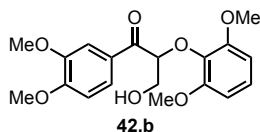
TLC (EtOAc/Hex, 2:1), R_f 0.40;

^{1}H NMR (500 MHz, CDCl$_3$) δ: 7.36 (s, 2H), 7.01 (ddd, J = 8.1, 7.5, 1.5 Hz, 1H), 6.92 (dd, J = 8.1, 1.2 Hz, 1H), 6.91 (dd, J = 8.0, 1.5 Hz, 1H), 6.84 (ddd, J = 8.0, 7.5, 1.2 Hz, 1H), 5.35 (dd, J = 5.7, 4.8 Hz, 1H), 4.09 (d, J = 5.7 Hz, 1H), 4.09 (d, J = 4.8 Hz, 1H), 3.92 (s, 3H), 3.87 (s, 6H), 3.85 (s, 3H), 2.86 (br, 1H);

^{13}C NMR (126 MHz, CDCl$_3$) δ: 195.6, 153.1 (2C), 150.5, 146.8, 143.3, 130.0, 123.7, 121.2, 118.4, 112.3, 106.6 (2C), 84.6, 63.5, 60.9, 56.3 (2C), 55.7;

HRMS (ESI): m/z calculated for C$_{19}$H$_{23}$O$_7^+$ [M+H]$^+$: 363.1438, found: 363.1446

Physical appearance: pale, yellow oil.

46.b
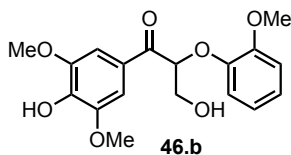
3-hydroxy-1-(4-hydroxy-3,5-dimethoxyphenyl)-2-(2-methoxyphenoxy)propan-1-one (46.b) was synthesized following the general procedure for Pd-mediated oxidation, 85%.
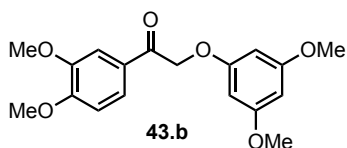
TLC (EtOAc/Hex, 1:4), R_f	0.07;
^{1}H NMR (500 MHz, CDCl$_3$) δ:	7.42 (s, 2H), 7.01 (ddd, J = 8.1, 7.4, 1.5 Hz, 1H), 6.92 (dd, J = 8.1, 1.2 Hz, 1H), 6.91 (dd, J = 8.0, 1.5 Hz, 1H), 6.84 (ddd, J = 8.0, 7.4, 1.2 Hz, 1H), 6.00 (s, 1H), 5.34 (dd, J = 6.4, 4.4 Hz, 1H), 4.09 (d, J = 6.4 Hz, 1H), 4.08 (d, J = 4.4 Hz, 1H), 3.92 (s, 6H), 3.86 (s, 3H);
^{13}C NMR (126 MHz, CDCl$_3$) δ:	195.3, 150.6, 147.0 (2C), 146.9, 140.6, 126.6, 123.9, 121.4, 118.5, 112.4, 106.6 (2C), 84.8, 63.8, 56.6 (2C), 55.9;
HRMS (ESI):	m/z calculated for C$_{18}$H$_{21}$O$_7^+$ [M+H]$^+$: 349.1282, found: 349.1285;
Physical appearance:	colorless solid.
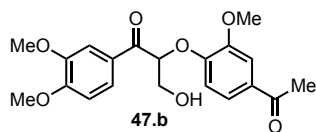
2-(4-acetyl-2-methoxyphenoxy)-1-(3,4-dimethoxyphenyl)-3-hydroxypropan-1-one (47.b) was synthesized following the general procedure for Pd-mediated oxidation, 78%.
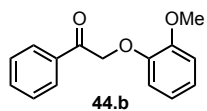
TLC (EtOAc/Hex, 2:1), R_f	0.21;
^{1}H NMR (500 MHz, CDCl$_3$) δ:	7.89 (d, $J = 8.9$ Hz, 2H), 7.74 (dd, $J = 8.4$, 1.9 Hz, 1H), 7.56 (d, $J = 1.9$ Hz, 1H), 6.92 (d, $J = 8.9$ Hz, 2H), 6.91 (d, $J = 8.4$ Hz, 1H), 5.63 (dd, $J = 6.2$, 3.9 Hz, 1H), 4.21 (dd, $J = 12.2$, 3.9 Hz, 1H), 4.15 (dd, $J = 12.2$, 6.2 Hz, 1H), 3.96 (s, 3H), 3.91 (s, 3H), 2.52 (s, 3H);
^{13}C NMR (126 MHz, CDCl$_3$) δ:	196.8, 194.0, 161.2, 154.5, 149.6, 131.4, 130.9 (2C), 127.6, 123.6, 114.9 (2C), 110.9, 110.4, 81.1, 63.7, 56.3, 56.2, 26.5;
HRMS (ESI):	m/z calculated for C$_{19}$H$_{21}$O$_6^+$ [M+H]$^+$: 345.1333, found: 345.1331;
Physical appearance:	pale yellow solid

Reaction conditions for redox-neutral fragmentation strategies

General procedure for reactions in Tables 6 – 10

Starting material was dissolved in the solvent of choice (0.05 M) in a 1 dr vial equipped with a Teflon coated magnetic stir bar, followed by the addition of photocatalyst (2 mol%), and then any exogenous reagents. Each reaction had argon gas bubbled through the solution for at least 60 s before sealing with a cap and parafilm. For volatile solvents, the solvent was removed by reduced pressure and then dried by high vacuum to afford the crude residue. For high-boiling solvents, the reaction solution was added to water (5x the volume) and the aqueous phase was extracted with 5 mL EtOAc (5x). The organic layers were then combined, washed twice with 5% $LiCl_{aq}$, once with brine, dried over magnesium, filtered, and concentrated under reduced pressure and high vacuum. The crude residue was dissolved in a minimal amount of $CDCl_3$, to which internal standard (1,4-dimethoxybenzene) was added. The resulting solution was diluted in a small aliquot of $CDCl_3$ in an NMR tube and ^{1}HNMR analysis was used to calculated starting material conversion.

Characterization of fragmentation products

This section describes the characterization of the fragmentation products and shows the yields for the product with respect to the procedure used to obtain said product. General procedures 1, 4, and 5 start from the ketone oxidation-state starting materials, whereas the general procedures 2 and 3 start from the alcohol oxidation-state starting materials.

General procedure for fragmentation 1 (GP 1) – Ir-mediated fragmentation in EtOH

Phenyl ketone (0.50 mmol – 1.0 mmol) was added to a round bottom flask or 4-dram vial with ^{i}Pr$_2$EtN (2.0 equiv), HCO$_2$H (1.0 equiv) and photocatalyst [Ir(ppy)$_2$(dtbbpy)]PF$_6$ (1 mol%). The reactants were diluted in EtOH (5 mL, 0.20 M in starting material), and irradiated by 1x4 W Blue LED strip until reaction completion (6-96 hours). At this point the ethanol was evaporated *in vacuo*, and the resulting oil was diluted in water and extracted with ethyl acetate. The organic portion was washed with 4 N HCl$_{aq}$, saturated sodium bicarbonate solution, brine and finally dried with sodium sulfate, after which it was concentrated to an oil. If the starting material contained acetophenone as the phenacyl fragment, 1 eq. of PhTMS was added to the oil and the mixture was diluted in CDCl$_3$. This was analyzed via ^{1}H NMR to obtain an accurate acetophenone yield. If the starting material yields an acetophenone derivative heavier than acetophenone, then the PhTMS standardization step was omitted. The crude reaction was purified by silica chromatography to afford the fragmentation products.

General procedure for fragmentation 2 (GP 2) – Pd-mediated oxidation and Ir-mediated fragmentation

Under air, a round bottom flask equipped with a stir bar and a reflux condenser was charged with Pd(OAc)$_2$ (0.02 mmol, 4.50 mg, 0.05 equiv), lignin system (0.4 mmol) and DMSO (1.0 mL). The resulting solution was stirred at 65 °C for 18 h under atmospheric air. Upon completion of the reaction, H$_2$O and CH$_2$Cl$_2$ were added to the reaction mixture. The phases were separated, and the aqueous layer was additionally extracted with CH$_2$Cl$_2$ (×3). The combined organic phases were washed with 5% aq. LiCl (×3) and brine (×2), dried over Na$_2$SO$_4$ and filtered. The solvent was removed *in vacuo* and the crude residue was combined with MeCN (1.0 mL), [Ir(ppy)$_2$(dtbbpy)]PF$_6$ (0.12 μmol, 110 μg, 0.0003 equiv), formic acid (HCO$_2$H, 0.04 mmol, 1.84 mg, 0.1 equiv) and diisopropylethylamine (^{i}Pr$_2$NEt, 0.48 mmol, 62.0 mg, 1.2 equiv). The resulting solution was sparged with N$_2$ for 30 seconds before irradiated with blue LEDs. After 32 h of irradiation, the solvent was removed *in vacuo* and the crude residue was purified by column chromatography to afford the desired products.

General procedure for fragmentation 3 (GP 3) – Electrocatalytic oxidation and Ir-mediated fragmentation

Acetonitrile (50 mL) were placed into a 100 mL flask capped with a rubber septum, which was punctured with two needles, one of them connected to an O$_2$ balloon. The reaction was sparged for 10 min. While sparging, two pieces of 2 x 5 cm of RVC panel (0.125 inch thick) were cut and submerged into concentrated nitric acid for 5 min, after which the RVC pieces were thoroughly rinsed first with water and then with acetone and let dry under air. In one of the RVC panels, a

hole was made in the middle-top part and a copper wire was coiled around the top part, leaving one end of the wire free (this panel acts as working electrode). The other panel was cut in two pieces, and a hole was made in the middle-top part of each piece. A copper wire was then inserted through the holes of both pieces and coiled around both of them, leaving uncoiled one of the ends of the wire (these panels act as auxiliary electrode) (Figure 46.a). While drying, the reaction mixture was prepared. The desired lignin substrate (0.32 mmol) was added to a 20 mL test tube (height: 5.5 cm; diameter: 2.2 cm) containing a stir bar, followed by 16 mL of MeCN (O_2 sparged for 10 min). The mixture was stirred for 5 min to ensure complete dissolution of the lignin substrate. Then KPF_6 (0.05 M, 147 mg) was added followed by NHPI (5.2 mg, 0.032 mmol, 10 mol%) while stirring. Finally, 2,6-lutidine (3.7 µL, 0.032 mmol, 10 mol%) was added to the mixture. A separator (panel of glass) was introduced into the reaction mixture and the electrodes where placed one on each side of the separator to avoid contact (Figure 46.b). The copper wires of both electrodes were maintained outside the solution at all times to avoid their oxidation during the reaction. The reference electrode (Ag/AgCl in 3 M KCl) was introduced in the reaction vessel next to the auxiliary electrode and no contact of the vycor with this electrode was ensured. The alligator clips of the electroanalyzer were correctly placed and the reaction was stirred at 850 rpm for 2-6 h at a constant voltage of 1.1 V (Figure 46.c). A chronoamperogram was recorded each time to follow the course of the reaction. After completion of the reaction, each electrode was rinsed with 1 mL of MeCN that was collected in the reaction vessel containing the reaction mixture.
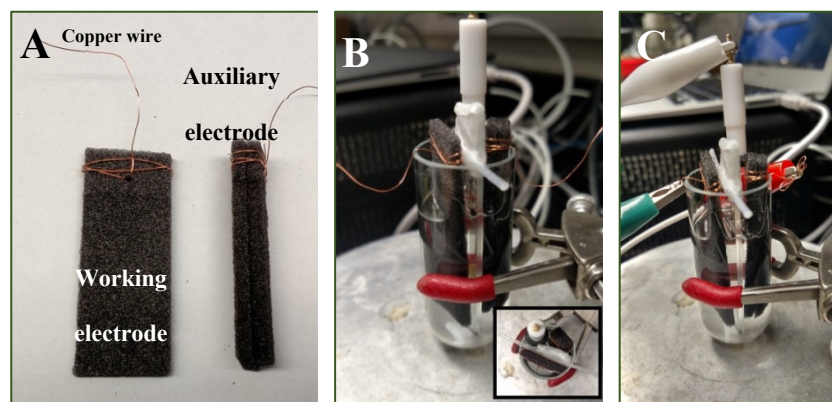
Figure 46 Pictures of the electrochemical cell components and the reaction setup.

Set-up of the flow reactor for the reductive cleavage: 10 m of 0.03-inch diameter PFA tubing were coiled around 4x25 mL test tubes (see Figure 30). 8 blue light strips (4 W each) where placed surrounding the tubing approximately 2 cm away from it in order to avoid. A peristaltic pump was used in order to control the flow of the reactor.

In the same reaction vessel used for the oxidation, Ir(ppy)$_2$(dtbbpy)PF$_6$ (1.4 mg, 0.5 mol%) was directly added to the mixture. Into another vial, ^{i}Pr$_2$EtN (61 µL, 0.35 mmol, 1.1 equiv) was dissolved in MeCN (1 mL) and formic acid (0.032 mmol, 1.2 µL, 10 mol%) was added. This mixture was carefully added to the reaction vessel while stirring. To this prepared reaction mixture, one of the ends of the flow reactor tubing was inserted and the blue LEDs were turned on. A 0.1

mL/min flow (residence time of 45 min) was selected and the reaction was flowed. The temperature of the flow reactor system was measured introducing a thermometer into one of the test tubes that supported the coiled tubing. This temperature was measured to reach an isothermal regime of 32 °C in within the first 10 min of the reaction. The collected mixture was concentrated, dissolved in CH_2Cl_2 and water, extracted with CH_2Cl_2 (x3) and washed with water and brine. The organic layer was dried over Na_2SO_4, filtered and concentrated at 100 mbar at 27 °C in order to avoid loss of volatile cleaved products formed during the reaction. The crude mixture was purified by column chromatography.

General procedure for fragmentation 4 – PhPTH-mediated fragmentation

A 2-dram vial with a magnetic stir bar was flame dried under a stream of nitrogen. The PhPTH (2.07 mg, 0.00750 mmol, 5 mol%), ketone substrate (0.150 mmol), and acetone (3.00 mL) were added to the vial. After, the ^{i}Pr$_2$EtN (52.3 µL, 0.300 mmol) and formic acid (0.150 mmol) were added, in that order. Nitrogen gas was bubbled through the solution for 1 minute, and the vial was sealed with a cap and parafilm and stirred at room temperature under irradiation with Kessil PR160 390 nm light (100% intensity, 6 cm away) for 3 h. The solution was then evaporated under reduced pressure to afford the crude product. The crude product was purified using a 13 g pre-packed silica column with a 5-step gradient up to 30% EtOAc/Hexanes (2 column volumes).

General procedure for fragmentation 5 – Electrochemical reductive fragmentation

Ketone starting material (0.3 mmol) was dissolved in 15 mL of a 50 mM KPF_6 MeCN solution followed by the addition of ^{i}Pr$_2$EtN (3 equiv). The solution was transferred to custom, house made electrochemical cell that was equipped with two graphite rod electrodes ($l = 2$ cm, $\phi = 0.6$ cm, one as anode and one as cathode) and an Ag/AgCl (3 M KCl_{aq}) reference electrode. The solution was sealed and degassed by bubbling nitrogen through the solution for at least 10 minutes. Electrolysis was started at ambient temperature with a constant potential of 1.2 V. The reaction progress was monitored by TLC, and the solution turned a dark red color as the reaction progressed. Depending on the desired product, each substrate was stopped at the indicated reaction time. Upon reaction completion, the solution was concentrated under reduced pressure and dried in vacuo. The crude residue was purified by column chromatography to give the products.

HO⟍
54.c
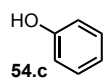
Phenol (54.c)

Yields obtained for:

General procedure 1:	55%
General procedure 2:	n/a
General procedure 3:	76%
General procedure 4:	n/a
General procedure 5:	n/a
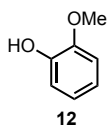
2-methoxyphenol (12)

^{1}H NMR (500 MHz, CDCl$_3$) δ:	6.95 – 6.91 (m, 1H), 6.88 (dd, J = 5.9, 3.2 Hz, 1H), 6.87 – 6.85 (m, 2H), 5.60 (br, 1H), 3.89 (s, 3H);
^{13}C NMR (126 MHz, CDCl$_3$) δ:	146.7, 145.7, 121.5, 120.2, 114.7, 110.9, 55.9;
HRMS (ESI):	m/z calculated for C$_7$H$_9$O$_2$ [M+H]$^+$: 125.0597, found: 125.0595.

Yields obtained for:
   General procedure 1:   up to 95%
   General procedure 2:   up to 92%
   General procedure 3:   up to 78%
   General procedure 4:   up to 95%
   General procedure 5:   n/a
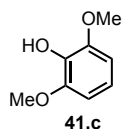
2,6-dimethoxyphenol (41.c)

^{1}H NMR (500 MHz, CDCl$_3$) δ:	6.79 (t, J = 8.4 Hz, 1H), 6.58 (d, J = 8.5 Hz, 2H), 5.55 (br, 1H), 3.87 (s, 6H);
^{13}C NMR (126 MHz, CDCl$_3$) δ:	147.3 (2C), 134.9, 119.1, 105.0 (2C), 56.3 (2C);
HRMS (ESI):	*m/z* calculated for C$_8$H$_{11}$O$_3$ [M+H]$^+$: 155.0703, found: 155.0702.

Yields obtained for:
    General procedure 1:   n/a
    General procedure 2:   82%
    General procedure 3:   71%
    General procedure 4:   up to 90%
    General procedure 5:   n/a
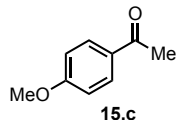
1-(4-methoxyphenyl)ethan-1-one (15.c)

^{1}H NMR (500 MHz, CDCl$_3$) δ:	7.93 (d, J = 8.9 Hz, 2H), 6.93 (d, J = 8.9 Hz, 2H), 4.00 (t, J = 5.3 Hz, 2H), 3.86 (s, 3H), 3.16 (t, J = 5.3 Hz, 2H), 2.85 (br, 1H);
^{13}C NMR (126 MHz, CDCl$_3$) δ:	199.2, 163.9, 130.5 (2C), 129.9, 113.9 (2C), 58.4, 55.6, 40.1;
HRMS (ESI):	*m/z* calculated for C$_{10}$H$_{12}$NaO$_3$ [M+Na]$^+$: 203.0679, found: 203.0677.

Yields obtained for:
General procedure 1:	72%
General procedure 2:	94%
General procedure 3:	75%
General procedure 4:	up to 92%%
General procedure 5:	78%
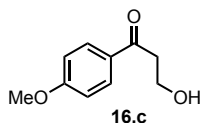
3-hydroxy-1-(4-methoxyphenyl)propan-1-one (16.c)

^{1}H NMR (500 MHz, CDCl$_3$) δ:	7.93 (d, J = 8.9 Hz, 2H), 6.93 (d, J = 8.9 Hz, 2H), 4.00 (t, J = 5.3 Hz, 2H), 3.86 (s, 3H), 3.16 (t, J = 5.3 Hz, 2H), 2.85 (br, 1H);
^{13}C NMR (126 MHz, CDCl$_3$) δ:	199.2, 163.9, 130.5 (2C), 129.9, 113.9 (2C), 58.4, 55.6, 40.1;
HRMS (ESI):	*m/z* calculated for C$_{10}$H$_{12}$NaO$_3$ [M+Na]$^+$: 203.0679, found: 203.0677.

Yields obtained for:

General procedure 1:	34%
General procedure 2:	83%
General procedure 3:	78%
General procedure 4:	91%
General procedure 5:	98%
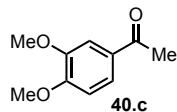
1-(3,4-dimethoxyphenyl)ethan-1-one (40.c)

^{1}H NMR (500 MHz, CDCl$_3$) δ:	7.57 (dd, J = 8.4, 1.9 Hz, 1H), 7.52 (d, J = 1.9 Hz, 1H), 6.88 (d, J = 8.4 Hz, 1H), 3.94 (s, 3H), 3.93 (s, 3H), 2.56 (s, 3H);
^{13}C NMR (126 MHz, CDCl$_3$) δ:	196.9, 153.4, 149.1, 130.6, 123.4, 110.2, 110.1, 56.2, 56.1, 26.3;
HRMS (ESI):	m/z calculated for C$_{10}$H$_{13}$O$_3$ [M+H]$^+$: 181.0859, found: 181.0858.

Yields obtained for:
    General procedure 1:   n/a
    General procedure 2:   95%
    General procedure 3:   80%
    General procedure 4:   91%
    General procedure 5:   78%
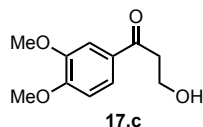
1-(3,4-dimethoxyphenyl)-3-hydroxypropan-1-one (17.c)

^{1}H NMR (500 MHz, CDCl$_3$) δ:	7.59 (dd, J = 8.4, 1.9 Hz, 1H), 7.53 (d, J = 1.9 Hz, 1H), 6.90 (d, J = 8.4 Hz, 1H), 4.02 (t, J = 5.4 Hz, 2H), 3.96 (s, 3H), 3.94 (s, 3H), 3.20 (t, J = 5.4 Hz, 2H), 2.70 (br, 1H);
^{13}C NMR (126 MHz, CDCl$_3$) δ:	199.3, 153.8, 149.3, 130.1, 123.1, 110.2, 110.1, 58.5, 56.3, 56.2, 40.0;
HRMS (ESI):	m/z calculated for C$_{11}$H$_{15}$O$_4$ [M+H]$^+$: 211.0965, found: 211.0968;

Yields obtained for:

General procedure 1:	29%
General procedure 2:	up to 86%
General procedure 3:	96%
General procedure 4:	87%
General procedure 5:	96%
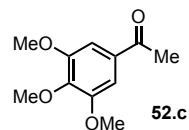
1-(3,4,5-trimethoxyphenyl)ethan-1-one (52.c)

^{1}H NMR (500 MHz, CDCl$_3$) δ:	7.22 (s, 2H), 3.92 (s, 6H, 2 × OCH$_3$), 3.92 (s, 3H, OCH$_3$), 2.59 (s, 3H, CH$_3$);
^{13}C NMR (126 MHz, CDCl$_3$) δ:	196.8, 153.0, 142.5, 132.4, 105.6, 60.8, 56.1, 26.5;

Yields obtained for:
General procedure 1:   n/a
General procedure 2:   n/a
General procedure 3:   n/a
General procedure 4:   n/a
General procedure 5:   63%
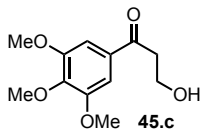
3-hydroxy-1-(3,4,5-trimethoxyphenyl)propan-1-one (45.c)

^{1}H NMR (500 MHz, CDCl$_3$) δ:	7.22 (s, 2H), 4.03 (t, J = 5.3 Hz, 2H), 3.92 (s, 3H), 3.92 (s, 6H), 3.21 (t, J = 5.3 Hz, 2H);
^{13}C NMR (126 MHz, CDCl$_3$) δ:	199.3, 153.3 (2C), 143.1, 132.0, 105.7 (2C), 61.1, 58.3, 56.5 (2C), 40.3;
Physical appearance:	white solid
HRMS (ESI):	m/z calculated for C$_{12}$H$_{17}$O$_5^+$ [M+H]$^+$: 241.1071, found: 241.1072.

Yields obtained for:
    General procedure 1:   n/a
    General procedure 2:   87%
    General procedure 3:   up to 91%
    General procedure 4:   n/a
    General procedure 5:   92%
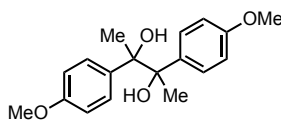
15.e

2,3-bis(4-methoxyphenyl)butane-2,3-diol (15.e) was obtained following the general procedure for electrochemical fragmentation.

TLC (EtOAc/Hex, 2:3), R_f 0.45;

^{1}H NMR (500 MHz, CDCl$_3$) δ: 7.32 – 7.10 (m, 4H), 6.89 – 6.76 (m, 4H), 3.80 (s, 3H, OCH$_3$), 3.79 (s, 3H, OCH$_3$), 2.57 (s, 1H, OH), 2.29 (s, 1H, OH), 1.56 (s, 3H, CH$_3$), 1.47 (s, 3H, CH$_3$);

^{13}C NMR (126 MHz, CDCl$_3$) δ: 158.51, 158.41, 136.00, 135.66, 128.52, 128.08, 112.54, 112.38, 78.70, 78.47, 55.19, 25.17, 25.01;

Physical appearance: white solid.

40.e
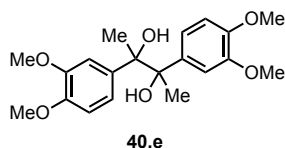
2,3-bis(3,4-dimethoxyphenyl)butane-2,3-diol (40.e) was obtained following the general procedure for electrochemical fragmentation.

TLC (EtOAc/Hex, 2:3), R_f	0.30;
^{1}H NMR (500 MHz, CDCl$_3$) δ:	6.95 – 6.95 (m, 2H), 6.90 – 6.88 (m, 2H), 6.84 – 6.83 (m, 2H), 4.86 (q, J = 15, 10 Hz, 1H, OH), 3.90 (s, 3H, OCH$_3$), 3.87 (s, 3H, OCH$_3$), 1.50 (s, 3H, CH$_3$), 1.48 (s, 3H, CH$_3$);
^{13}C NMR (126 MHz, CDCl$_3$) δ:	148.02, 132.46, 120.95, 112.04, 109.66, 82.43, 60.32, 55.82, 55.75, 35.08;
Physical appearance:	yellow solid.

55.e
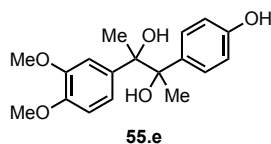
2-(3,4-dimethoxyphenyl)-3-(4-hydroxyphenyl)butane-2,3-diol (55.e) was obtained following the general procedure for electrochemical fragmentation.

TLC (EtOAc/Hex, 2:3), R_f	0.35;
^{1}H NMR (500 MHz, CDCl$_3$) δ:	7.23 (d, J = 10 Hz, 2H), 6.95 – 6.94 (m, 1H), 6.90 – 6.88 (m, 1H), 6.84 – 6.79 (m, 3H), 3.89 (s, 3H, OCH$_3$), 3.87 (s, 3H, OCH$_3$), 1.50 – 1.46 (m, 6H, 2 × CH$_3$);
^{13}C NMR (126 MHz, CDCl$_3$) δ:	154.94, 149.07, 148.38, 138.47, 138.09, 126.87, 117.52, 115.24, 110.99, 108.63, 70.27, 69.99, 55.94, 55.85, 25.06, 25.00;
Physical appearance:	yellow solid.

2,3-bis(3,4,5-trimethoxyphenyl)butane-2,3-diol (52.e) was obtained following the general procedure for electrochemical fragmentation.

|	
TLC (EtOAc/Hex, 2:3), R_f	0.30;
^{1}H NMR (500 MHz, CDCl$_3$) δ:	6.60 (s, 4H), 3.87 (s, 12H, 4 × OCH$_3$), 4.87 – 4.82 (m, 2 × OH), 3.83 (s, 6H, 2 × OCH$_3$), 1.50 (s, 3H, CH$_3$), 1.49 (s, 3H, CH$_3$);
^{13}C NMR (126 MHz, CDCl$_3$) δ:	153.27, 141.65, 137.11, 102.19, 70.61, 60.82, 56.08, 25.22;
Physical appearance:	yellow solid.

16.e
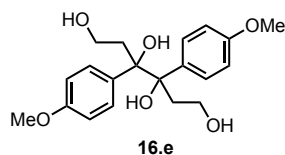
3,4-bis(4-methoxyphenyl)hexane-1,3,4,6-tetraol (16.e) was obtained following the general procedure for electrochemical fragmentation.

TLC (EtOAc/Hex, 3:2), R_f 0.30;

^{1}H NMR (500 MHz, CD$_3$CN) δ: 7.04 – 6.76 (m, 8H), 4.68 (s, 2H, 2 × OH), 3.76 (s, 6H, 2 × CH$_3$), 3.42 – 3.32 (m, 4H, 2 × CH$_2$), 2.93 (s, 2H, 2 × OH), 2.32 – 2.26 (m, 2H, CH$_2$), 1.76 – 1.73 (m, 2H, CH$_2$);

^{13}C NMR (126 MHz, CD$_3$CN) δ: 159.40, 134.30, 130.38, 112.99, 82.40, 60.07, 55.74, 36.41;

Physical appearance: white solid.

17.e
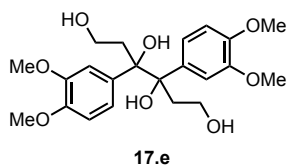
3,4-bis(3,4-dimethoxyphenyl)hexane-1,3,4,6-tetraol (17.e) was obtained following the general procedure for electrochemical fragmentation.

TLC (EtOAc/Hex, 3:2), R_f	0.10;
^{1}H NMR (500 MHz, CDCl$_3$) δ:	6.94 – 6.83 (m, 6H), 4.93 – 4.91 (m, 2H, 2 × OH), 3.90 – 3.88 (m, 12H, 4 × OCH$_3$), 3.88 – 3.73 (m, 4H, 2 × CH$_2$), 2.69 (br s, OH), 2.31 (br s, OH), 2.08 – 2.00 (m, 2H, CH$_2$), 1.94 – 1.90 (m, 2H, CH$_2$);
^{13}C NMR (126 MHz, CDCl$_3$) δ:	148.02, 132.46, 120.95, 112.04, 109.66, 82.43, 60.32, 55.82, 55.75, 35.08;
Physical appearance:	yellow solid.

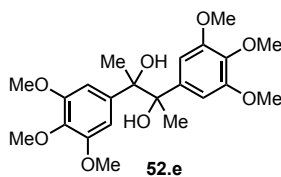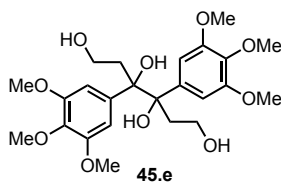**3,4-bis(3,4,5-trimethoxyphenyl)hexane-1,3,4,6-tetraol** (45.e) was obtained following the general procedure for electrochemical fragmentation.

TLC (EtOAc/Hex, 3:2), R_f	0.10;
^{1}H NMR (500 MHz, CDCl$_3$) δ:	6.60 (s, 2H), 4.90 (dd, J = 10, 5 Hz, 2H, 2 × OH), 3.92 – 3.89 (m, 4H, 2 × CH$_2$), 3.87 (s, 12H, 4 × OCH$_3$), 3.83 (s, 6H, 2 × OCH$_3$), 2.86 (br s, 1H, OH), 2.29 (br s, 1H, OH), 2.06 -1.90 (m, 4H, 2 × CH$_2$);
^{13}C NMR (126 MHz, CDCl$_3$) δ:	153.62, 140.52, 137.45, 102.75, 74.92, 61.91, 61.18, 56.43, 40.92;
Physical appearance:	yellow solid.

General procedure for photocatalytic Depolymerization of Polymers 48, 49.a, 50.a, 48-OH, 49.a-OH, 50-OH.

A 2-dram screw-cap vial equipped with a magnetic stir bar was charged with polymer (1 equiv) and [Ir(dtbbpy)(ppy)$_2$]PF$_6$ (1 mol%). Subsequently, in the following order, acetonitrile (0.2 M), ^{i}Pr$_2$NEt (3 equiv), and HCO$_2$H (3 equiv) were added via syringe. The vial was sealed with the screw cap and irradiated with a 4W blue LED strip while stirring rapidly. The reactions were heterogeneous upon the start of the reaction. There were no special precautions taken to avoid oxygen or moisture and no external heating was used (except for the ambient heat from the proximal LEDs). After 48 h of irradiation, the reaction mixtures were mostly homogeneous. The reaction mixture was concentrated *in vacuo* to afford a yellow or yellow-brown oil. The crude residue was purified via column chromatography to afford monomeric material. It is worth to note that attempting an aqueous, acidic workup of the reaction mixture typically afforded lower yields. Increasing methoxy substitution on the arene ring affords more polar monomer units that may be water soluble.
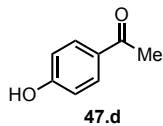
1-(4-hydroxyphenyl)ethan-1-one (47.d)

TLC (EtOAc/Hex, 3:1), R_f	0.24;
^{1}H NMR (500 MHz, CDCl$_3$) δ:	7.91 (d, $J = 8.6$ Hz, 2H), 6.89 (d, $J = 8.6$ Hz, 2H), 5.73 (br, 1H), 2.57 (br, 3H);
^{13}C NMR (126 MHz, CDCl$_3$) δ:	198.2, 161.0, 131.3 (2C), 130.1, 115.6 (2C), 26.5;
HRMS (ESI):	m/z calculated for C$_8$H$_9$O$_2$$^+$ [M+H]$^+$: 137.0597, found: 137.0596
Physical appearance:	white solid
Yields:	97% from polymer **48**, 67% from polymer **48-OH**
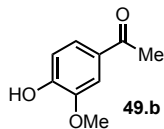
1-(4-hydroxy-3-methoxyphenyl)ethan-1-one (49.b)

TLC (EtOAc/Hex, 3:2), R_f	0.26;
^{1}H NMR (400 MHz, CDCl$_3$) δ:	7.53 (dd, J = 3.9, 2.4 Hz, 2H), 6.94 (m, 1H), 6.15 (s, 1H), 3.95 (s, 3H), 2.55 (s, 3H);
^{13}C NMR (126 MHz, CDCl$_3$) δ:	196.9, 150.5, 146.7, 130.4, 124.1, 113.9, 109.9, 56.2, 26.3;
Physical appearance:	white solid
Yields:	80% from polymer **49**, 58% from polymer **49.a-OH**
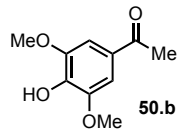
1-(4-hydroxy-3,5-dimethoxyphenyl)ethan-1-one (50.b)

TLC (acetone/Hex, 3:7), R_f	0.28;
^{1}H NMR (500 MHz, CDCl$_3$) δ:	7.23 (s, 2H), 3.93 (s, 6H), 2.56 (s, 3H);
^{13}C NMR (126 MHz, CDCl$_3$) δ:	196.7, 146.8, 139.8, 128.9, 105.8, 56.6, 26.4;
Physical appearance:	white solid
Yields:	80% from polymer **50**, 58% from polymer **50.a-OH**
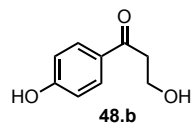
3-hydroxy-1-(4-hydroxyphenyl)propan-1-one (48.b)

TLC (Hex/CH$_2$Cl$_2$/acetone/MeOH, 5:2:2:1), R_f	0.24;
^{1}H NMR (400 MHz, acetone-d$_6$) δ:	9.16 (s, 1H), 7.91 (d, J = 8.8 Hz, 2H), 6.92 (d, J = 8.8 Hz, 2H), 3.91 (q, J = 6.0 Hz, 2H), 3.57 (t, J = 5.8 Hz, 1H), 3.13 (t, J = 6.2 Hz, 2H);
^{13}C NMR (126 MHz, acetone-d$_6$) δ:	198.1, 162.7, 131.4, 130.5, 116.0, 58.7, 41.6;
Physical appearance:	white solid
Yield:	12% from polymer **48-OH**
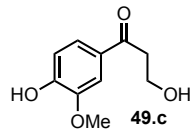
3-hydroxy-1-(4-hydroxy-3-methoxyphenyl)propan-1-one (49.c)

TLC (Hex/CH$_2$Cl$_2$/acetone/MeOH, 6:2:1:1), R_f	0.25;
^{1}H NMR (400 MHz, CDCl$_3$) δ:	7.55 (d, J = 8.0 Hz, 2H), 6.95 (d, J = 8.0 Hz, 1H), 6.42–6.14 (br, 1H), 4.02 (t, J = 5.3 Hz, 2H), 3.95 (s, 3H), 3.18 (t, J = 5.3 Hz, 2H), 2.92–2.78 (br, 1H);
^{13}C NMR (126 MHz, CDCl$_3$) δ:	199.2, 151.0, 146.9, 129.7, 123.8, 114.1, 109.7, 58.5, 56.2, 39.9;
Physical appearance:	yellow oil
Yield:	28% from polymer **49.a-OH**
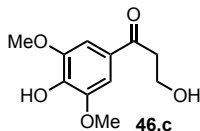
3-hydroxy-1-(4-hydroxy-3,5-dimethoxyphenyl)propan-1-one (46.c)

TLC (Hex/CH$_2$Cl$_2$/acetone/MeOH, 6:2:1:1), R_f	0.20;
^{1}H NMR (500 MHz, CDCl$_3$) δ:	7.25 (s, 2H), 4.03 (t, J = 5.3 Hz, 2H), 3.96 (s, 6H), 3.19 (t, J = 5.3 Hz, 2H);
^{13}C NMR (176 MHz, CDCl$_3$) δ:	199.0, 147.0, 140.3, 128.4, 105.6, 58.4, 56.6, 40.0;
Physical appearance:	white solid
Yield:	9% from polymer **50.a-OH**

<div align="center">References Cited</div>

[1] Koehn, F. E.; Carter, G. T. The Evolving Role of Natural Products in Drug Discovery. *Nature Reviews Drug Discovery*. **2005**, *4*, 206.

[2] Baran, P. S. Natural Product Total Synthesis: As Exciting as Ever and Here To Stay. *J. Am. Chem. Soc.* **2018**, *140*, 4751.

[3] Li, J.; Eastgate, M. D. Current Complexity: A Tool for Assessing the Complexity of Organic Molecules. *Org. Biomol. Chem.* **2015**, *13*, 7164.

[4] Michaudel, Q.; Ishihara, Y.; Baran, P. S. Academia–Industry Symbiosis in Organic Chemistry. *Acc. Chem. Res.* **2015**, *48*, 712.

[5] Brown, D. G.; Bostrom, J. Analysis of Past and Present Synthetic Methodologies on Medicinal Chemistry: Where Have All the New Reactions Gone? *J. Med. Chem.* **2016**, *59*, 4443.

[6] Gomberg, M. An Instance of Trivalent Carbon: Triphenylmethyl. *J. Am. Chem. Soc.* **1900**, *22*, 757.

[7] Romero, K. J.; Galliher, M. S.; Pratt, D. A.; Stephenson, C. R. J. Radicals in Natural Product Synthesis. *Chem. Soc. Rev.* **2018**, *47*, 7851.

[8] Wender, P. A.; Howbert, J. J. Synthetic Studies on Arene-olefin Cycloadditions: Total Synthesis of (±)-α-cedrene. *J. Am. Chem. Soc.* **1981**, *103*, 688.

[9] Winkler, J. D.; Rouse, M. B.; Greaney, M. F.; Harrison, S. J.; Jeon, Y. T. The First Total Synthesis of (±)-ingenol. *J. Am. Chem. Soc.* **2002**, *124*, 9726.

[10] Crimmins, M. T.; Pace, J. M.; Nantermet, P. G.; Kim-Meade, A. S.; Thomas, J. B. Watterson, S. H.; Wagman, A. S. *J. Am. Chem. Soc.* **2000**, *122*, 8453.

[11] Kavarnos, G. J.; Turro, N. J. Photosensitization by Reversible Electron Transfer: Theories, Experimental Evidence, and Examples. *Chem. Rev.* **1986**, *86*, 401.

[12] Turro, N. J.; Ramamurthy, V.; Scaiano, J. C. *Modern Molecular Photochemistry of Organic Molecules*; University Science Books, 2010.

[13] Kärkäs, M. D.; Porco Jr., J. A.; Stephenson, C. R. J. Photochemical Approaches to Complex Chemotypes: Applications in Natural Product Synthesis. *Chem. Rev.* **2016**, *116*, 9683.

[14] Narayanam, J. M. R.; Stephenson, C. R. J. Visible Light Photoredox Catalysis: Applications in Organic Synthesis. *Chem. Soc. Rev.* **2011**, *40*, 102.

[15] Prier, C. K.; Rankic, D. A.; MacMillan, D. W. C. Visible Light Photoredox Catalysis with Transition Metal Complexes: Applications in Organic Synthesis. *Chem. Rev.* **2013**, *113*, 5322.

[16] Romero, N. A.; Nicewicz, D. A. Organic Photoredox Catalysis. *Chem. Rev.* **2016**, *116*, 10075.

[17] Juris, A.; Balzani, V.; Barigelletti, F.; Campagna, S.; Bleser, P.; Von Zelewsky, A. Ru(II) Polypyridine Complexes: Photophysics, Photochemistry, Electrochemistry, and Chemiluminescence. *Coordination Chemistry Reviews* **1988**, *84*, 85.

[18] Roth, H. G.; Romero, N. A.; Nicewicz, D. A. Experimental and Calculated Electrochemical Potentials of Common Organic Molecules for Applications to Single-Electron Redox Chemistry. *Synlett* **2016**, *27*, 714.

[19] Wrighton, M.; Markham, J. Quenching of the Luminescent State of tris(2,2'-bipyridine)ruthenium(II) by Electronic Energy Transfer. *J. Phys. Chem.* **1973**, *77*, 3042.

[20] Lu, Z.; Yoon, T. P. Visible Light Photocatalysis of [2+2] Styrene Cycloadditions by Energy Transfer. *Angew. Chem., Int. Ed.* **2012**, *51*, 10329.

[21] Singh, K.; Staig, S. J.; Weaver, J. D. Facile Synthesis of Z-Alkenes via Uphill Catalysis. *J. Am. Chem. Soc.* **2014**, *136*, 5275.

[22] Blum, T. R.; Miller, Z. D.; Bates, D. M.; Guzei, I. A.; Yoon, T. P. Enantioselective Photochemistry through Lewis Acid-catalyzed Triplet Energy Transfer. *Science* **2016**, *354*, 1391.

[23] Welin, E. R.; Le, C.; Arias-Rotondo, D. M.; McCusker, J. K.; MacMillan, D. W. C. Photosensitized, Energy Transfer-mediated Organometallic Catalysis through Electronically Excited Nickel(II). *Science.* **2017**, *355*, 380.

[24] Huang, X.; Quinn, T. R.; Harms, K.; Webster, R. D.; Zhang, L.; Wiest, O.; Meggers, E. Direct Visible-light-excited Asymmetric Lewis Acid Catalysis of Intermolecular [2+2] Photocycloadditions. *J. Am. Chem. Soc.* **2017**, *139*, 9120.

[25] Miller, Z. D.; Lee, B. J.; Yoon, T. P. Enantioselective Crossed Photocycloadditions of Styrenic Olefins by Lewis Acid Catalyzed Triplet Sensitization. *Angew. Chem., Int. Ed.* **2017**, *56*, 11891.

[26] Lei, T.; Zhou, C.; Huang, M.-Y.; Yang, B.; Ye, C.; Xiao, H.; Meng, Q.-Y.; Ramamurthy, V.; Tung, C.-H.; Wu, L.-Z. General and Efficient Intermolecular [2+2] Photodimerization of Chalcones and Cinnamic Acid Derivatives in Solution through Visible-light Catalysis. *Angew. Chem., Int. Ed.* **2017**, *56*, 15407.

[27] Julliard, M.; Chanon, M. Photoelectron-Transfer Catalysis: Its Connections with Thermal and Electrochemical Analogs. *Chem. Rev.* **1983**, *83*, 425.

[28] Singh-Rachford, T. N.; Castellano, F. N. Photon Upconversion Based on Sensitized Triplet–Triplet Annihilation. *Coordination Chemistry Reviews* **2010**, *254*, 2560.

[29] Ni, T.; Caldwell, R. A.; Melton, L. A. The Relaxed and Spectroscopic Energies of Olefin Triplets. *J. Am. Chem. Soc.* **1989**, *111*, 457.

[30] Sherbrook, E. M.; Yoon, T. P. Asymmetric Catalysis of Triplet-State Photoreactions. *Photochemistry* **2019**, *46*, 432.

[31] DiRocco, D. A.; Dykstra, K.; Krska, S.; Vachal, P.; Conway, D. V.; Tudge, M. Late-Stage Functionalization of Biologically Active Heterocycles through Photoredox Catalysis. *Angew. Chem., Int. Ed.* **2014**, *53*, 4802.

[32] Beatty, J. W.; Douglas, J. J.; Miller, R.; McAtee, R. C.; Cole, K. P.; Stephenson, C. R. J. Photochemical Perfluoroalkylation with Pyridine N-Oxides: Mechanistic Insights and Performance on a Kilogram Scale. *Chem* **2016**, *1*, 456.

[33] Douglas, J. J.; Sevrin, M. J.; Cole, K. P.; Stephenson, C. R. J. Preparative Scale Demonstration and Mechanistic Investigation of a Visible Light-mediated Radical Smiles Rearrangement. *Org. Process Res. Dev.* **2016**, *20*, 1148.

[34] Yayla, H. G.; Peng, F.; Mangion, I. K.; McLaughlin, M.; Campeau, L.-C.; Davies, I. W.; DiRocco, D. A.; Knowles, R. R. Discovery and Mechanistic Study of a Photocatalytic Indoline Dehydrogenation for the Synthesis of Elbasvir. *Chem. Sci.* **2016**, *7*, 2066.

[35] Le, C.; Wismer, M. K.; Shi, Z.-C.; Zhang, R.; Conway, D. V.; Li, G.; Vachal, P.; Davies, I. W.; MacMillan, D. W. C. A General Small-Scale Reactor to Enable Standardization and Acceleration of Photocatalytic Reactions. *ACS Cent. Sci.* **2017**, *3*, 647.

[36] Bissonnette, N. B.; Boyd, M. J.; May, G. D.; Giroux, S.; Nuhant, P. C-H Functionalization of Heteroarenes Using Unactivated Alkyl Halides through Visible-light Photoredox Catalysis under Basic Conditions. *J. Org. Chem.* **2018**, *83*, 10933.

[37] Harper, K. C.; Moschetta, E. G.; Bordawekar, S. V.; Wittenberger, S. J. A Laser Driven Flow Chemistry Platform for Scaling Photochemical Reactions with Visible Light. *ACS Cent. Sci.* **2019**, *5*, 109.

[38] Abas, N.; Kalair, A.; Khan, N. Review of Fossil Fuels and Future Energy Technologies. *Futures* **2015**, *69*, 31.

[39] Obama, B. The Irreversible Momentum of Clean Energy. *Science* **2017**, *355*, 126.

[40] *Commercial Biotechnology: An International Analysis*. Chapter 9 Commodity Chemicals and Energy Production. Office of Technology Assessment, OTA-BA-218: Washington D.C., U.S. Congress, January 1984.

[41] McFarlane, J.; Robinson, S. M. *Survey of Alternative Feedstocks for Commodity Chemical Manufacturing*; Report to the U.S. Department of Energy under contract DE-AC05-00OR22725; Oak Ridge National Laboratory: Oak Ridge, TN, March 2007.

[42] Monthly Energy Review – October 2018.

[43] Perlack, R. D.; Wright, L. L.; Turhollow, A. F.; Graham, R. L.; Stokes, B. J.; Erbach, D. C. *Biomass as Feedstock for a Bioenergy and Bioproducts Industry: The Technical Feasibility of a Billion-Ton Annual Supply*; 1216415; 2005.

[44] McCarthy, J. L.; Islam, A. Lignin Chemistry, Technology, and Utilization: A Brief History. In *Lignin: Historical, Biological, and Materials Perspectives*; ACS Symposium Series; American Chemical Society, 1999; Vol. 742, pp 2–99.

[45] Rinaldi, R.; Jastrzebski, R.; Clough, M. T.; Ralph, J.; Kennema, M.; Bruijnincx, P. C. A.; Weckhuysen, B. M. Paving the Way for Lignin Valorisation: Recent Advances in Bioengineering, Biorefining and Catalysis. *Angew. Chem.*, *Int. Ed.* **2016**, *55*, 8164

[46] Kärkäs, M. D.; Matsuura, B. S.; Monos, T. M.; Magallanes, G.; Stephenson, C. R. J. Transition-metal Catalyzed Valorization of Lignin: The Key to a Sustainable Carbon-neutral Future. *Org. Biomol. Chem.* **2016**, *14*, 1853.

[47] de Jong, E.; Jungmeier, G. Chapter 1 - Biorefinery Concepts in Comparison to Petrochemical Refineries. In *Industrial Biorefineries & White Biotechnology*; Pandey, A., Höfer, R., Taherzadeh, M., Nampoothiri, K. M., Larroche, C., Eds.; Elsevier: Amsterdam, 2015; pp 3–33.

[48] Ragauskas, A. J.; Beckham, G. T.; Biddy, M. J.; Chandra, R.; Chen, F.; Davis, M. F.; Davison, B. H.; Dixon, R. A.; Gilna, P.; Keller, M.; Langan, P.; Naskar, A. K.; Saddler, J. N.; Tschaplinski, T. J.; Tuskan, G. A.; Wyman, C. E. Lignin Valorization: Improving Lignin Processing in the Biorefinery. *Science* **2014**, *344*, 1246843.

[49] Ralph, J.; Peng, J.; Lu, F.; Hatfield, R. D.; Helm, R. F. Are Lignins Optically Active? *J. Agric. Food Chem.* **1999**, *47*, 2991.

[50] Crestini, C.; Melone, F.; Sette, M.; Saladino, R. Milled Wood Lignin: A Linear Oligomer. *Biomacromolecules* **2011**, *12*, 3928.

[51] Zakzeski, J.; Bruijnincx, P. C. A.; Jongerius, A. L.; Weckhuysen, B. M. The Catalytic Valorization of Lignin for the Production of Renewable Chemicals. *Chem. Rev.* **2010**, *110*, 3552.

[52] Galkin, M. V.; Samec, J. S. M. Lignin Valorization through Catalytic Lignocellulose Fractionation: A Fundamental Platform for the Future Biorefinery. *ChemSusChem* **2016**, *9*, 1544.

[53] Shaw, M. H.; Twilton, J.; MacMillan, D. W. C. Photoredox Catalysis in Organic Chemistry. *J. Org. Chem.* **2016**, *81*, 6898.

[54] Sauer, J.; Adkins, H. The Selective Hydrogenation of Unsaturated Esters to Unsaturated Alcohols. *J. Am. Chem. Soc.* **1937**, *59*, 1.

[55] Harris, E. E.; D'Ianni, J.; Adkins, H. Reaction of Hardwood Lignin with Hydrogen. *J. Am. Chem. Soc.* **1938**, *60*, 1467.

[56] Shimada, M.; Habe, T.; Umezawa, T.; Higuchi, T.; Okamoto, T. The C–C Bond Cleavage of a Lignin Model Compound, 1,2-diarylpropane-1,3-diol, with a Heme-Enzyme Model Catalyst Tetraphenylporphyrinatoiron(III) Chloride in the Presence of *tert*-Butylhydroperoxide. *Biochem. Biophys. Res. Commun.* **1984**, *122*, 1247.

[57] Schoemaker, H. E.; Harvey, P. J.; Bowen, R. M.; Palmer, J. M. On the Mechanism of Enzymatic Lignin Breakdown. *FEBS Letters* **1985**, *183*, 7.

[58] DiCosimo, R.; Szabo, H.-C. Oxidation of Lignin Model Compounds Using Single-Electron-Transfer Catalysis. *J. Org. Chem.* **1988**, *53*, 1673.

[59] DCA is known to have a large singlet excited state, but there are inconsistent reports for its excited state reduction potential. Nicewicz and Romero have listed the excited state reduction potential as +1.99 V vs. SCE.[16] Lacombe has reported +2.17 V, and Mariano reported +2.80 V.[60] It is clear that DCA is highly oxidizing in its photoexcited state, but reports of the exact reduction potential seem to be inconsistently reported. Blanc, S.; Pigot, T.; Cugnet, C.; Brown, R.; Lacombe, S. *Phys. Chem. Chem. Phys.* **2010**, *12*, 11280.

[60] Cho, D. W.; Parthasarathi, R.; Pimentel, A. S.; Maestas, G. D.; Park, H. J.; Yoon, U. C.; Dunaway-Mariano, D.; Gnanakaran, S.; Langan, P.; Mariano, P. S. Nature and Kinetic Analysis of Carbon–Carbon Bond Fragmentation Reactions of Cation Radicals Derived from SET-Oxidation of Lignin Model Compounds. *J. Org. Chem.* **2010**, *75*, 6549.

[61] Lim, S. H.; Nahm, K.; Ra, C. S.; Cho, D. W.; Yoon, U. C.; Latham, J. A.; Dunaway-Mariano, D.; Mariano, P. S. Effects of Alkoxy Groups on Arene Rings of Lignin β-O-4 Model Compounds

on the Efficiencies of Single Electron Transfer-Promoted Photochemical and Enzymatic C–C Bond Cleavage Reactions. *J. Org. Chem.* **2013**, *78*, 9431.

[62] Son, S.; Toste, F. D. Non-Oxidative Vanadium-Catalyzed C–O Bond Cleavage: Application to Degradation of Lignin Model Compounds. *Angew. Chem., Int. Ed.* **2010**, *49*, 3791.

[63] Chan, J. M. W.; Bauer, S.; Sorek, H.; Sreekumar, S.; Wang, K.; Toste, F. D. Studies on the Vanadium-Catalyzed Nonoxidative Depolymerization of *Miscanthus giganteus*-derived Lignin *ACS Catal.* **2013**, *3*, 1369.

[64] Tucker, J. W.; Stephenson, C. R. J. Shining Light on Photoredox Catalysis: Theory and Synthetic Applications. *J. Org. Chem.* **2012**, *77*, 1617.

[65] Narayanam, J. M. R.; Tucker, J. W.; Stephenson, C. R. J. Electron-transfer Photoredox Catalysis: Development of a Tin-Free Reductive Dehalogenation Reaction. *J. Am. Chem. Soc.* **2009**, *131*, 8756.

[66] Nguyen, J. D.; D'Amato, E. M.; Narayanam, J. M. R.; Stephenson, C. R. J. Engaging Unactivated Alkyl, Alkenyl and Aryl Iodides in Visible-light-mediated Free Radical Reactions. *Nat. Chem.* **2012**, *4*, 854.

[67] Devery III, J. J.; Nguyen, J. D.; Dai, C.; Stephenson, C. R. J. Light-Mediated Reductive Debromination of Unactivated Alkyl and Aryl Bromides. *ACS Catal.* **2016**, *6*, 5962.

[68] Douglas, J. J.; Albright, H.; Sevrin, M. J.; Cole, K. P.; Stephenson, C. R. J. A Visible-light-mediated Radical Smiles Rearrangement and its Application to the Synthesis of a Difluoro-substituted Spirocyclic ORL-1 Antagonist. *Angew. Chem., Int. Ed.* **2015**, *54*, 14898.

[69] Monos, T. M.; McAtee, R. C.; Stephenson, C. R. J. Arylsulfonylacetamides as Bifunctional Reagents for Alkene Aminoarylation. *Science* **2018**, *361*, 1369.

[70] Kim, S.; Chmely, S. C.; Nimlos, M. R.; Bomble, Y. J.; Foust, T. D.; Paton, R. S.; Beckham, G. T. Computational Study of Bond Dissociation Enthalpies for a Large Range of Native and Modified Lignins. *J. Phys. Chem. Lett.* **2011**, *2*, 2846.

[71] Beatty, J. W.; Stephenson, C. R. J. Amine Functionalization via Oxidative Photoredox Catalysis: Methodology Development and Complex Molecule Synthesis. *Acc. Chem. Res.* **2015**, *48*, 1474.

[72] Condie, A. G.; González-Gómez, J. C.; Stephenson, C. R. J. Visible-Light Photoredox Catalysis: Aza-Henry Reactions via C–H Functionalization. *J. Am. Chem. Soc.* **2010**, *132*, 1464.

[73] Beatty, J. W.; Stephenson, C. R. J. Synthesis of (–)-Psuedoatabersonine, (–)-Pseudovincadifformine, and (+)-Coronaridine Enabled by Photoredox Catalysis in Flow. *J. Am. Chem. Soc.* **2014**, *136*, 10270.

[74] Staveness, D.; Sodano, T. M.; Burnham, E. A.; Jackson, K. D.; Stephenson, C. R. J. Providing a New Aniline Bioisostere through the Photochemical Production of 1-Aminonorbornanes. *Chem.* **2018**, *5*, 215.

[75] Hasegawa, E.; Takizawa, S.; Seida, T.; Yamaguchi, A.; Yamaguchi, N.; Chiba, N.; Takahashi, T.; Ikeda, H.; Akiyama, K. Photoinduced Electron-Transfer Systems Consisting of Electron-Donating Pyrenes or Anthracenes and Benzimidazolines for Reductive Transformation of Carbonyl Compounds. *Tetrahedron* **2006**, *62*, 6581.

[76] Larraufie, M.-H.; Pellet, R.; Fensterbank, L.; Goddard, J.-P.; Lacôte, E.; Malacria, M.; Ollivier, C. Visible-light-induced Photoreductive Generation of Radicals from Epoxides and Aziridines. *Angew. Chem., Int. Ed.* **2011**, *50*, 4463.

[77] Nguyen, J. D.; Matsuura, B. S.; Stephenson, C. R. J. A Photochemical Strategy for Lignin Degradation at Room Temperature. *J. Am. Chem. Soc.* **2014**, *136,* 1218.

[78] Monos, T. M.; Magallanes, G.; Sebren, L. J.; Stephenson, C. R. J. Visible Light Mediated Reduction of Ethers, Amines, and Sulfides. *J. Photochem. Photobio. A.* **2016**, *328, 240.*

[79] Roberts, B. P. Polarity-reversal Catalysis of Hydrogen-atom Abstraction Reactions: Concepts and Applications in Organic Chemistry. *Chem. Soc. Rev.* **1999**, *28*, 25.

[80] Sergeev, A. G.; Hartwig, J. F. Selective, Nickel-catalyzed Hydrogenolysis of Aryl Ethers. *Science* **2011**, *332*, 439.

[81] Galkin, M. V.; Samec, J. S. M. Selective Route to 2-propenyl Aryls Directly from Wood by a Tandem Organosolv and Palladium-catalysed Transfer Hydrogenolysis. *ChemSusChem* **2014**, *7*, 2154.

[82] Wang, M.; Li, L. H.; Lu, J. M.; Li, H. J.; Zhang, X. C.; Liu, H. F.; Luo, N. C.; Wang, F. Acid Promoted C–C Bond Oxidative Cleavage of β-O-4 and β-1 Lignin Models to Esters Over a Copper Catalyst. *Green Chem.* **2017**, *19*, 702.

[83] Zhu, C.; Ding, W.; Shen, T.; Tang, C.; Sun, C.; Xu, S.; Chen, Y.; Wu, J.; Ying, H. Metallo-Deuteroporphyrin as a Biomimetic Catalyst for the Catalytic Oxidation of Lignin to Aromatics. *ChemSusChem* **2015**, *8*, 1768.

[84] Sedai, B.; Díaz-Urrutia, C.; Baker, R. T.; Wu, R.; Silks, L. A.; Hanson, S. K. Aerobic Oxidation of β-1 Lignin Model Compounds with Copper and Oxovanadium Catalysts. *ACS Catal.* **2013**, *3*, 3111.

[85] Rahimi, A.; Ulbrich, A.; Coon, J. J.; Stahl, S. S. Formic-Acid Induced Depolymerization of Oxidized Lignin to Aromatics. *Nature* **2014**, *515*, 249.

[86] Lancefield, C. S.; Ojo, O. S.; Tran, F.; Westwood, N. J. Isolation of Functionalized Phenolic Monomers Through Selective Oxidation and C−O Bond Cleavage of the β-O-4 Linkages in Lignin. *Angew. Chem., Int. Ed*. **2015**, *54*, 258.

[87] Chan, J. M. W.; Bauer, S.; Sorek, H.; Sreekumar, S.; Wang, K.; Toste, F. D. Studies on the Vanadium-Catalyzed Nonoxidative Depolymerization of Miscanthus giganteus-Derived Lignin. *ACS Catal*. **2013**, *3*, 1369.

[88] Galkin, M. V.; Sawadjoon, S.; Rohde, V.; Dawange, M.; Samec, J. S. M. Mild Heterogeneous Palladium-Catalyzed Cleavage of β-O-4′-Ether Linkages of Lignin Model Compounds and Native Lignin in Air. *ChemCatChem* **2014**, *6*, 179.

[89] Rahimi, A.; Azarpira, A.; Kim, H.; Ralph, J.; Stahl, S. S. Chemoselective Metal-free Aerobic Alcohol Oxidation in Lignin. *J. Am. Chem. Soc.* **2013**, *135*, 6415.

[90] Das, A.; Rahimi, A.; Ulbrich, A.; Alherech, M.; Motagamwala, A. H.; Bhalla, A.; da Costa Sousa, L.; Balan, V.; Dumesic, J. A.; Hegg, E. L.; Dale, B. E.; Ralph, J.; Coon, J. J.; Stahl, S. S. Lignin Conversion to Low-molecular-weight Aromatics via an Aerobic Oxidation-hydrolysis Sequence: Comparison of Different Lignin Sources. *ACS Sustainable Chem. Eng.* **2018**, *6*, 3367.

[91] Kärkäs, M. D.; Bosque, I.; Matsuura, B. S.; Stephenson, C. R. J. Photocatalytic Oxidation of Lignin Model Systems by Merging Visible-light Photoredox and Palladium Catalysis. *Org. Lett.* **2016**, *18*, 5166.

[92] Ortiz de Montellano, P. R. Hydrocarbon Hydroxylation by Cytochrome P450 Enzymes. *Chem. Rev.* **2010**, *110*, 932.

[93] Poulos, T. L. Heme Enzyme Structure and Function. *Chem. Rev.* **2014**, *114*, 3919.

[94] Kleingardner, J. G.; Bren, K. L. Biological Significance and Applications of Heme c Proteins and Peptides. *Acc. Chem. Res.* **2015**, *48*, 1845.

[95] Piera, J.; Bäckvall, J.-E. Catalytic Oxidation of Organic Substrates by Molecular Oxygen and Hydrogen Peroxide by Multistep Electron Transfer–A Biomimetic Approach. *Angew. Chem., Int. Ed.,* **2008**, *47*, 3506.

[96] Allen, S. E.; Walvoord, R. R.; Padilla-Salinas, r.; Kozlowski, M. C. Aerobic Copper-Catalyzed Organic Reactions. *Chem. Rev.* **2013**, *113*, 6234.

[97] Wang, D.; Weinstein, A. B.; White, P. B.; Stahl, S. S. Ligand-promoted Palladium-catalyzed Aerobic Oxidation Reactions. *Chem. Rev.* **2018**, *118*, 2636.

[98] Larock, R. C.; Hightower, T. R. Synthesis of Unsaturated Lactones via Palladium-Catalyzed Cyclization of Alkenoic Acids. *J. Org. Chem.* **1993**, *58*, 5298.

[99] Van Benthem, R. A. T. M.; Hiemstra, H.; Michels, J. J.; Speckamp, W. N. Palladium(II)-catalysed Oxidation of Allylic Amines with Molecular Oxygen. *J. Chem. Soc., Chem. Commun.* **1994**, 357.

[100] Ochen, A.; Whitten, R.; Aylott, H. E.; Ruffell, K.; Williams, G. D.; Slater, F.; Roberts, A.; Evans, P.; Steves, J. E.; Sanganee, M. J. Development of a Large-Scale Copper(I)/TEMPO-Catalyzed Aerobic Alcohol Oxidation for the Synthesis of LSD1 Inhibitor GSK2879552. *Organometallics* **2019**, *38*, 176.

[101] Nichols, J. M.; Bishop, L. M.; Bergman, R. G.; Ellman, J. A. Catalytic C–O Bond Cleavage of 2-Aryloxy-1-arylethanols and Its Application to the Depolymerization of Lignin-related Polymers. *J. Am. Chem. Soc.* **2010**, *132*, 12554.

[102] Knowles, J. P.; Elliott, L. D.; Booker–Milburn, K. I. Flow Photochemistry: Old Light through New Windows. *Beilstein J. Org. Chem.* **2012**, *8*, 2025.

[103] Garlets, Z. J.; Nguyen, J. D.; Stephenson, C. R. J. The Development of Visible-light Photoredox Catalysis in Flow. *Isr. J. Chem.* **2014**, *54*, 351.

[104] Cambié, D.; Bottecchia, C.; Straathof, N. J. W.; Hessel, V.; Noël, T. Applications of Continuous-flow Photochemistry in Organic Synthesis, Material Science, and Water Treatment. *Chem. Rev.* **2016**, *116*, 10276.

[105] Plutschacks, M. B.; Pieber, B.; Gilmore, K.; Seeberger, P. H. The Hitchhiker's Guide to Flow Chemistry. *Chem. Rev.* **2017**, *117*, 11796.

[106] Arias-Rotondo, D. M.; McCusker, J. K. The Photophysics of Photoredox Catalysis: A Roadmap for Catalyst Design. *Chem. Soc. Rev.* **2016**, *45*, 5803.

[107] Magallanes, G.; Kärkäs, M. D.; Bosque, I.; Lee, S.; Maldonado, S.; Stephenson, C. R. J. Selective C–O Bond Cleavage of Lignin Systems and Polymers Enabled by Sequential Palladium-catalyzed Aerobic Oxidation and Visible-light Photoredox Catalysis. *ACS Catalysis* **2019**, *9*, 2252.

[108] This idea is further supported by the fact that the reaction progress proceeds normally when done in the presence of other Brønsted acids, such as HCl and HNO$_3$

[109] The equation for estimating the excited-state redox potentials is: $E_{ox}^{o*} = E_{ox}^{o'} - E^{0-0}$ and $E_{red}^{o*} = E_{red}^{o'} - E^{0-0}$; where E^{o-o} = energy gap between the zeroth vibrational levels of the ground and excited states (can be estimated from emission spectra compared at room temperature and at cryogenic temperatures (77K), also from the wavelength intersection of the absorbance spectra and the emission spectra using the following equation): $E^{0-0} = E_{photon}(eV) = \frac{1240}{\lambda(nm)}$. For additional

reading on this topic, see: Brennan, J. L.; Keyes, T. E.; Forster, R. J. Photonic Electrochemical Properties of Adsorbed [Ru(dpp)2(Qbpy)]2+ Luminophores. *Langmuir* **2006**, *22*, 10754.

[110] Weinberg, N. L.; Weinberg, N. R. Electrochemical Oxidation of Organic Compounds. *Chem. Rev*. **1968**, *68*, 449.

[111] Horn, E. J.; Rosen, B. R.; Baran, P. S. Synthetic Organic Electrochemistry: An Enabling and Innately Sustainable Method. *ACS Cent. Sci*. **2016**, *2*, 302.

[112] Stromskaya, G. I.; Chupka, E. I. Electrochemical Reduction of Lignin in Liquid Ammonia. 1. Change in the Chromophore and Molecular-weight Composition During Electrochemical Reduction in Liquid Ammonia. *Koksnes Kimija* **1983**, *2*, 60.

[113] Tolba, R.; Tian, M.; Wen, J.; Jiang, Z.-H.; Chen, A. Electrochemical Oxidation of Lignin at IrO2-based Oxide Electrodes. *J. Electroanal. Chem*. **2010**, *649*, 9.

[114] Parpot, P.; Bettencourt, A. P.; Carvalho, A. M.; Belgsir, E. M. Biomass Conversion: Attempted Electrooxidation of Lignin for Vanillin Production. *J. Appl. Electrochem*. **2000**, *30*, 727.

[115] Reichert, E.; Wintringer, R.; Volmer, D. A.; Hempelmann, R. Electro-catalytic Oxidative Cleavage of Lignin in a Protic Ionic Liquid. *Phys. Chem. Chem. Phys*. **2012**, *14*, 5214.

[116] Bailey, A.; Brooks, H. M. Electrolytic Oxidation of Lignin. *J. Am. Chem. Soc*. **1946**, *68*, 445.

[117] Liu, M.; Xia, H.; Lu, W.; Xu, T.; Zhu, Z.; Chen, W. Electrocatalytic Degradation of Organic Contaminants Using Carbon Fiber Coupled with Cobalt Phthalocyanine Electrode. *J. Appl. Electrochem*. **2016**, *46*, 583.

[118] Francke, R.; Little, R. D. Redox Catalysis in Organic Electrosynthesis: Basic Principles and Recent Developments. *Chem. Soc. Rev*. **2014**, *43*, 2492.

[119] Masui, M.; Ueshima, T.; Ozaki, S. *N*-Hydroxyphthalimide as an Effective Mediator for the Oxidation of Alcohols by Electrolysis. *J. Chem. Soc., Chem. Commun.* **1983**, 479.

[120] Shiraishi, T.; Takano, T.; Kamitakahara, H.; Nakatsubo, F. Studies on Electro-oxidation of Lignin and Lignin Model Compounds. Part 2: *N*-Hydroxyphthalimide (NHPI)-mediated Indirect Electro-oxidation of Non-phenolic lignin Model Compounds. *Holzforschung* **2012**, *66*, 311.

[121] Nguyen, B. H.; Perkins, R. J.; Smith, J. A.; Moeller, K. D. Solvolysis, Electrochemistry, and Development of Synthetic Building Blocks from Sawdust. *J. Org. Chem.* **2015**, *80*, 11953.

[122] Rafiee, M.; Miles, K. C.; Stahl, S. S. Electrocatalytic Alcohol Oxidation with TEMPO and Bicyclic Nitroxyl Derivatives: Driving Force Trumps Steric Effects. *J. Am. Chem. Soc.* **2015**, *137*, 14751.

[123] Hickey, D. P.; Schiedler, D. A.; Matanovic, I.; Doan, P. V.; Atanassov, P.; Minteer, S. D.; Sigman, M. S. Predicting Electrocatalytic Properties: Modeling Structure−Activity Relationships of Nitroxyl Radicals. *J. Am. Chem. Soc.* **2015**, *137*, 16179.

[124] Badalyan, A.; Stahl, S. S. Cooperative Electrocatalytic Alcohol Oxidation with Electron-proton-transfer Mediators. *Nature* **2016**, *535*, 406.

[125] For detailed instructions on running a cyclic voltammetry experiment, see: Graham, D. J. Standard Operating Procedures for Cyclic Voltammetry. https://sop4cv.com/index.html (accessed March 2019).

[126] Elgrishi, N.; Rountree, K. J.; McCarthy, B. D.; Rountree, E. S.; Eisenhart, T. T.; Dempsey, J. L. A Practical Beginner's Guide to Cyclic Voltammetry. *J. Chem. Ed.* **2018**, *95*, 197.

[127] Saveant, J.-M. Elements of Molecular and Biomolecular Electrochemistry; John Wiley & Sons: Hoboken, NJ, 2006.

[128] Horn, E. J.; Rosen, B. R.; Chen, Y.; Tang, J.; Chen, K.; Eastgate, M. D.; Baran, P. S. Scalable and Sustainable Electrochemical Allylic C−H Oxidation. *Nature* **2016**, *533*, 77.

[129] Hibino, T.; Shibata, D.; Ito, T.; Tsuchiya, D.; Higuchi, T.; Pollet, B.; Lapierre, C. Chemical Properties of Lignin from Aralia Cordata. *Phytochemistry* **1994**, *37*, 445.

[130] Coseri, S. Phthalimide-N-oxyl (PINO) Radical, a Powerful Catalytic Agent: Its Generation and Versatility Towards Various Organic Substrates. *Catal. Rev.: Sci. Eng.* **2009**, *51*, 218.

[131] Recupero, F.; Punta, C. Free Radical Functionalization of Organic Compounds Catalyzed by *N*-hydroxyphthalimide. *Chem. Rev.* **2007**, *107*, 3800.

[132] Simmons, E. M.; Hartwig, J. F. On the Interpretation of Deuterium Kinetic Isotope Effects in C–H Bond Functionalizations by Transition-metal Complexes. *Angew. Chem., Int. Ed.* **2012**, *51*, 3066.

[133] Bosque, I.; Magallanes, G.; Rigoulet, M.; Kärkäs, M. D.; Stephenson, C. R. J. Redox Catalysis Facilitates Lignin Depolymerization. *ACS Cent. Sci.* **2017**, *3*, 621.

[134] Warren, J. J.; Tronic, T. A.; Mayer, J. M. Thermochemistry of Proton-coupled Electron Transfer Reagents and its Implications. *Chem. Rev.* **2010**, *110*, 6961.

[135] Gentry, E. C.; Knowles, R. R. Synthetic Applications of Proton-coupled Electron Transfer. *Acc. Chem. Res.* **2016**, *49*, 1546.

[136] Both sequential transfer mechanisms are not feasible, since the base (2,6-lutidine, pK_a 12 (in MeCN)) is not able to deprotonate NHPI (pK_a NHPI 23.5 (in MeCN)) to any extent.

[137] Konya, K. G.; Paul, T.; Lin, S.; Lusztyk, J.; Ingold, K. U. Laser Flash Photolysis Studies on the First Superoxide Thermal Source. First Direct Measurements of the Rates of Solvent-assisted 1,2-

hydrogen Atom Shifts and a Proposed New Mechanism for this Unusual Rearrangement. *J. Am. Chem. Soc.* **2000**, *122*, 7518.

[138] Bothe, E.; Behrens, G.; Schulte-Frohlinde, D. Mechanism of the First Order Decay of 2-hydroxy-propyl-2-peroxyl Radicals and of $O_2^{-\bullet}$ Formation in Aqueous Solution. *Z. Naturforsch., B: J. Chem. Sci.* **1977**, *32b*, 886.

[139] Valgimigli, L.; Amorati, R.; Fumo, M. G.; DiLabio, G. A.; Pedulli, G. F.; Ingold, K. U.; Pratt, D. A. The Unusual Reaction of Semiquinone Radicals with Molecular Oxygen. *J. Org. Chem.* **2008**, *73*, 1830.

[140] Treat, N. J.; Sprafke, H.; Kramer, J. W.; Clark, P. G.; Barton, B. E.; Read de Alaniz, J.; Fors, B. P.; Hawker, C. J. Metal-free Atom Transfer Radical Polymerization. *J. Am. Chem. Soc.* **2014**, *136*, 16096.

[141] Pan, X.; Lamson, M.; Yan, J.; Matyjaszewski, K. Photoinduced Metal-Free Atom Transfer Radical Polymerization of Acrylonitrile. *ACS Macro Lett.* **2015**, *4*, 192.

[142] Chen, M.; MacLeod, M. J.; Johnson, J. A. Visible-light Controlled Living Radical Polymerization from a Trithiocarbonate Iniferter Mediated by an Organic Photoredox Catalyst. *ACS Macro Lett.* **2015**, *4*, 566.

[143] Discekici, E. H.; Treat, N. J.; Poelma, S. O.; Mattson, K. M.; Hudson, Z. M.; Luo, Y.; Hawker, C. J.; de Alaniz, J. R. A Highly Reducing Metal-free Photoredox Catalyst: Design and Application in Radical Dehalogenations. *Chem. Commun.* **2015**, *51*, 11705.

[144] Yayla, H. G.; Wang, H.; Tarantino, K. T.; Orbe, H. S.; Knowles, R. R. Catalytic Ring-opening of Cyclic Alcohols Enabled by PCET Activation of Strong O–H Bonds. *J. Am. Chem. Soc.* **2016**, *138*, 10794.

[145] Eisuke, O.; Wang, H.; Frye, N. L.; Knowles, R. R. A Redox Strategy for Light-driven, Out-of-equilibrium Isomerizations and Applications to Catalytic C–C Bond Cleavage Reactions. *J. Am. Chem. Soc.* **2019**, *141*, 1457.

[146] Zhou, W.; Nakahashi, J.; Miura, T.; Murakami, M. Light/Copper Relay for Aerobic Fragmentation of Lignin Model Compounds. *Asian J. Org. Chem.* **2018**, *7*, 2431.

[147] Sedai, B.; Diaz-Urrutia, C.; Baker, R. T.; Wu, R.; Silks, L. A.; Hanson, S. K. Comparison of Copper and Vanadium Homogeneous Catalysts for Aerobic Oxidation of Lignin Models. *ACS Catal.* **2011**, *1*, 794.

[148] Choi, G. J.; Zhu, Q.; Miller, D. C.; Gu, C. J.; Knowles, R. R. Catalytic Alkylation of Remote C–H Bonds Enabled by Proton-coupled Electron Transfer. *Nature* **2016**, *539*, 268.

[149] Jeffrey, J. L.; Terrett, J. A.; MacMillan, D. W. C. O–H Hydrogen Bonding Promotes H-atom Transfer from α C–H Bonds for C-alkylation of Alcohols. *Science* **2015**, *349*, 1532.

[150] Shuai, L.; Amiri, M. T.; Questell-Santiago, Y. M.; Héroguel, F.; Li, Y.; Kim, H.; Meilan, R.; Chapple, C.; Ralph, J.; Luterbacher, J. S. Formaldehyde Stabilization Facilitates Lignin Monomer Production During Biomass Depolymerization. *Science.* **2016**, *354*, 329.

[151] Lan, W.; Amiri, M. T.; Hunston, C. M.; Luterbacher, J. S. Protection Group Effects During α,γ-diol Lignin Stabilization Promote High-selectivity Monomer Production. *Angew. Chem., Int. Ed.* **2018**, *57*, 1356.